Fall 11-21-2016

From Drought Monitoring to Forecasting: a Combined Dynamical-Statistical Modeling Framework

Hongxiang Yan
Portland State University

Recommended Citation
Yan, Hongxiang, "From Drought Monitoring to Forecasting: a Combined Dynamical-Statistical Modeling Framework" (2016). *Dissertations and Theses.* Paper 3292.
https://doi.org/10.15760/etd.3283

From Drought Monitoring to Forecasting:

A Combined Dynamical-Statistical Modeling Framework

by

Hongxiang Yan

A dissertation submitted in partial fulfillment of the
requirements for the degree of

Doctor of Philosophy
in
Civil and Environmental Engineering

Dissertation Committee:
Hamid Moradkhani, Chair
Dacian Daescu
Ian Dinwoodie
Faryar Etesami

Portland State University
2016

Abstract

Drought is the most costly hazard among all natural disasters. Despite the significant improvements in drought modeling over the last decade, accurate provisions of drought conditions in a timely manner is still one of the major research challenges. In order to improve the current drought monitoring and forecasting skills, this study presents a hybrid system with a combination of remotely sensed data assimilation based on particle filtering and a probabilistic drought forecasting model. Besides the proposed drought monitoring system through land data assimilation, another novel aspect of this dissertation is to seek the use of data assimilation to quantify land initial condition uncertainty rather than relying entirely on the hydrologic model or the land surface model to generate a single deterministic initial condition. Monthly to seasonal drought forecasting products are generated using the updated initial conditions. The computational complexity of the distributed data assimilation system required a modular parallel particle filtering framework which was developed and allowed for a large ensemble size in particle filtering implementation. The application of the proposed system is demonstrated with two case studies at the regional (Columbia River Basin) and the Conterminous United States. Results from both synthetic and real case studies suggest that the land data assimilation system significantly improves drought monitoring and forecasting skills. These results also show how sensitive the seasonal drought forecasting skill is to the initial conditions, which can lead to better facilitation of the state/federal drought preparation and response actions.

Acknowledgements

This dissertation would not have been possible without the help of a large number of people. First, I would like to express the deepest appreciation to my advisor, Dr. Hamid Moradkhani, who helped me choose my courses, taught me the advanced skills, guided me to the frontier research topics, and gave me advice about my future career. Thanks to his guidance and persistent encouragement, I have completed research of greater complexity than I had imagined four years ago. Secondly, I would like to thank my committee members, Dr. Dacian Daescu, Dr. Ian Dinwoodie, and Dr. Faryar Etesami. Thanks so much for your time and willingness to serve on my committee and guide my research. Thirdly, I would like to thank Dr. Karen Karavanic from the Computer Science Department, and all of the members in the Remote Sensing and Water Resources Lab. Thanks for your guidance, hard work, and great attitude during our collaborations. Special thanks to Mahkameh Zarekarizi and Benjamin Beal, who worked on the same project and helped to prepare several results. Last but not least, I would like to thank my family and my friends for their support, especially my big brother Yuan Yan and my best friend Tianyuan Zhang. Your encouragement has helped me to get through the most difficult parts and to chase my dream.

Table of Contents

List of Tables

List of Figures

List of Abbreviations

AFDM…….....African Flood and Drought Monitor

AMI…….....Advanced Microwave Instrument

AMSR-E……Advanced Microwave Scanning Radiometer for Earth Observing System

AMSR2…….Advanced Microwave Scanning Radiometer2

ARK……Arkansas-Red

ASCAT……...Advanced Scatterometer

BOR……..Bureau of Reclamation

BPA……. Bonneville Power Administration

CALI……..California

CCI……Climate Change Initiative

CDF…….Cumulative Distribution Function

CFS……....Climate Forecast System

COLOR…….Colorado River

CONUS…….Contiguous United States

CPC…….....Climate Prediction Center

CRB……Columbia River Basin

DA…….……Data Assimilation

DTF……Drought Task Force

EAST……East Coast

EnKF……...Ensemble Kalman Filter

ENSO……..El Niño-Southern Oscillation

ERS……..……Economic Research Service

ESP……Ensemble Streamflow Prediction

ESRI…….…..Environmental Systems Research Institute

GCM…….Global Circulation Model

GCOM-W1…….Global Change Observation Mission1-Water

GIDMaPS……Global Integrated Drought Monitoring and Prediction System

GLAKES……Great Lakes Drainage

GLDAS……...…Global Land Data Assimilation System

GRB……....Great Basin

GSFC……...Goddard Space Flight Center

GULF……...South Central

HPC…….……..High Performance Computing

HRU……Hydrologic Response Unit

I/O……..Input/Output

JAXA…….Japan Aerospace Exploration Agency

KGE…….Kling-Gupta Efficiency

LDAS……..Land Data Assimilation System

LOW…….Lower Mississippi

LPRM……...….Land Parameter Retrieval Model

LSM……..Land Surface Model

MCMC……...Markov Chain Monte Carlo

MLE……..Maximum Likelihood Estimation

MO…….Missouri River

MPI……..Message Passing Interface

NARR…….North American Regional Reanalysis

NASA……National Aeronautics and Space Administration

NCEP……..National Centers for Environmental Prediction

NDMC……..National Drought Mitigation Center

NESDIS…….NOAA Environmental Satellite, Data, and Information Service

NIC……Normalized Information Contribution

NLDAS……North American Land Data Assimilation System

NMME……North American Multimodel Ensemble

NOAA.....National Oceanic and Atmospheric Administration

NRNI……....No Regulation No Irrigation

NWP……..Numerical Weather Prediction

NWS……..Numerical Weather Service

OHD……...Office of Hydrologic Development

OHIO……..Ohio

OIT……..…Office of Information Technology

OL……Open Loop

OSSE……..Observing System Simulation Experiment

PDF……..Probability Density Function

PDO……Pacific Decadal Oscillation

PET……..….Potential Evapotranspiration

PF…….Particle Filter

PF-SIR……..Particle Filter-Sampling Importance Resampling

PMCMC……...Particle Markov Chain Monte Carlo

PNW……..Pacific Northwest

PRMS……..Precipitation-Runoff Modeling System

PSU……Portland State University

RAM……...Random-access Memory

RMSE…….Root Mean Square Error

RIO……..Rio Grande

SCE……..……Shuffled Complex Evolution

SDO…….Seasonal Drought Outlook

SIR……...Sampling Importance Resampling

SMAP……..Soil Moisture Active Passive

SMMR……...Scanning Multichannel Microwave Radiometer

SMOS……..Soil Moisture Ocean Salinity

SR……..Solar Radiation

SSM/I……..Special Sensor Microwave Imager

SWM…….Surface Water Monitor

TMI……..Microwave Imager

TRMM……...…Tropical Rainfall Measure Mission

USACE……...United States Army Corps of Engineers

UCI……University of California Irvine

UP…….Upper Mississippi

USDA……United States Department of Agriculture

USDM…….United States Drought Monitoring

USGS…….United States Geological Survey

UW……...University of Washington

VIC…….Variable Infiltration Capacity

WCRP……..World Climate Research Program

Chapter 1 Introduction

Water sustainability is one of the grand challenges facing society in the twenty-first century. With ongoing land development driven by population growth and climate change, many regions of the world are facing the exacerbated floods and droughts, which threaten the long-term sustainability of water resources. Accurate monitoring and forecasting of hydrometeorologic extreme events plays a significant role in developing appropriate policies to plan for available water resources. Despite multitude of studies conducted that proposed promising methods to improve extreme events monitoring and forecasts, the observed effects of climate change on floods and droughts across different regions of the globe in recent decades highlights the need for more sophisticated methods (Mishra and Singh 2010; DeChant and Moradkhani, 2015a; Rana and Moradkhani, 2016; Halmstad et al. 2012; Risley et al. 2011).

1.1 Drought Background

What is drought? Drought is a complex natural hazard and impacts hydrological, environmental, ecological, and social systems in many ways. Currently, no universal definition of drought exists (Lloyd-Hughes, 2014). The National Drought Mitigation Center (NDMC) at the University of Nebraska, Lincoln defines drought as: "*drought is a protracted period of deficient precipitation resulting in extensive damage to crops, resulting in loss of yield*". Other definitions can also be found in Wilhite (2000), Keyantash and Dracup (2002), Mishra and Singh (2010), Sheffield and Wood (2011), and Van Loon (2015). Generally, drought can be described as a deficiency in precipitation,

soil moisture, and surface/ground water over an extended period, which has huge negative impacts on agricultural, ecological, and socio-economic systems. A drought event can be short, lasting for just a few months, or it can persist for multiple years.

What causes drought? Drought is caused by natural variability (i.e., meteorological anomalies) or anthropogenic activities (i.e., groundwater abstraction). Natural variability indicates the variations of our climate system caused by natural factors, including external factors such as solar radiation, and internal factors such as the El Niño-Southern Oscillation (ENSO) or the Pacific Decadal Oscillation (PDO). Anthropogenic activities, such as water transfer projects or groundwater over abstraction, can also influence water input, storage, and output and therefore break the local water balance modifying the propagation of drought (Liu et al., 2015). Moreover, human-induced global warming can further exacerbate a drought event in terms of both duration and severity (Ahmadalipour et al., 2016; Cheng et al., 2016; Rana et al., 2016).

What are the types of drought? In general, drought can be classified into four categories: meteorological, agricultural, hydrological, and socio-economic (Figure 1-1) (Dai et al., 2004). Meteorological drought results from a deficiency of precipitation, such as the number of days with precipitation less than a specified threshold; agricultural drought relates to a shortage of available water in the root-zone layer for plant growth, and is assessed as insufficient soil moisture; hydrological drought is a deficiency in the surface/ground water supply, such as a dry reservoir; and socio-economic drought is characterized by the water and food market, such as hydroelectric power and loss of fish.

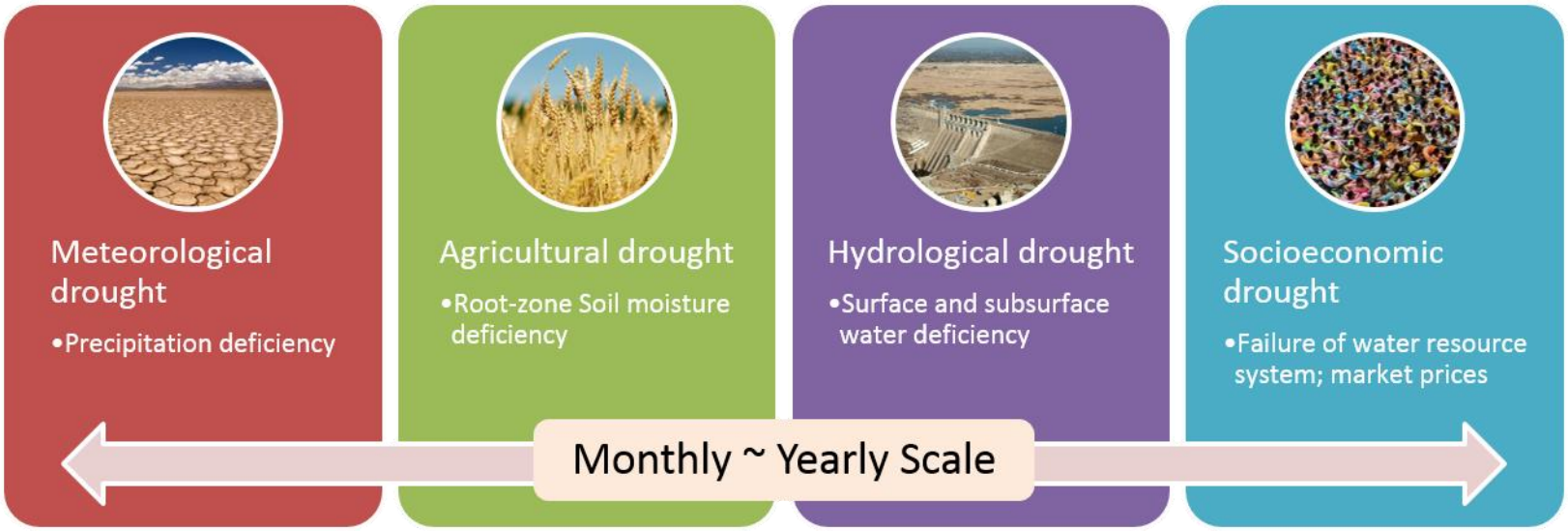

Figure 1-1. The description of four types of drought.

Why is drought important? Among all natural disasters, drought is the most costly extreme event (Sheffield et al., 2014) that may result in water scarcity (Jaeger et al., 2013). For example, the North American drought in 1988 cost nearly $62 billion (in 2002 dollars), which was more than the cost of the 1993 Mississippi River flood and Hurricane Andrew combined (Ross and Lott, 2003). Severe drought events can have devastating effects on crop production, agriculture, and even water supplies (Mishra and Cherkauer, 2010). For instances, the 2012 summertime flash drought event across the Great Plains resulted in a major curtailment of crop yields, and caused about $12 billion economic loss (Hoerling et al., 2014). In 2015, California faced its fourth year of a multiple year drought event. The economic losses of this year were estimated to be $2.7 billion, which is equivalent to about 5% of annual agricultural production (Howitt et al., 2015). Figure 1-2 shows the percent area of the United States under drought from January 2000 to October 2016, according to the NDMC.

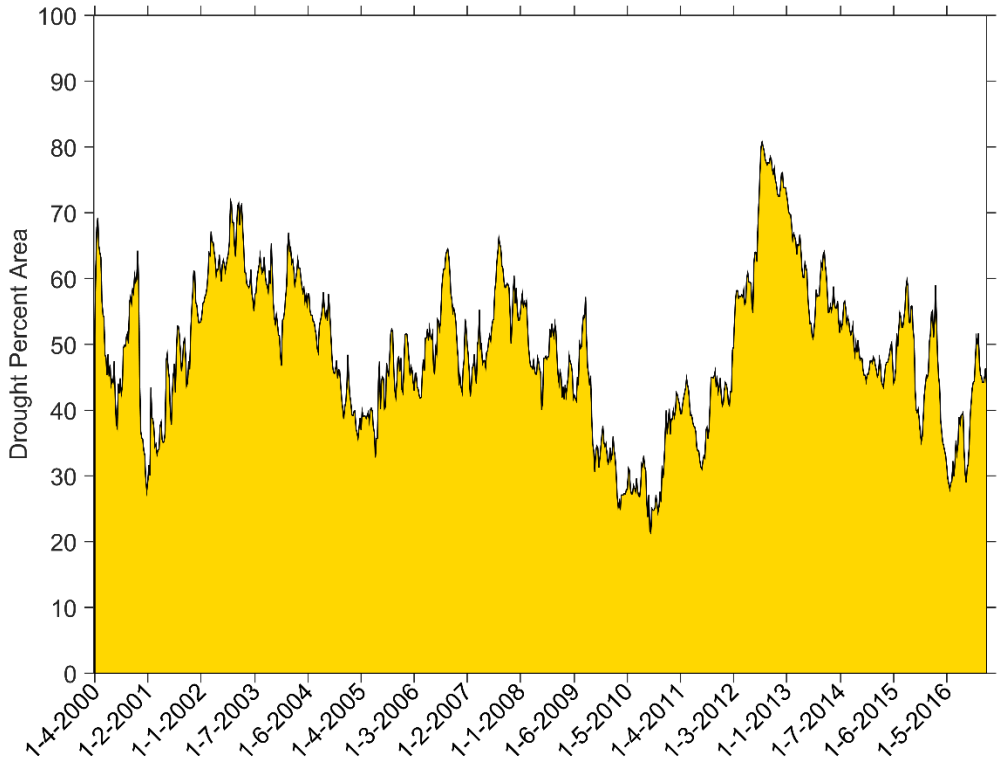

Figure 1-2. Percent area of the United States in drought, 2000-2016, according to the NDMC.

How can we reduce drought risk? One possible reason for such huge losses from a drought event is the lack of prompt preparation and effective response actions due to the lack of accurate knowledge about the behavior of drought development (Figure 1-3). Different from other natural disasters, drought has a slow onset and develops over large areas, which makes it difficult to detect until severe damage has already occurred (Luo and Wood, 2007; Sheffield and Wood, 2011; Wood et al., 2015). Therefore, a drought monitoring and forecasting system that can sense drought conditions in a timely manner is essential for drought preparedness and risk reduction (Ahmadalipour et al., 2017; Madadgar and Moradkhani, 2014a, 2013a; Sheffield et al., 2014).

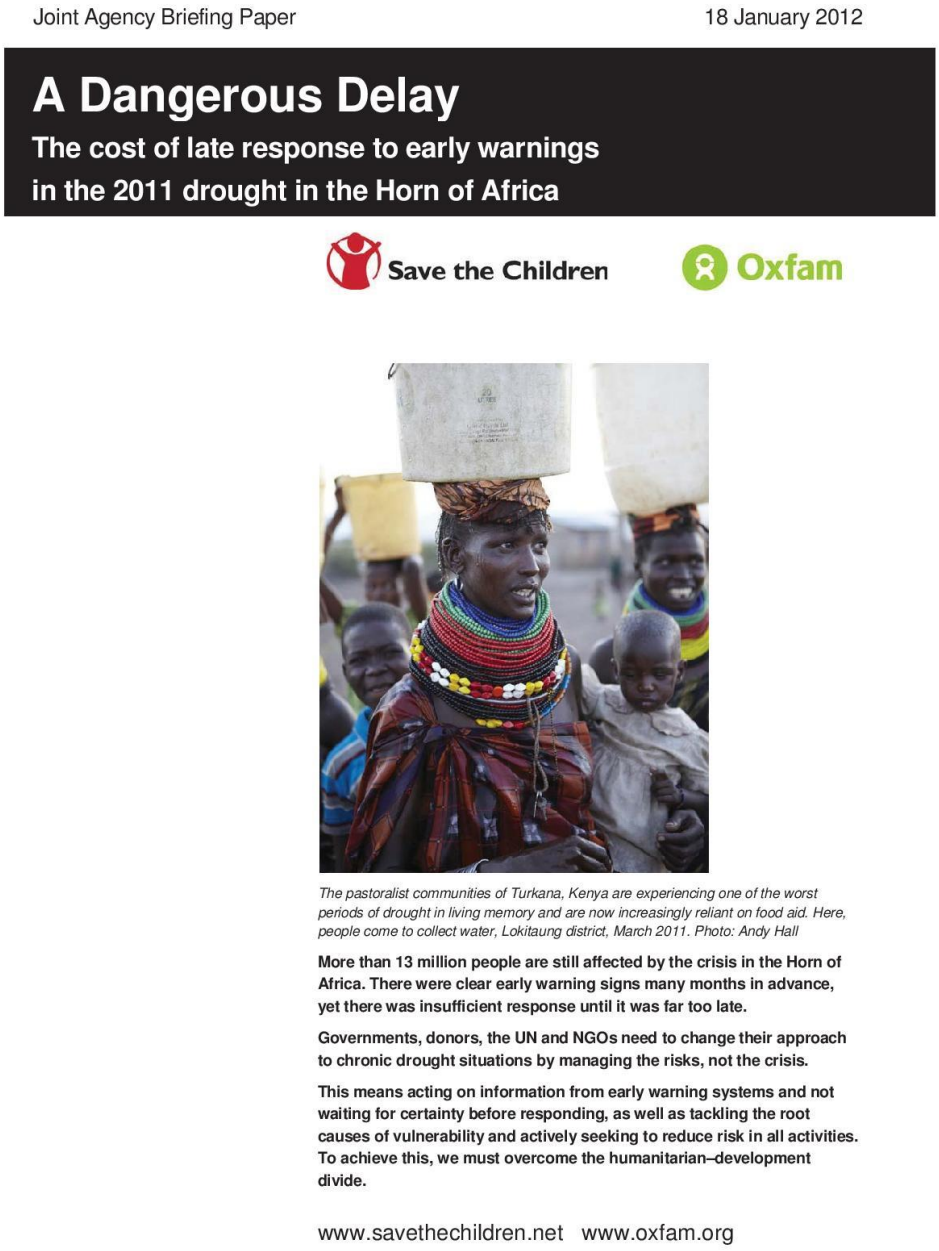

Joint Agency Briefing Paper 18 January 2012

A Dangerous Delay

The cost of late response to early warnings in the 2011 drought in the Horn of Africa

Save the Children Oxfam

The pastoralist communities of Turkana, Kenya are experiencing one of the worst periods of drought in living memory and are now increasingly reliant on food aid. Here, people come to collect water, Lokitaung district, March 2011. Photo: Andy Hall

More than 13 million people are still affected by the crisis in the Horn of Africa. There were clear early warning signs many months in advance, yet there was insufficient response until it was far too late.

Governments, donors, the UN and NGOs need to change their approach to chronic drought situations by managing the risks, not the crisis.

This means acting on information from early warning systems and not waiting for certainty before responding, as well as tackling the root causes of vulnerability and actively seeking to reduce risk in all activities. To achieve this, we must overcome the humanitarian–development divide.

www.savethechildren.net www.oxfam.org

Figure 1-3. The late response to the 2011 drought in the Horn of Africa resulted in severe food shortage and affected more than 13 million people. (Source: Hillier & Dempsey, 2012)

1.2 Soil Moisture

Among the four types of drought, agricultural drought, which is characterized by root-zone soil moisture receives special attention due to its direct relationships with crop yields and food security (Champagne et al., 2011; Sheffield et al., 2014). Especially for developing counties, an agricultural drought event can have devastating effects on the food supply and even the political stability. For instances, in Ethiopia and Sudan, the incidences of the agricultural drought events in 1983-1985 resulted in hundreds of thousands of deaths due to the poor plant growth and agricultural yields (Pickering and Owen, 1997). In 2011, the Horn of Africa experienced the most severe agricultural drought event of this century, which affected more than thirteen million people, with hundreds of thousands placed at risk of starvation and fifty to one hundred thousand deaths (Hillier and Dempsey, 2012). Considering the huge negative impacts of agriculture drought events, the focus of this dissertation is on the study of agriculture drought in order to improve future agricultural drought relief efforts. For the remainder of this dissertation, the term "drought" will be used to indicate agricultural drought only, as opposed to other types of drought.

Root-zone soil moisture refers to the amount of water stored in the root-zone layer and is a critical variable in drought monitoring and forecasting (Brocca et al., 2012; Kumar et al., 2014a; Samaniego et al., 2013; Shukla et al., 2011; Xiao et al., 2016). Quantitative analysis of drought requires consistent and long-term time-series of root-zone soil moisture observations (Luo and Wood, 2007; Mishra and Singh, 2011; Svoboda et al., 2002). Currently, three approaches are used to retrieve soil moisture: 1) *in-situ*

measurements; 2) model simulations; and 3) remotely sensed retrievals. The *in-situ* measurements can provide continuous and reliable soil moisture measurements, with an extended length of record. The main limitation of this approach, however, is that it is only available for few regions, and cannot represent the spatial heterogeneity of soil moisture (Figure 1-4). As an alternative, model simulations can estimate soil moisture on a continental or global scale, but these simulations are potentially biased due to the errors in model parameters, forcing data, and the deficiencies in the model structure. In the third approach, remotely sensed soil moisture observations (spaceborne or airborne) can provide an unprecedented spatial and temporal resolution of soil moisture across a range of scales. Recently, two L-band spaceborne sensors have been specifically designed to estimate soil moisture, the Soil Moisture Ocean Salinity (SMOS) (Kerr et al., 2010) and the Soil Moisture Active Passive (SMAP) missions (Entekhabi et al., 2010). One major drawback of remotely sensed observation is the sensing depth. Microwaves (C-, X-, and L-bands) can only penetrate the top five centimeters, retrieving only the surface soil moisture rather than the root-zone soil moisture (Crow et al., 2008; Jackson et al., 2010; Njoku et al., 2003; Yan et al., 2015). Another drawback of remotely sensed data is the short length of record (less than a decade of data), which makes them insufficient to monitor drought from a climate perspective (Yan and Moradkhani, 2016a). One possible solution is to use the spatial regionalization method (Yan and Moradkhani, 2016b, 2015, 2014; Yan, 2012).

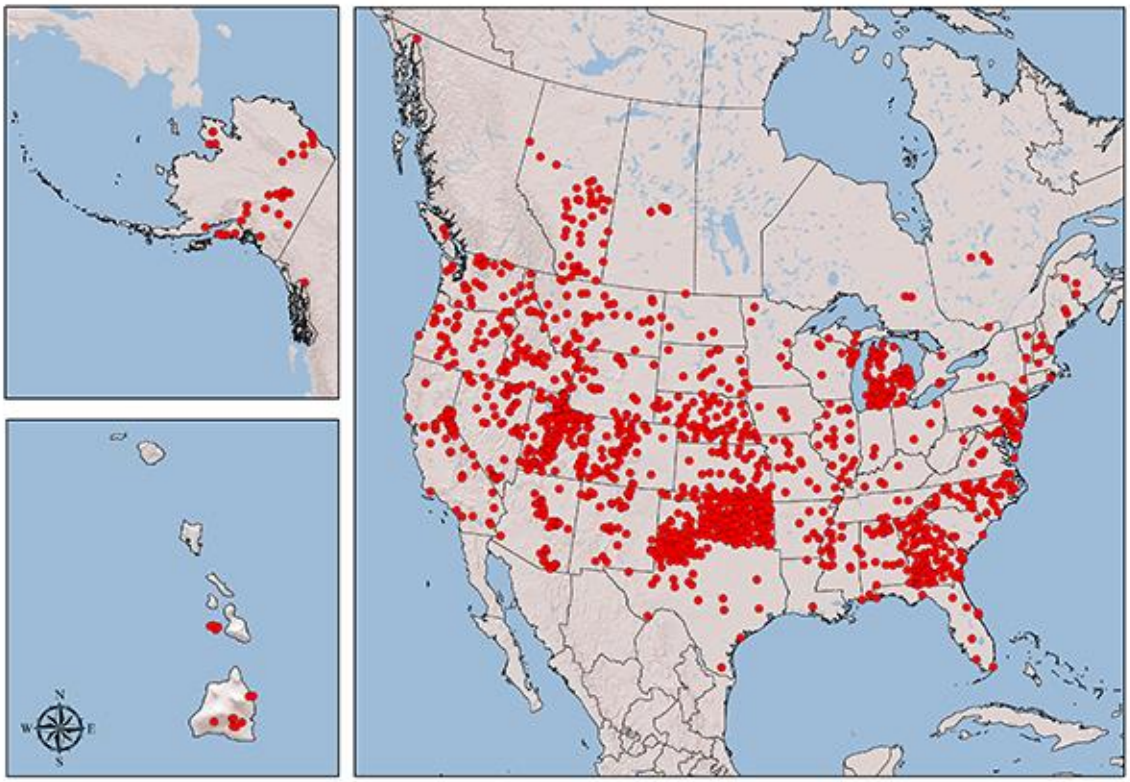

Figure 1-4. The TAMU North American Soil Moisture Database. Source: http://soilmoisture.tamu.edu/

Root-zone soil moisture is an indicator in drought monitoring and forecasting, and has been used in different forms, such as the root-zone soil moisture anomaly (Sheffield and Wood, 2008), the standardized root-zone soil moisture index (Hao and AghaKouchak, 2013), and the normalized root-zone soil moisture (Dutra et al., 2008). But the most commonly used form in hydrology community is the root-zone soil moisture percentile (Kumar et al., 2014a, 2014b; Luo and Wood, 2007; Mao et al., 2015; Mo and Lettenmaier, 2015; Samaniego et al., 2013; Shukla and Lettenmaier, 2011; Wang et al., 2009). The root-zone soil moisture percentile is estimated based on a historical reference period (normally 30-year time blocks). This historical reference period is also called as climatology. According to the NDMC, the drought intensity can be classified into five categories based on the root-zone soil moisture percentile: D0 (abnormally dry, percentile $\leq$ 30%), D1 (moderate drought, percentile $\leq$ 20%), D2 (severe drought, percentile $\leq$ 10%), D3 (extreme drought, percentile $\leq$ 5%), and D4 (exceptional drought, percentile $\leq$ 2%) (Table 1-1) (Svoboda et al., 2002). For the sake of convenience, in the remainder of this dissertation the term “soil moisture” will be used to indicate the root-zone soil moisture only, as opposed to the surface soil moisture.

Table 1-1. Drought classification based on the soil moisture percentile, according to the National Drought Mitigation Center.

Drought Category	Drought Intensity	Soil Moisture Percentile
D0	Abnormally Dry	(0.2, 0.3]
D1	Moderate Drought	(0.1, 0.2]
D2	Severe Drought	(0.05, 0.1]
D3	Extreme Drought	(0.02, 0.05]
D4	Exceptional Drought	(0, 0.02]

1.3 Limitations of the Current Systems

In United States, there are a number of operational federal and research drought monitoring and forecasting systems, including the NDMC United States Drought Monitoring (USDM) (Svoboda et al., 2002), the National Oceanic and Atmospheric Administration (NOAA) Climate Prediction Center's (CPC's) Seasonal Drought Outlook (SDO) (Steinemann, 2006), the University of Washington Experimental Surface Water Monitor (SWM) (Wood and Lettenmaier, 2006), the Princeton African Flood and Drought Monitor (AFDM) (Sheffield et al., 2014). Due to the abundance of available information in prior literature, the description of each system is not provided in this dissertation. Table 1-2 summarizes the basic information of each system. For more details, the above references are suggested as useful resources.

Table 1-2. Summary of the current drought monitoring and forecasting system.

System	USDM	SDO	SWM	AFDM	GIDMaPS
Institution	NDMC	NOAA/CPC	UW	Princeton	UCI
Study Area	U.S.	U.S.	U.S. and Mexico	Africa	Globe
Drought Monitoring	√	-	√	√	√
Drought Forecasting	-	√	√	√	√
Drought Index	Composite	Composite	Soil Moisture	Soil Moisture	Soil Moisture and Precipitation
Updated Period	Weekly	Monthly	Daily	Daily	Monthly
Model	CPC Soil Moisture Model	CPC Soil Moisture Model	VIC	VIC	-
Forecasting Approach	-	NWP	ESP	NWP	ESP
Forecasting Period	-	3-month	3-month	3-month	4-month
Ensemble Modeling	-	-	√	-	-

Generally speaking, all of the above drought monitoring and forecasting systems are based on simulated soil moisture using dynamical hydrologic models or land surface models (LSMs), but coupled with different drought forecasting approaches. While the above systems have been well received among the federal/local agencies and research communities, there still exist areas for continued development. For instance, the 2012 Central U.S. flash drought event (May-August) resulted in about $12 billion economic loss, but the SDO issued on 17 May 2012 did not forecast this event (Hoerling et al., 2014). The USDM also did not capture this event until late June (Mo and Lettenmaier, 2015). In the latest summary paper of National Oceanic and Atmospheric Administration (NOAA) Drought Task Force (DTF) research, Wood et al. (2015) concluded that one of the current critical challenges in drought study is "*the development of objective, science-based integration approaches for merging multiple information sources*".

Following this trend, there exists three ways to improve the current drought monitoring and forecasting systems: 1) improve the quality of soil moisture estimation by integrating remotely sensed observations (for drought monitoring); 2) develop new objective, science-based drought forecasting approach (for drought forecasting); and 3) objectively quantify the uncertainty of initial conditions (for drought forecasting). The following three paragraphs explain or illustrate each point in details.

1). The quality of soil moisture estimation. There are three main uncertainty sources affecting the quality of simulated soil moisture: the forcing data, the model parameter, and the model structure (DeChant and Moradkhani, 2014a; Moradkhani and Sorooshian, 2008). Addressing each of these uncertainties is beyond the scope of this

dissertation, and several recent progresses can be found in DeChant and Moradkhani (2014b), Samaniego et al. (2013). Only the model parameter uncertainty issue is briefly discussed here, since an interesting distinction exists on the model parameter estimation between the LSM and hydrologic modeling communities. For LSMs, these parameters are typically set to default values or estimated using look-up tables based on similarity between sites as a function of soil and vegetation (Clark et al., 2015; Mendoza et al., 2015). However, sensitivity analysis suggests that this methodology is overly simplistic and can lead to significant errors in flux estimations, including soil moisture (Rosero et al., 2010). For dynamical hydrologic models, the parameters are often calibrated based on streamflow observations using sophisticated optimization techniques (Duan et al., 1994). Although after intensive calibration, the simulated streamflow can match the observed streamflow, but other fields (i.e., soil moisture) may be significantly biased (Yan and Moradkhani, 2016a). The "parameter equifinality" (Beven, 2006), where multiple parameter sets satisfy the observations, further complicates the parameter calibration problem. It is possible that multiple parameter sets give the same results for a given cost function, but give different results when using other cost functions (Gupta et al., 2008). Specifically, finding robust model parameters, that are able to produce reliable flux estimations is still one of the grand challenges of contemporary hydrology (Wood et al., 2011). As a result, questions still remain regarding the quality of the simulated soil moisture in these systems.

2). The drought forecasting approaches. The drought forecasting approaches used in the aforementioned systems can be classified as climatological forecasts (including the

SWM and GIDMaPS) or numerical weather prediction (NWP) forecasts (including the SDO and AFDM). The climatological drought forecasting approach relies on the ensemble streamflow prediction (ESP) framework, which originated from probabilistic streamflow forecasting at National Weather Service (NWS) (Day, 1985). The ESP resamples the climatological stochastic forcing to it to run dynamical hydrologic models/LSMs or the climatological soil moisture directly to forecast future drought conditions. However, the main limitation of this approach is that the sampled forcing/soil moisture are not necessarily representative of the future climate, especially under a non-stationary world (Demirel and Moradkhani, 2016; Milly et al., 2008; Pathiraja et al., 2016a, 2016b; Yan and Edwards, 2013). As an alternative, instead of using the climatological data, the NWP drought forecasting approach seeks the use of NWP products, such as the Climate Forecast System version 2 (CFSv2) or the North American Multimodel Ensemble (NMME) (Yuan et al., 2011). Although the NWP products can provide future climate information, the current NWP products are subject to high uncertainty and exhibit low skill beyond a one month lead time (DeChant and Moradkhani, 2015b, 2014b; Hayes et al., 2005). So far, the NWP drought forecasts have met with mixed success, and the major stumbling block is the low skill of forecasting precipitation (Hayes et al., 2005). As a result, the World Climate Research Program (WCRP) identified seasonal drought forecasting as one of the major research gaps, and the development of an objective, reliable, and cost effective drought forecasting approach is still an undergoing research (Madadgar and Moradkhani, 2014a, 2013a; WCRP, 2010).

3). The role of initial condition on drought forecasting. Besides the aforementioned forecasting approaches, another important factor playing a crucial role in drought forecasting is the initial condition (DeChant and Moradkhani, 2015, 2014a, 2011a; Koster et al., 2010; Li et al., 2009; Shukla and Lettenmaier, 2011; Wood and Lettenmaier, 2008; Yossef et al., 2013). Initial condition refers to the land surface states or storage (i.e., soil moisture) at the initialization date of each forecasting, providing a starting point for trajectories in changes of the earth system states. For instances, Shukla et al. (2013) suggested that soil moisture predictability at seasonal lead times (one to six months) is sensitive to initial conditions. DeChant and Moradkhani (2015) emphasized that better estimates of the initial conditions could lead to improvements in drought forecasting skill. Currently, characterization of initial condition is performed through model simulations, or called as the "spin-up" period, where historical forcing data are available up to an initialization date of a forecast (Sheffield et al., 2014; Wood and Lettenmaier, 2006). As a result, the "spin-up" initial conditions are potentially biased due to the errors in forcing data, model parameter estimation, and the deficiencies in model structure. In addition, these "spin-up" initial conditions are treated as deterministic quantities and the epistemic uncertainties associated with them are not accounted for. The initial condition uncertainty that arises from the properties of the earth chaotic system is unavoidable due to the inability to accurately observe land surface states (Stainforth et al., 2005). Without quantification of the initial condition uncertainty, though such systems lead to probabilistic drought forecasts, these forecasts are generally over-

confident and underestimate the drought forecasting uncertainty (DeChant and Moradkhani, 2014b; Wood and Schaake, 2008).

1.4 Proposed Solutions

In order to improve the current drought monitoring and forecasting skills, this study attempts to propose three possible solutions to address the three challenges of the current systems discussed in the previous section. In the following three paragraphs, each proposed solution is discussed in details. It is noted that the proposed solutions are resulted from the recent improvements in computational resources, algorithm developments, and data availability.

1). Assimilation of remotely sensed surface soil moisture observations. A plausible approach to improve the quality of simulated soil moisture is to exploit the soil moisture observations to update the model states (Brocca et al., 2012; De Lannoy et al., 2012; Han et al., 2014; Li et al., 2010; Q. Liu et al., 2011; Massari et al., 2015; Moradkhani, 2008; Reichle and Koster, 2004; Yan and Moradkhani, 2016a; Yan et al., 2015). This method of integrating model simulations and observations is referred to as data assimilation (DA) (Doucet and Johansen, 2011; Evensen, 1994; Moradkhani et al., 2005a, 2005b). Recently, the advent of satellite microwave observations has created for the first time the possibility of large-scale soil moisture monitoring, which has led us to the era of "big data", or the "fourth paradigm" as described in Jim Gray's book *The Fourth Paradigm: Data-Intensive Scientific Discovery* (Table 1-3) (Hey et al., 2009). The remotely sensed big data provide newly emerging opportunities for DA applications in both soil moisture estimations and drought monitoring. Ahmadalipour et al. (2017) suggested that remotely sensed soil moisture played an important role in improving the current drought monitoring skill based on hydrologic models/LSMs. Yan and

Moradkhani (2016a) compared the root-mean-square-error of soil moisture prediction before and after assimilating satellite data, and found out that the soil moisture prediction biases were reduced significantly after data assimilation (Figure 1-5).

Table 1-3. The four science paradigms according to Jim Gray.

Science Paradigms	Date	Category	Description
1st	Thousand years ago	Empirical	Describing natural phenomena
2nd	Last few hundred years	Theoretical	Using models, generalizations
3rd	Last few decades	Computational	Simulating complex phenomena
4th	Today	Data exploration	Unifying theory, experiment, and simulation

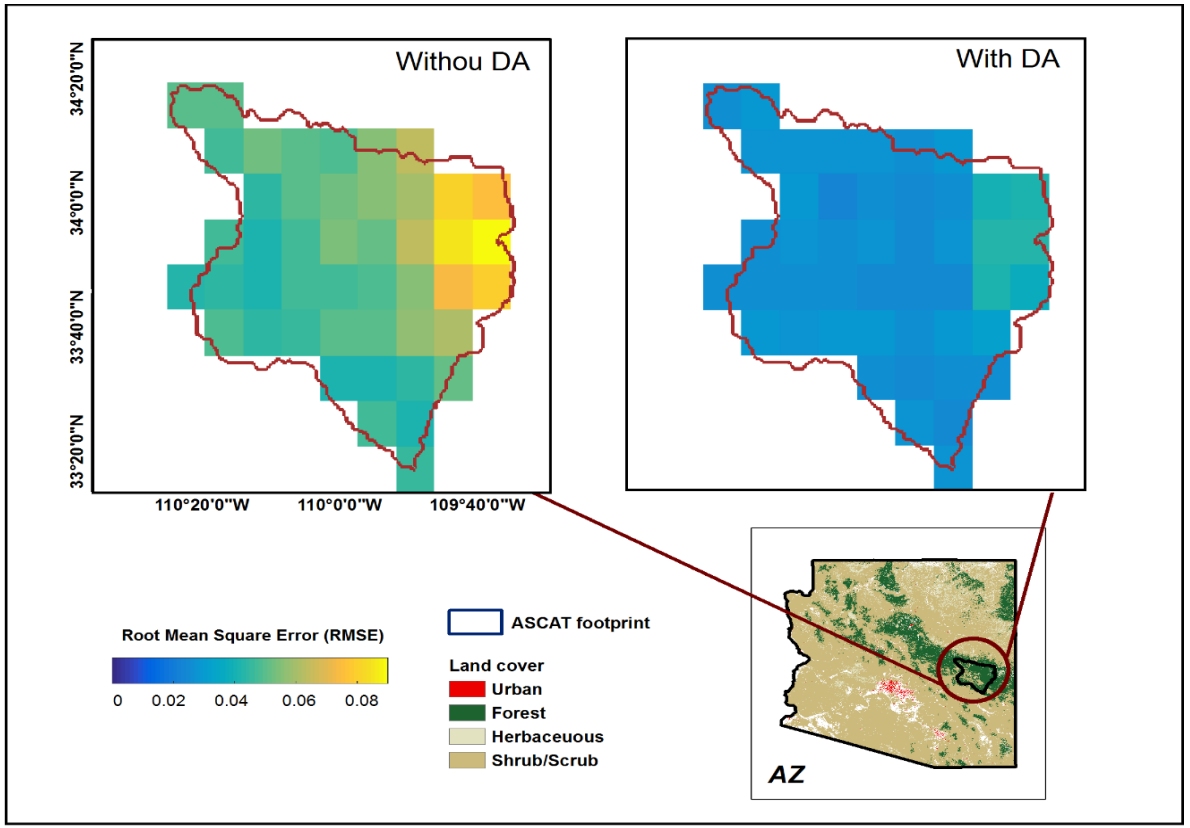

Figure 1-5. The root mean square error (m^3/m^3) between the simulated soil moisture and synthetic truth with/without assimilation of the satellite soil moisture (Yan and Moradkhani, 2016a).

2). Implementation of statistical drought forecasting approach. Soil moisture shows a distinctive characteristic called persistence, as it exhibits much less variability relative to climate variables (Seneviratne et al., 2010). Due to this persistence property, the drought states of a location at a particular time are affected by their earlier status to some extent. The persistence property directly motivates the use of the Markov network to model soil moisture in drought forecasting system instead of relying on the low skill climatological/future climate as implemented in the current system (Madadgar and Moradkhani, 2016, 2014b, 2013b; Mishra and Desai, 2005; Nicolai-Shaw et al., 2016; Pan et al., 2013; Wood et al., 2015). Recently, Madadgar and Moradkhani (2013a) proposed a newly statistical drought forecasting approach based on multivariate copula. They indicated that compared against the ESP approach a statistical copula-based model could lead to better seasonal drought forecasting skill. Madadgar and Moradkhani (2014a) further emphasized the importance of persistence in drought forecasting, and suggested that the persistence property played a key role during monthly to seasonal time scales.

3). Quantification of initial condition uncertainty. Accurate characterization of initial condition uncertainty is a challenge, but much progress has been made in the field of ensemble DA (DeChant and Moradkhani, 2015b, 2014b, 2011b; Leisenring and Moradkhani, 2012; Moradkhani, 2008; Moradkhani et al., 2012). A number of studies have investigated the ability of the ensemble DA to estimate soil moisture uncertainty showing promising results (Figure 1-6) (Yan and Moradkhani, 2016a; Yan et al., 2015). In addition, DeChant and Moradkhani (2011a) combined the ESP framework with the

initial condition uncertainty quantified through ensemble DA, and suggested that accounting for initial condition uncertainty improves the reliability of hydrologic forecasts.

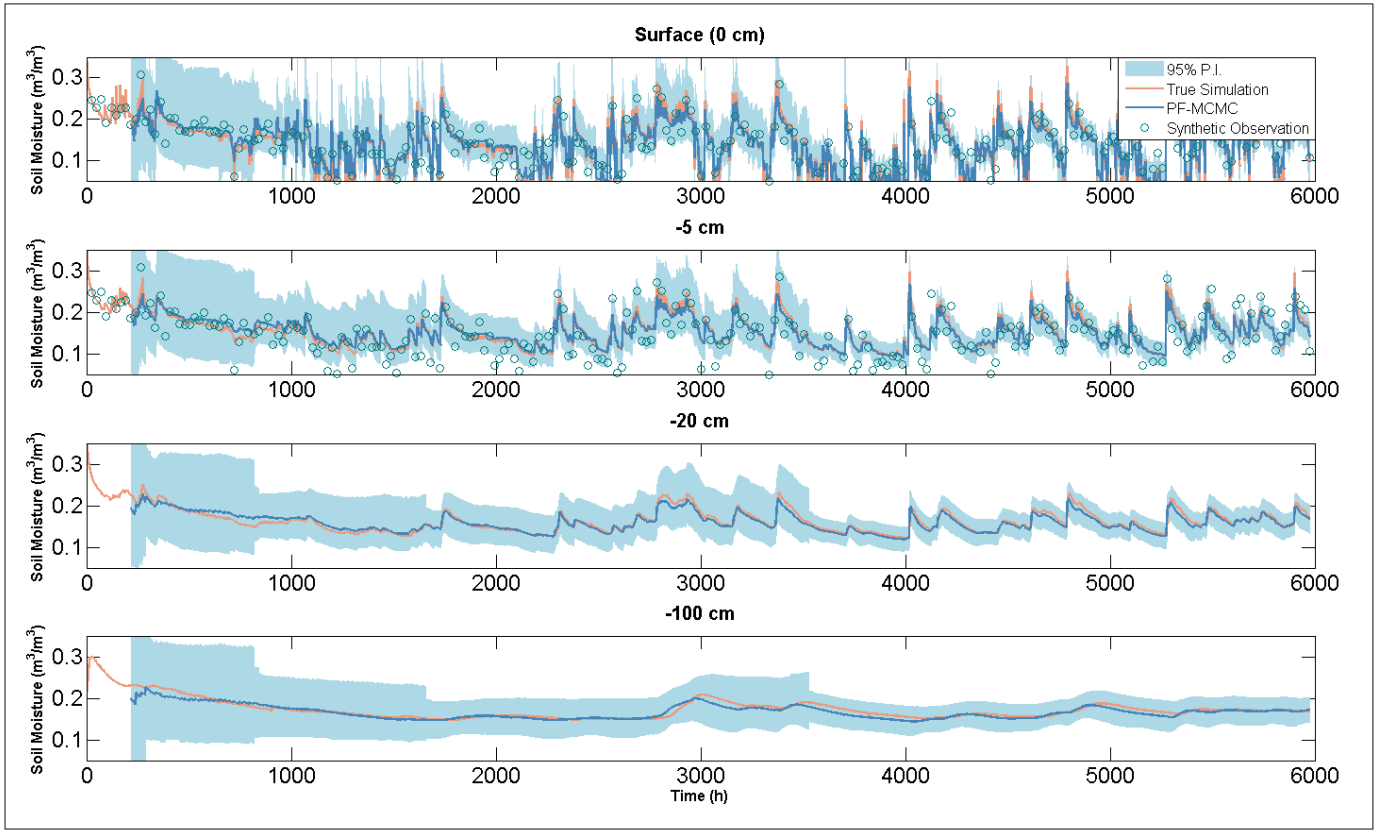

Figure 1-6. Assimilation of synthetic AMSR-E soil moisture (temporal resolution: one day) for quantifying soil moisture initial condition uncertainty (Yan et al., 2015).

1.5 Objective of Dissertation

Based on the above discussions, the objective of this dissertation is to improve the current drought monitoring and forecasting skills through the assimilation of remotely sensed surface soil moisture. Besides the proposed drought monitoring system through ensemble DA, another novel aspect of this dissertation is to propose a dynamical-statistical hybrid drought forecasting framework using both ensemble DA and multivariate copula. In the hybrid framework, this dissertation seeks the use of ensemble DA to improve soil moisture initialization by quantifying the initial condition uncertainty. It is hypothesized that ensemble DA would lead to an improved simulated soil moisture field, which translates into a drought monitoring skill; a more accurate quantification of initial condition uncertainty would lead to an improved drought forecasting skill.

After the brief introduction, the rest of the dissertation is organized as follows. Chapter 2 presents the framework of the proposed drought monitoring and forecasting system, including the dynamical hydrologic modeling, DA algorithm, the parallelization of DA, and the probabilistic multivariate copula. Chapter 3 illustrates the proposed system with two drought case studies in Columbia River Basin and Contiguous United States. Chapter 4 and 5 present and discuss the synthetic and real case study results for the Columbia River Basin case study, respectively. Chapter 6 and 7 present and discuss the synthetic and real case study results for the Contiguous United States case study, respectively. Finally, Chapter 8 concludes the dissertation and discusses future studies.

Chapter 2 Methodology

The proposed drought monitoring and hybrid drought forecasting systems are composed of three main parts: 1) dynamical hydrologic modeling, 2) ensemble DA, and 3) probabilistic multivariate copula model. First, the hydrologic model is calibrated for the study region. Next, the remotely sensed surface soil moisture observations are assimilated into the calibrated model through the ensemble DA. At this point, better drought monitoring skills can be achieved with the updated soil moisture field. For each forecasting date, the soil moisture initial condition uncertainty can be quantified through a probability density function (PDF) estimated using the ensemble DA. Last, the initial conditions sampled from the PDF are used in the probabilistic multivariate copula to generate drought forecasts. Figure 2-1 illustrates the framework of the proposed drought monitoring and forecasting systems.

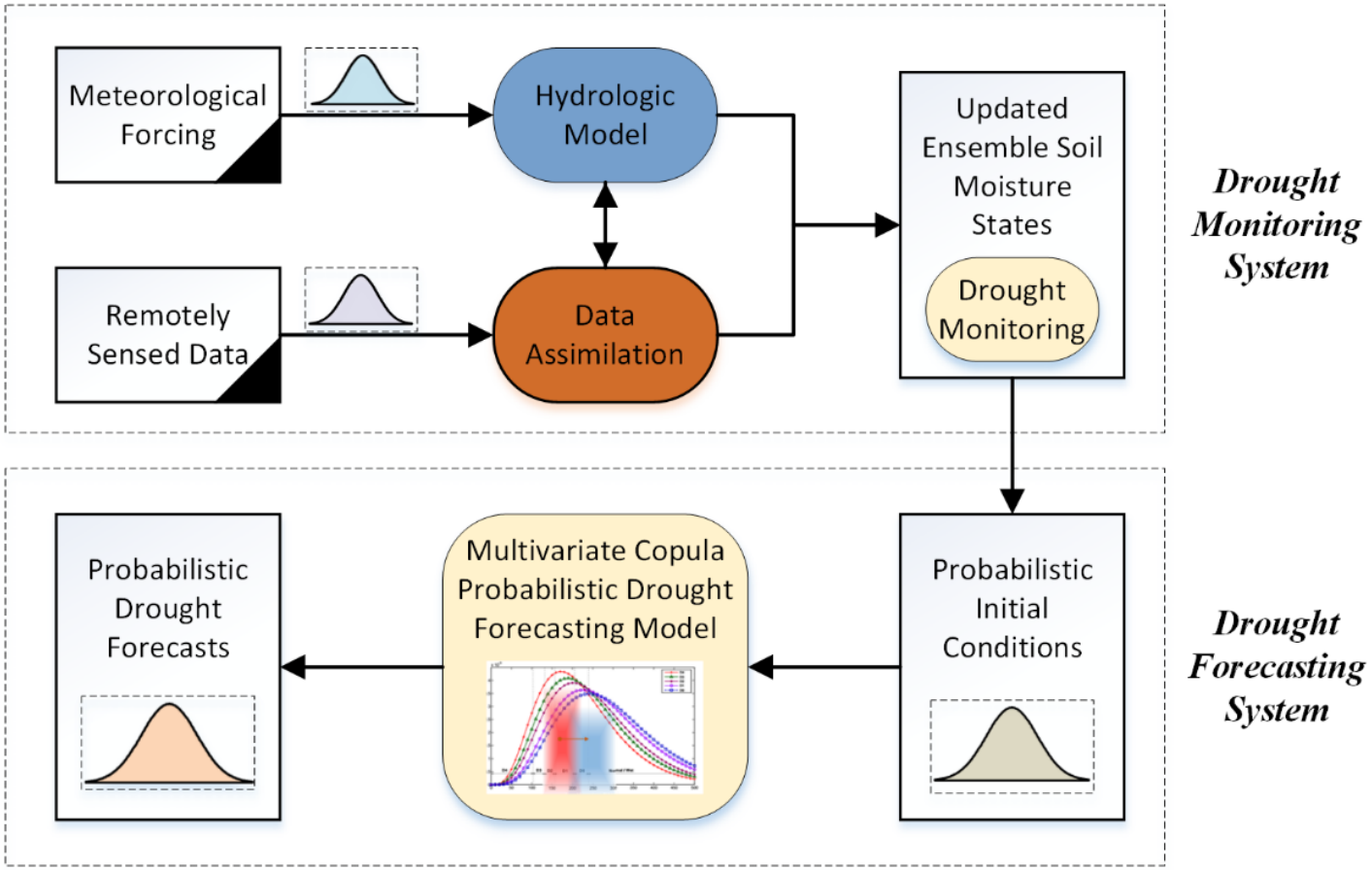

Figure 2-1. The framework of the proposed drought monitoring and forecasting systems.

2.1 VIC Model

The Variable Infiltration Capacity (VIC) model is a physically based and semi-distributed macroscale hydrologic model. As such, it shares several basic features with other LSMs that are usually coupled with global circulation models (GCMs). The VIC model was developed by Liang et al. (1994) and later improved by Lohmann et al. (1998), and Liang and Xie (2001). The VIC model includes both water-balance and energy-balance parameterizations and two types of runoff-yielding mechanisms.

The land surface is modeled as a grid of large, flat, and uniform cells. The VIC model balances both surface energy and water over each grid cell. The VIC model represents sub-grid variability in soils, topography, and vegetation. This allows for the representation of the non-linear dependence of the partitioning of precipitation into infiltration and direct runoff, which is determined by soil moisture in the upper soil layer and its spatial heterogeneity. The VIC model partitions the vadose zone into three soil layers. The first soil layer has a fixed depth of 10 cm, and responds quickly to changes in surface conditions and precipitation. The second and third soil layer depths are spatially varied, which is the same as in the Land Data Assimilation System (LDAS) retrospective simulations (Maurer et al., 2002). Moisture movement between the three soil layers is governed by gravity drainage, with diffusion from the second to the first layer allowed in unsaturated conditions. Water drained from the second layer to the third layer is entirely controlled by gravity. Base flow is a non-linear function of the soil moisture content of the third layer (Shukla et al., 2011).

The minimum meteorological forcing data for VIC model are the time series of daily or sub-daily precipitation, maximum and minimum air temperature, and wind speed. In this dissertation, the root-zone soil moisture is estimated as the total column soil moisture (sum of the three soil layers). Figure 2-2 presents the spatial variability of root-zone soil depth (the combination of three soil layers) across the Contiguous United States.

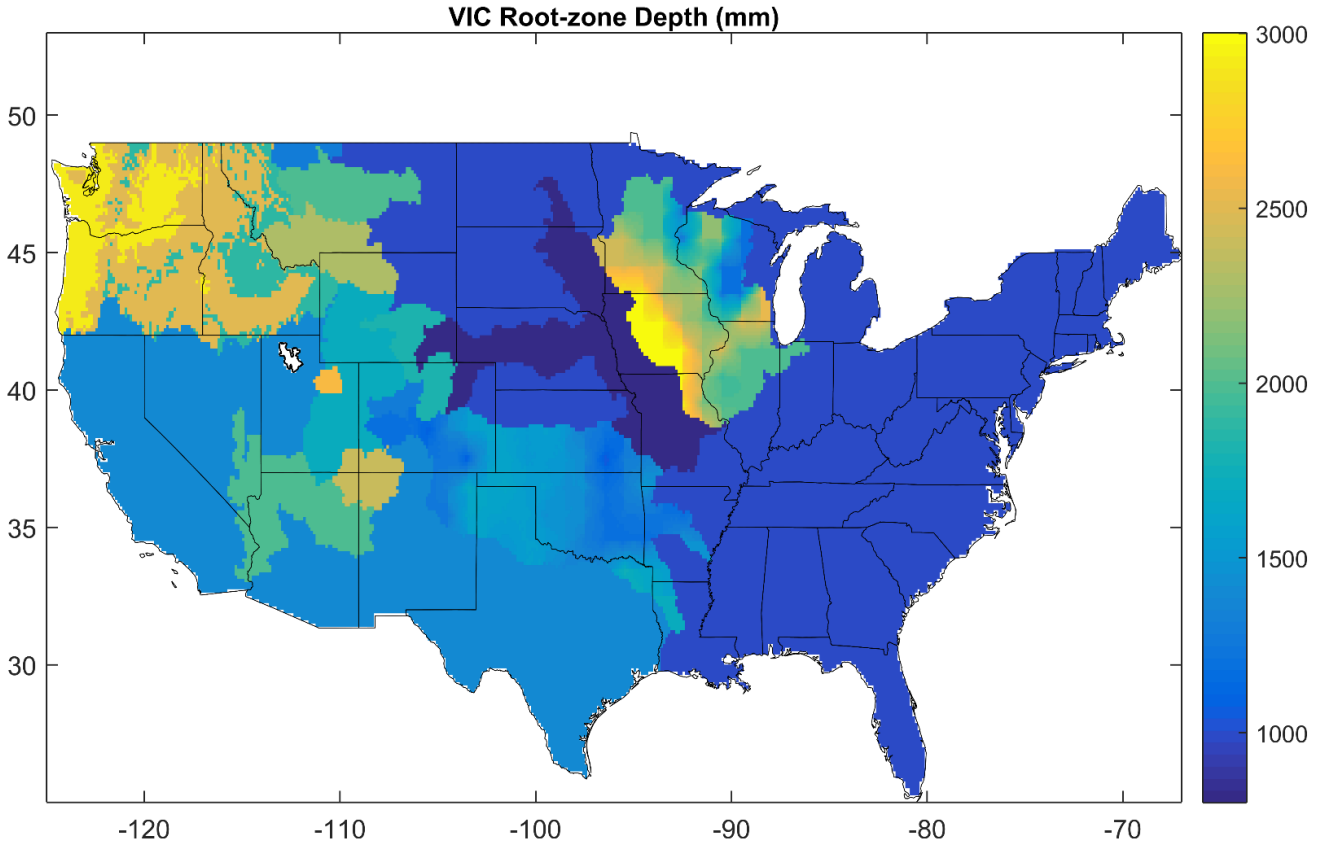

Figure 2-2. The VIC root-zone soil layer depth across the Contiguous United States.

2.2 PRMS Model

The Precipitation-Runoff Modeling System (PRMS) (Leavesley et al., 1983) is a modular deterministic, distributed-parameter, and physical-process watershed model (Markstrom et al., 2008). The land surface hydrologic process simulated by PRMS includes the evapotranspiration, runoff, infiltration, interflow, snowpack, and soil moisture.

Instead of delineating a watershed into uniform grid cells, the PRMS partitions a watershed into hydrologic response units (HRUs) that are based on the physical attributes of the watershed such as land-surface elevation, slope and aspect, vegetation type, soil type, and spatiotemporal climate patterns (Markstrom et al., 2015). The physical attributes and hydrologic response of each HRU are assumed to be homogeneous. The meteorological forcing data for PRMS are precipitation, and minimum and maximum temperature. Excess runoff is routed to the outlet through the cascade and Muskingum routing methods.

The PRMS version 4.0.1 (PRMS-IV) released on March 15, 2015 is used in this study. The PRMS-IV takes soil moisture into account in three reservoir systems: the preferential-flow reservoir, the capillary reservoir, and the gravity reservoir. The preferential-flow reservoir represents the water content between preferential-flow threshold and total soil saturation; it is available for fast interflow and Dunnian surface runoff. The capillary reservoir represents the moisture content between wilting point and field capacity; it is only available for evapotranspiration and not for drainage. The gravity reservoir is limited to the water content between field capacity and preferential-flow

threshold. The water content in this reservoir is available for slow interflow, groundwater recharge, and Dunnian surface runoff (Markstrom et al., 2015). In this dissertation, root-zone soil moisture is estimated as the total column soil moisture (sum of the three soil reservoirs).

2.3 Data Assimilation Algorithm

Currently the most commonly used DA method in the hydrologic community is the ensemble Kalman filter (EnKF) (Evensen, 1994; Kumar et al., 2016, 2014a; Reichle and Koster, 2004; Reichle et al., 2008). Although the EnKF is popular for hydrologic applications, many studies have shown that the Gaussian error assumption of the EnKF is often violated in hydrologic modeling, and suggest that the particle filter (PF) is a more robust technique (DeChant and Moradkhani, 2014a, 2012; Dong et al., 2015; Montzka et al., 2011; Moradkhani et al., 2012, 2005a; Plaza et al., 2012; Yan et al., 2015). Compared with the popular EnKF, the advantage of PF is that it relaxes the Gaussian assumption for error distributions, potentially characterizing multimodal or skewed distribution in state variables. Therefore, it can quantify a more complete representation of the posterior distribution for a non-linear non-Gaussian system. In addition, instead of updating the state variables as EnKF, the PF resamples the ensemble states and thus can maintain water balance. The PF ensemble DA is based on the sequential Bayesian theory and is described in the following paragraphs.

Following Moradkhani (2008), the state-space models that describe the generic earth system are as follows:

$$x_t = f(x_{t-1}, u_t, \theta) + w_t \quad (1)$$

$$y_t = h(x_t) + v_t \quad (2)$$

where $x_t \in \mathbb{R}^n$ is a vector of the uncertain state variables at current time step, $y_t \in \mathbb{R}^m$ is a vector of observation data, u_t is the uncertain forcing data, $\theta \in \mathbb{R}^d$ is the model parameters, $h(\cdot)$ is a non-linear function that relates the states x_t to the observations y_t,

w_t represents the model error, and v_t indicates the observation error. The errors w_t and v_t are assumed to be white noise with a mean of zero and covariance Q_t and R_t, respectively. The white noise implies that a model or observation error follows a Gaussian distribution with a mean of zero and a diagonal covariance matrix.

Under the assumption of independence in time series, the posterior distribution of the state variables x_t given a realization of the observations $y_{1:t}$ is as follows:

$$p(x_t|y_{1:t}) = p(x_t|y_{1:t-1}, y_t) = \frac{p(y_t|x_t)p(x_t|y_{1:t-1})}{p(y_t|y_{1:t-1})} = \frac{p(y_t|x_t)p(x_t|y_{1:t-1})}{\int p(y_t|x_t)p(x_t|y_{1:t-1})dx_t} \tag{3}$$

$$p(x_t|y_{1:t-1}) = \int p(x_t, x_{t-1}|y_{1:t-1})dx_{t-1} = \int p(x_t|x_{t-1})p(x_{t-1}|y_{1:t-1})dx_{t-1} \tag{4}$$

where $p(y_t|x_t)$ is the likelihood, $p(x_t|y_{1:t-1})$ is the prior distribution, and $p(y_t|y_{1:t-1})$ is the normalization factor. The marginal likelihood function $p(y_{1:t})$ can be computed as:

$$p(y_{1:t}) = p(y_1)\prod_{k=2}^{t} p(y_k|y_{1:k-1}) \tag{5}$$

where the normalization factor $p(y_t|y_{1:t-1})$ is:

$$p(y_t|y_{1:t-1}) = \int p(y_t, x_t|y_{1:t-1})dx_t = \int p(y_t|x_t)\, p(x_t|y_{1:t-1})dx_t \tag{6}$$

Equation (3) shows mathematically that a posterior conditional probability distribution of model predicted states x_t, given all previous observations $y_{1:t-1}$ and the current observation y_t can be computed sequentially in time. In practice, Equation (3) does not have an analytic solution except for a few special cases. Instead, the posterior

distribution $p(x_t|y_{1:t})$ is usually approximated using a set of Monte Carlo (MC) random samples as:

$$p(x_t|y_{1:t}) \approx \sum_{i=1}^{N} w_t^{i+} \delta(x_t - x_t^i) \tag{7}$$

where w_t^{i+} is the posterior weight of the i^{th} particle, δ is the Dirac delta function, and N is the ensemble size. The normalized weights are calculated as follows:

$$w_t^{i+} = w_t^{i-} \frac{p(y_t|x_t^i)}{\sum_{i=1}^{N} w_t^{i-} p(y_t|x_t^i)} \tag{8}$$

where w_t^{i-} is the prior particle weights, and $p(y_t|x_t^i)$ can be computed from the likelihood $L(y_t|x_t^i)$. Generally, a Gaussian distribution is used to estimate $L(y_t|x_t^i)$:

$$L(y_t|x_t^i) = \frac{1}{\sqrt{(2\pi)^m |R_t|}} exp\left[-\frac{1}{2}\left(y_t - h(x_t^i)\right)^T {R_t}^{-1}\left(y_t - h(x_t^i)\right)\right] \tag{9}$$

To obtain approximate samples from $p(x_t|y_{1:t})$, a resampling operation is necessary in order to address the weight degeneration issue (all but one of the importance weights are close to zero). Moradkhani et al. (2005a) suggests to resample the particles with a probability greater than the uniform probability. After resampling, all the particle weights are set equal to $1/N$.

To further reduce the weight degeneration problem in large-scale applications, the particle filter with a sampling importance resampling (PF-SIR) algorithm can be combined with a Markov chain Monte Carlo (MCMC) move (Moradkhani et al., 2012). The recently developed particle Markov chain Monte Carlo (PMCMC) (Andrieu et al., 2010) is used in this dissertation for large-scale DA drought applications. The PMCMC is

an extension of the PF-SIR and uses the PF-SIR to design efficient high-dimensional proposal distributions for the MCMC algorithm.

The PMCMC consists of the following three steps: 1) Initialization ($j = 0$): run PF-SIR targeting $p(x_t|y_{1:t})$, sample $X_t(0) \sim p(x_t|y_{1:t})$ and let $p(y_{1:t})(0)$ denote the corresponding marginal likelihood estimate. 2) Iteration ($j \geq 1$): sample $X_t^* \sim p(x_t|y_{1:t})$ again and let $p(y_{1:t})^*$ denote the corresponding marginal likelihood estimate. 3) Calculate the acceptance ratio as:

$$min\left\{1, \quad \frac{p(y_{1:t})^*}{p(y_{1:t})(j-1)}\right\} \tag{10}$$

and set $X_t(j) = X_t^*$ and $p(y_{1:t})(j) = p(y_{1:t})^*$; otherwise set $X_t(j) = X_t(j-1)$ and $p(y_{1:t})(j) = p(y_{1:t})(j-1)$.

2.4 Code Parallelization

Dynamical distributed hydrologic models (such as the VIC and RPMS models) are usually very computationally expensive and often need to be run on high-performance computing (HPC) clusters. Especially for simulations that are performed on a large-scale with a high spatial resolution, code parallelization is an essential requirement to reduce computational times. Fortunately, the natural parallelism in the ensemble DA algorithm can be used to implement parallel programming, since each ensemble state can be simulated independently from the others.

Generally, there are two parallelization strategies for ensemble DA algorithm: the model decomposition (Figure 2-3) and the domain decomposition (Figure 2-4). The model decomposition schema is to distribute the ensemble members of DA over all available processors. However, it would lead to a significant amount of data communication between different processors in each state updating step of DA. Therefore, the model decomposition schema is more suitable for small-scale DA applications using multi-processing strategy (i.e., OpenMP) in a single computer system with shared-memory. As an alternative, the domain decomposition implementation gains more popularity in the community due to the avoidance of the huge amount of data passing. The domain decomposition distributes the large scale study region over all available processors. As a result, each processor only updates the domain states that belong to its own, and other domain states can be updated concurrently. Currently, domain decomposition is the standard parallelization strategy in the large-scale dynamical models using Message Passing Interface (MPI) (Nerger and Hiller, 2013).

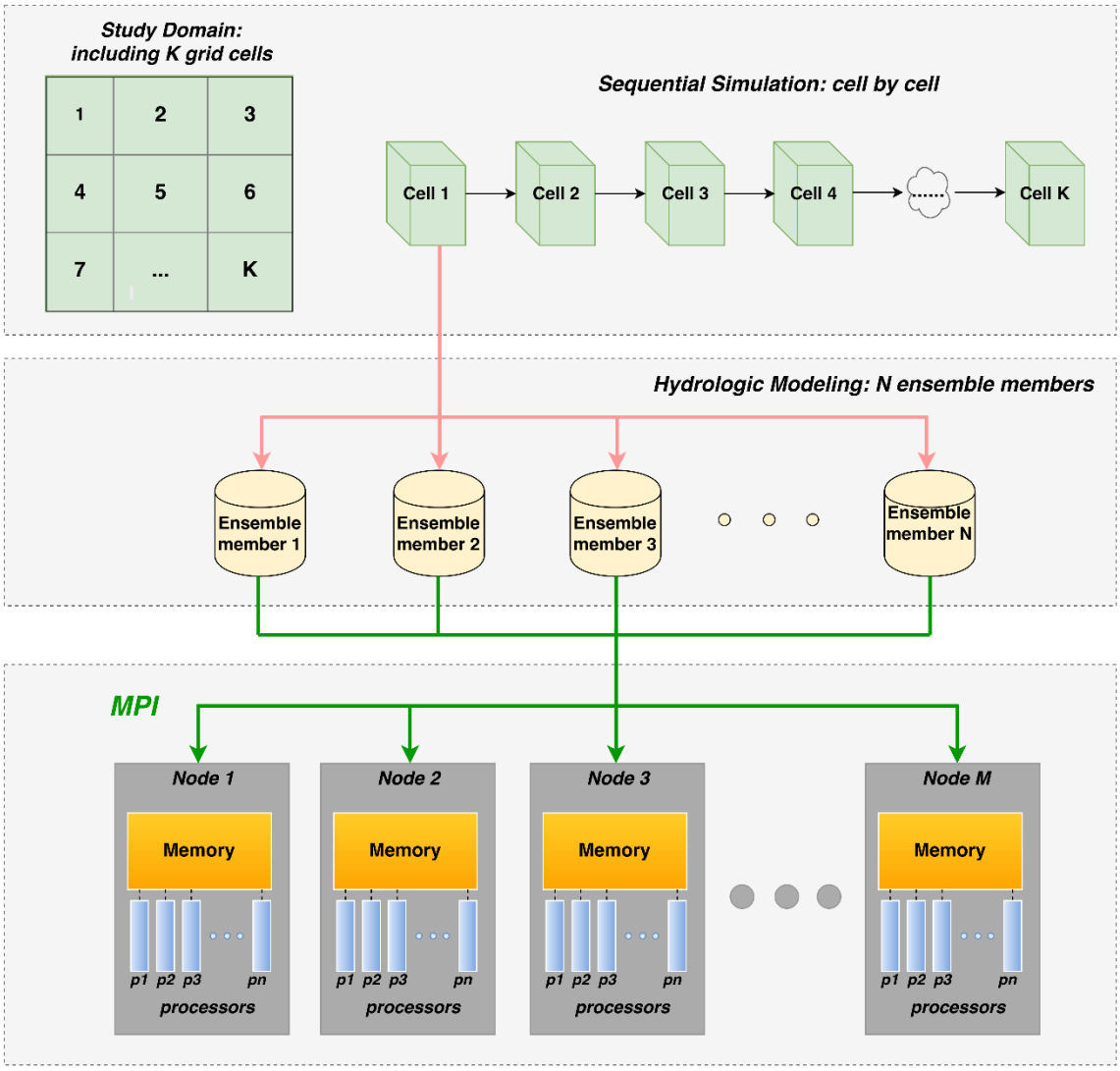

Figure 2-3. The schematic framework of the model decomposition parallelization strategy.

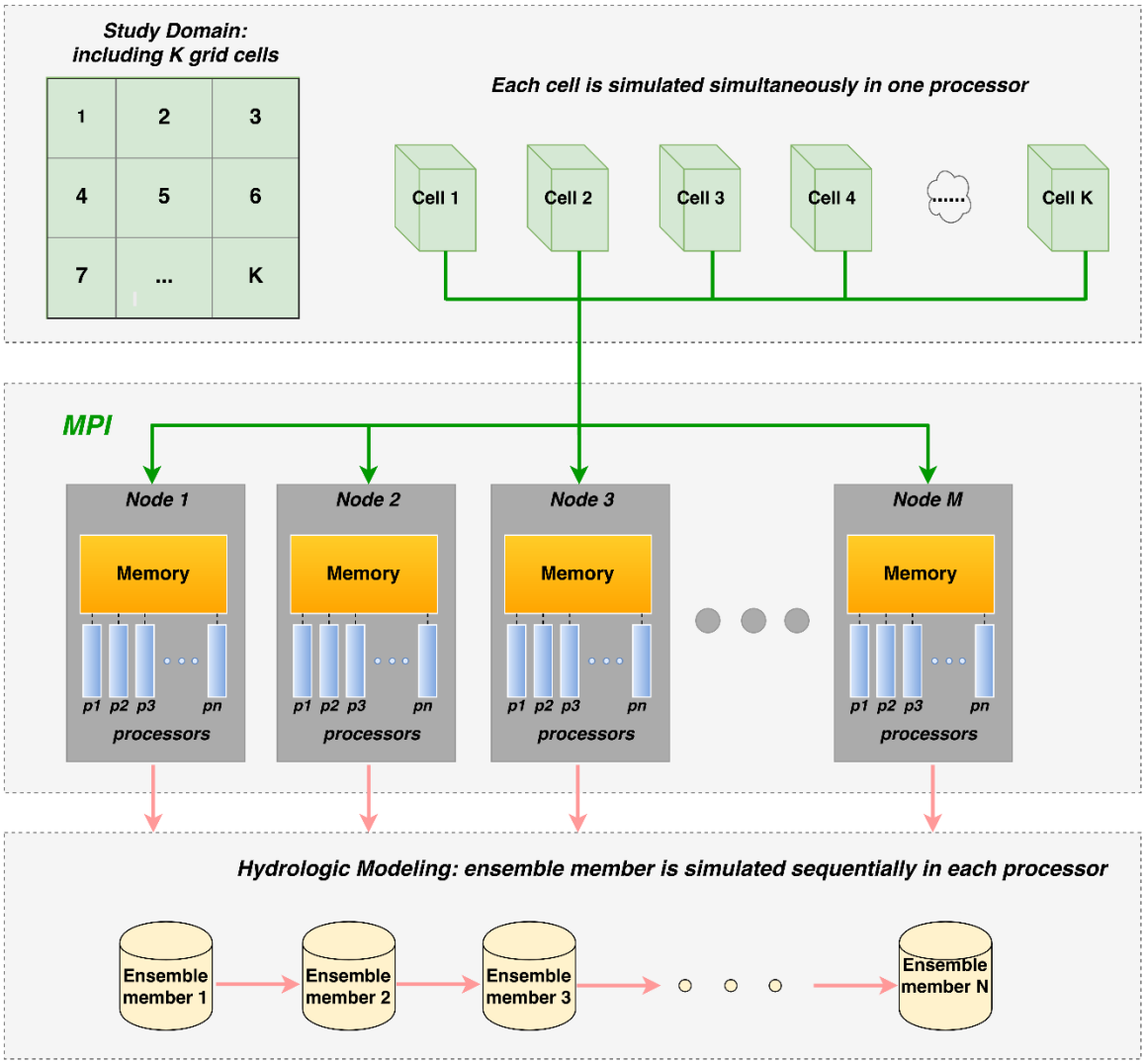

Figure 2-4. The schematic framework of the domain decomposition parallelization strategy.

Besides the two DA parallelization strategies, there are also two strategies to couple the hydrologic model and DA algorithm: online coupling and offline coupling (Kurtz et al., 2016). For online coupling implementation, the DA algorithm is a subroutine of the dynamical model routines and they are all compiled into a single program. Data is exchanged via the main memory. The main advantage of the online coupling is that it is computationally more efficient since the exchange of data using files can be avoided. In addition, the model only needs to execute the start-up phase once and there is no additional start-up cost. However, the online coupling schema requires modification to the model source code in order to be compatible with the DA subroutine. For offline coupling schema, there are two separate programs used for model execution and DA, respectively. Data is then exchanged via the input/output (I/O) files of the model. Obviously, the offline coupling is more ad hoc since there is no need to modify the model source code. In addition, the offline coupling is the only option when the source code of the model is not available or not open source. One limitation of the offline coupling is that it generates a large amount of files on the local drive, and it produces a lot of I/O overhead. One simple solution is to use the RAM disk to catch these I/O files.

In general, an ideal parallel DA framework should provide a generic DA environment that can be coupled with any hydrologic model. Therefore, the offline coupling schema and domain decomposition strategy is used in this study to provide a generic parallel DA framework for VIC model. Figure 2-5 describes the detailed PMCMC-VIC offline coupling interface in this study. Similar flowchart can be used for PMCMC-PRMS offline coupling too.

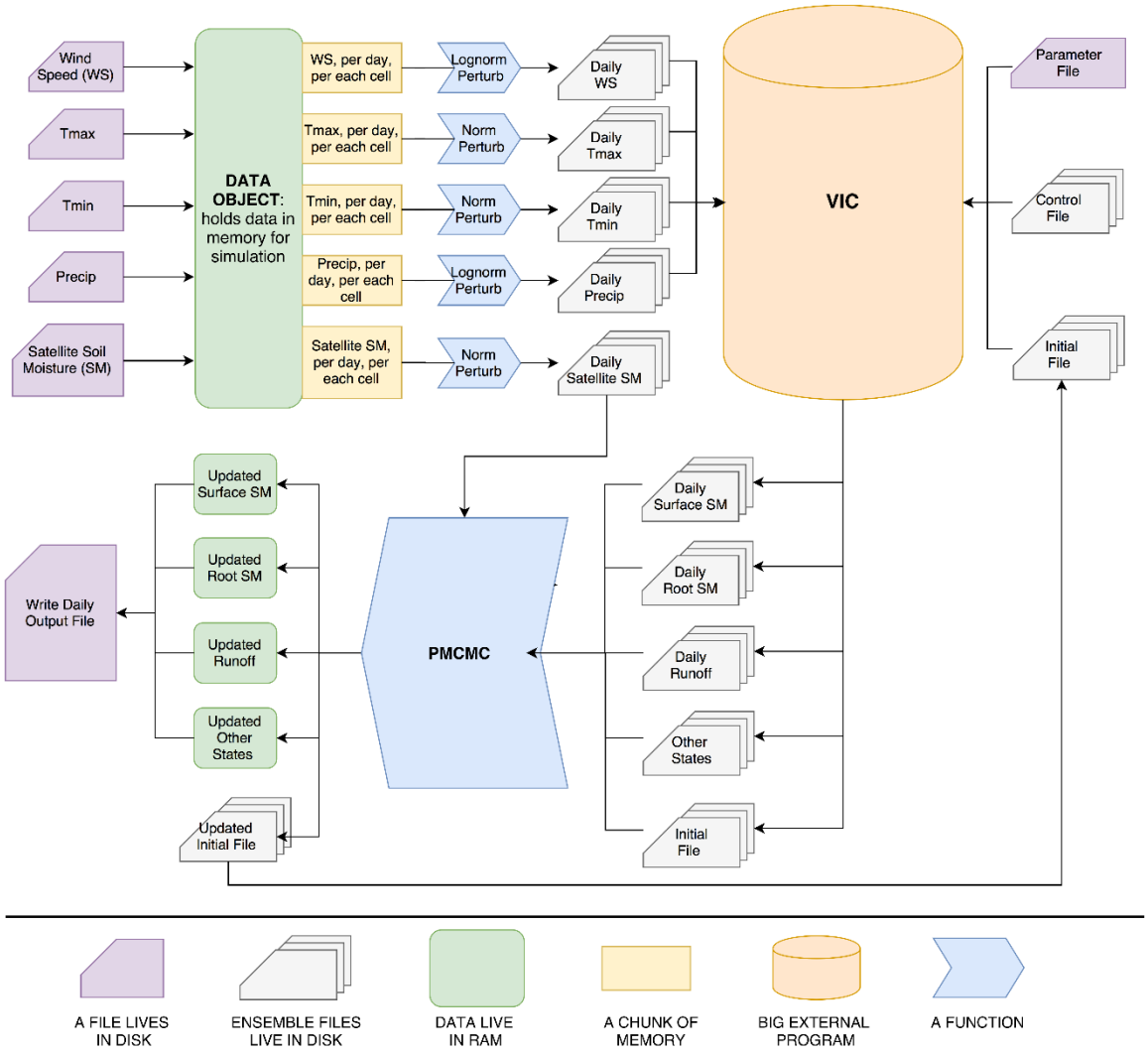

Figure 2-5. The particle filter-VIC offline coupling interface.

2.5 Probabilistic Multivariate Copula

A newly developed probabilistic drought forecasting method based on copula functions is used here which is coupled with the initial condition uncertainty through DA (Madadgar and Moradkhani, 2014a, 2013a). The core of this forecast model is to apply a multivariate distribution function to forecast future drought conditions given the current drought status.

Following Sklar (1959), the joint cumulative distribution function (CDF) of two temporal continuous state variables (i.e., soil moisture) $P(x_t, x_{t+1})$ could be written as:

$$P(x_t, x_{t+1}) = C[P(x_t), P(x_{t+1})] = C[u_t, u_{t+1}] \tag{11}$$

where C is the CDF of the copula and $P(x)$ is the marginal CDF of x denoted by u. Then the PDF of the copula is:

$$c[u_t, u_{t+1}] = \frac{\partial^2 C[u_t, u_{t+1}]}{\partial u_t \partial u_{t+1}} \tag{12}$$

and the joint PDF of $p(x_t, x_{t+1})$ is calculated as:

$$p(x_t, x_{t+1}) = c[u_t, u_{t+1}]p(x_t)p(x_{t+1}) \tag{13}$$

the conditional PDF of x_{t+1} given x_t is:

$$p(x_{t+1}|x_t) = \frac{p(x_t, x_{t+1})}{p(x_t)} = c[u_t, u_{t+1}]p(x_{t+1}) \tag{14}$$

Using Equation (14), the probabilistic forecast of drought states in time $t+1$ given the drought condition at time t can be examined. The mode of the $p(x_{t+1}|x_t)$ is correspondent to the maximum likelihood estimation (MLE) of x_{t+1}.

Figure 2-6 illustrates how the copula drought forecasting model works using a seasonal drought forecasting example. In this example, the future drought condition in

spring is forecasted using the drought statuses in the past winter. In Figure 2-6, the five distributions of drought condition in spring conditional on the drought statuses in winter have been developed. Each curve represents the PDF associated with a particular drought status in winter (D0-D4). More red color means that more severe drought happened in winter. For instances, if a D4 drought occurred in winter, the MLE drought statuses in the coming spring is a D1 drought; while if a D0 drought occurred in winter, it is most likely to have a normal condition in spring.

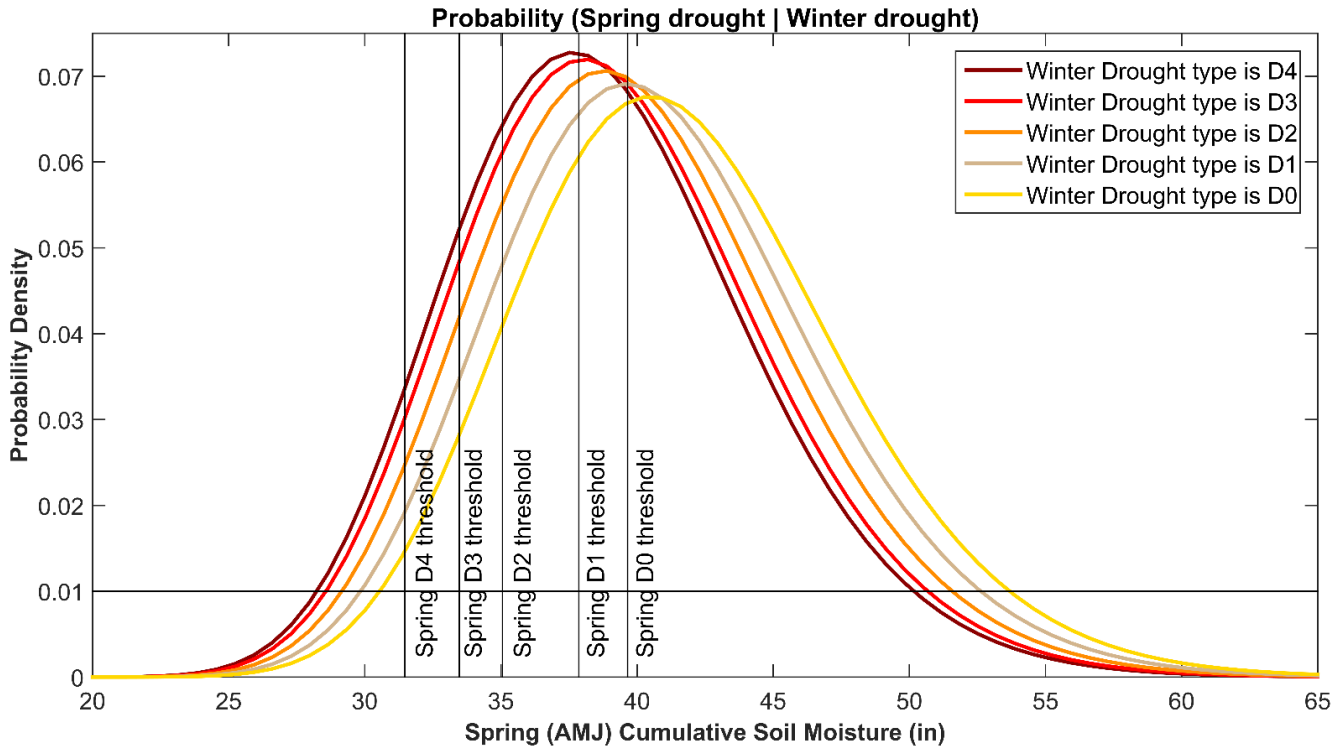

Figure 2-6. The conditional distributions of spring drought given winter drought status.

2.6 Monthly to Seasonal Forecasting Framework

Figure 2-7 describes the proposed monthly to seasonal drought forecasting framework. Based on Figure 2-7, the drought forecasting framework composes of three components: monthly (short-term), bimonthly (middle-term), and seasonal forecasts (long-term). The "stars" indicate the sampled initial conditions through the PDF of the initial conditions. The "arrow" directs the corresponding PDF of drought forecast. The drought forecast can be generated from whether one sampled initial condition (i.e., posterior mean) or multiple sampled initial conditions as shown in Figure 2-7. If multiple initial conditions are used to generate drought forecasts, the final forecast can be the average of each drought forecast, as the "thick line" shown in the figure.

The probabilistic drought conditions in each monthly/bimonthly/seasonal are forecasted using the drought status in the previous month/bimonth/season. The drought forecast initializes on the first day of each month (i.e., 1 January and 2 February), and provides three forecasting products for decision-makers and water resources managers. The monthly forecasting products can provide drought information for the following month, and can be used for irrigation, reservoir operations, and water supply plans. The bimonthly and seasonal forecasting products offer the seasonal drought information sooner (up to three-month preparation time), and can be used for drought risk assessment and drought preparation.

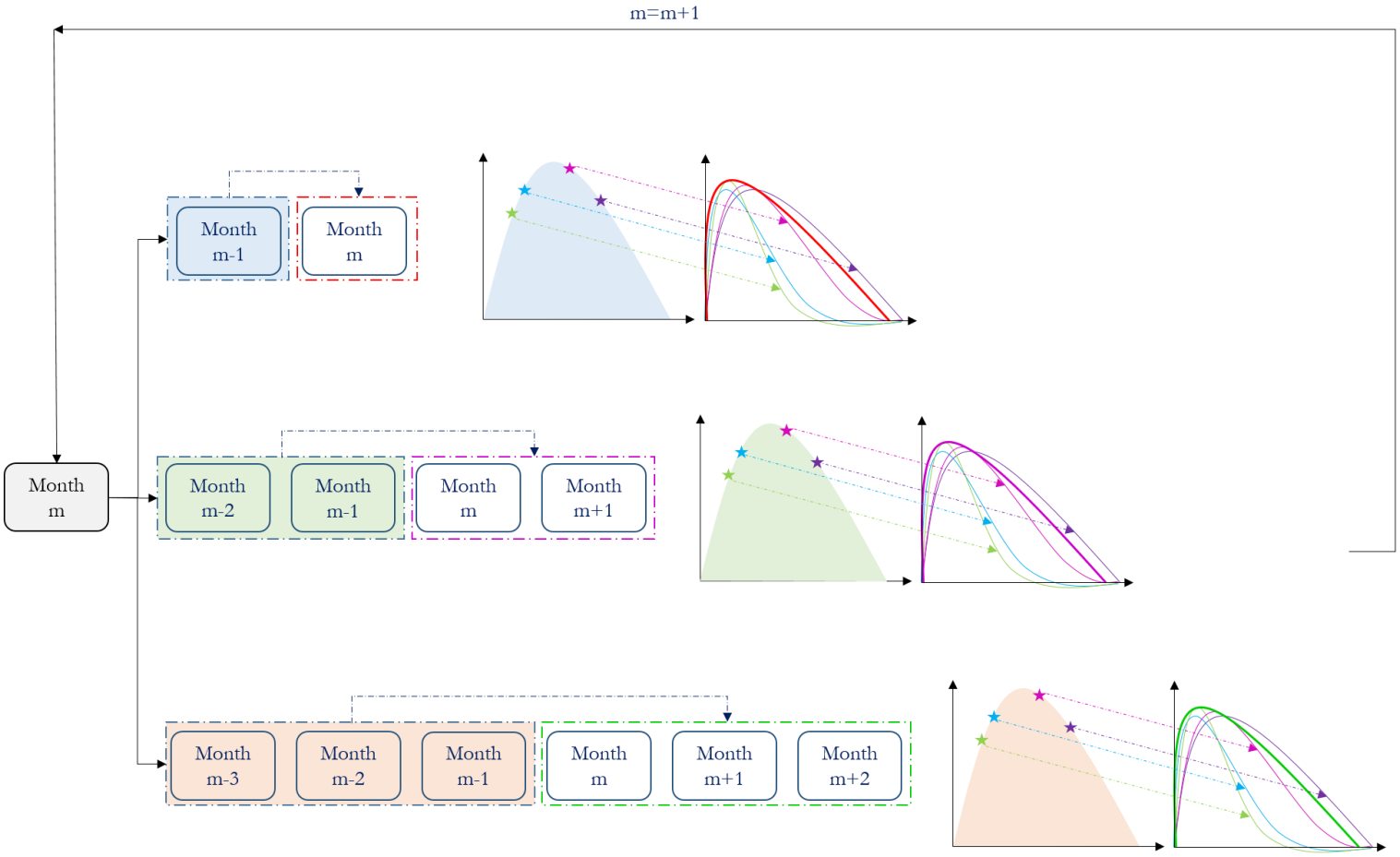

Figure 2-7. The monthly to seasonal drought forecasting framework using the multivariate copula model.

Chapter 3 Study Area and Data Sources

3.1 Case Study 1: Study Area and Drought Event

The first case study area of this dissertation is the regional scale analysis. The Columbia River Basin (CRB), located in the Pacific Northwest (PNW), covers about 674,500 km^2 of U.S. (~85%) and Canada (~15%). In the U.S., the CRB spans seven states, including Washington, Oregon, Idaho, Montana, Utah, Wyoming, and Nevada (Figure 3-1). The CRB encompasses a wide range of physiographic provinces and ecoregions ranging from semiarid in central plateaus to wet forests in the Cascade Mountains (Omernik and Bailey, 1997). The mean annual precipitation ranges from about 200 mm in the central plateaus to about 3,550 mm in the Cascade Mountains. The Columbia River is the 4th largest river in North America, originating in the Rocky Mountain and flowing to the Pacific Ocean, with a mean annual discharge of 247 million cubic meters. More than 450 dams have been built on this river system to provide hydroelectricity, flood control, irrigation, and stream regulation. The Columbia River is dominated by snow hydrology: snow accumulating in winter and melting in spring. It generally shows a characteristic of low flow in winter and peak flow in spring (Hamlet and Lettenmaier, 1999).

Recently, the CRB droughts have received increasing attention due to the low snowpack and rising temperature. Two drought events are studied in this dissertation. 1) In spring 2013, drought declarations were issued for nine counties in the southern Idaho. Three months later, a total of 19 counties in Idaho issued drought emergence. 2) In winter 2015, the PNW received historically low snowpack conditions. In June 2015, the

Washington State Governor Jay Inslee declared the statewide drought and Oregon State Governor Kate Brown declared drought emergencies for 19 out of 36 Oregon counties (about 80% of the state's landmass). The Washington Department of Agriculture (2015) calculated that the economic loss of the 2015 state drought was more than $335 million.

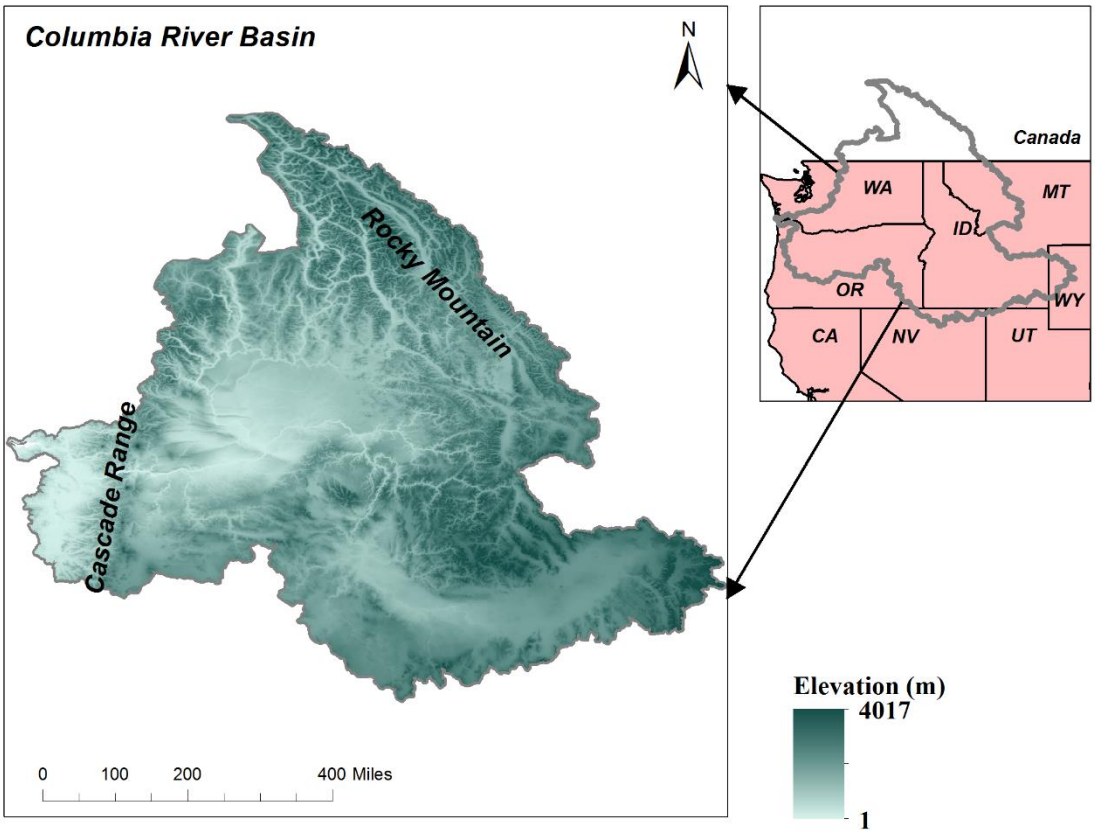

Figure 3-1. The location of the Columbia River Basin.

3.2 Case Study 2: Study Area and Drought Event

The second case study area of this dissertation is the continental scale analysis. The Contiguous United States (CONUS) (25˚–53˚N, 125˚–67˚W) consists of the 48 states on the continent of North America and occupies an area of about 3,119,884.69 square miles, which is equal to about 1.6% of the total surface area of Earth. The greatest distance in CONUS domain is about 2,802 miles between the Florida and Washington states. The state-wide averages of annual precipitation range from a high of 60.1 inches in Louisiana to a low of 9.5 inches in Nevada. The annual average amount of precipitation over CONUS domain is about 30.2 inches. The CONUS domain is divided into 13 river basin oriented regions (Figure 3-2). They are: 1) Northwest and Columbia (CRB); 2) California (CALI); 3) Great Basin (GRB); 4) Colorado River (COLOR); 5) Rio Grande (RIO); 6) Missouri River (MO); 7) Arkansas-Red (ARK); 8) South Central (GULF); 9) Great Lakes Drainage (GLAKES); 10) Upper Mississippi (UP); 11) Lower Mississippi (LOW); 12) Ohio (OHIO); and 13) East Coast (EAST).

The 2012 summertime (May-August) drought over Central U.S. is selected as the case drought event in this dissertation. The 2012 drought event developed rapidly in May and reached peak intensity in August. The two main causes for this drought event were the precipitation deficits and high temperatures. The rainfall season for Central U.S. occurs mostly during May-August, however, in 2012 the rainfall failed. The combination of substantial precipitation deficits and high temperatures caused the soil moisture to decrease rapidly, and the drought type propagated from meteorological drought to agricultural drought quickly. According to the USDM, during May-August, over three-

quarters of CONUS experienced at least D0 drought conditions and the Central U.S. experienced D2-D4 drought conditions.

This drought event attracts attention due to two reasons. First, it was the most severe seasonal drought in 117 years. It caused significant economic loss, and heavily impacted food security and commodity prices (PaiMazumder and Done, 2016). Second, the current drought forecasting systems failed to capture this drought event (Hoerling et al., 2014; Mo and Lettenmaier, 2015).

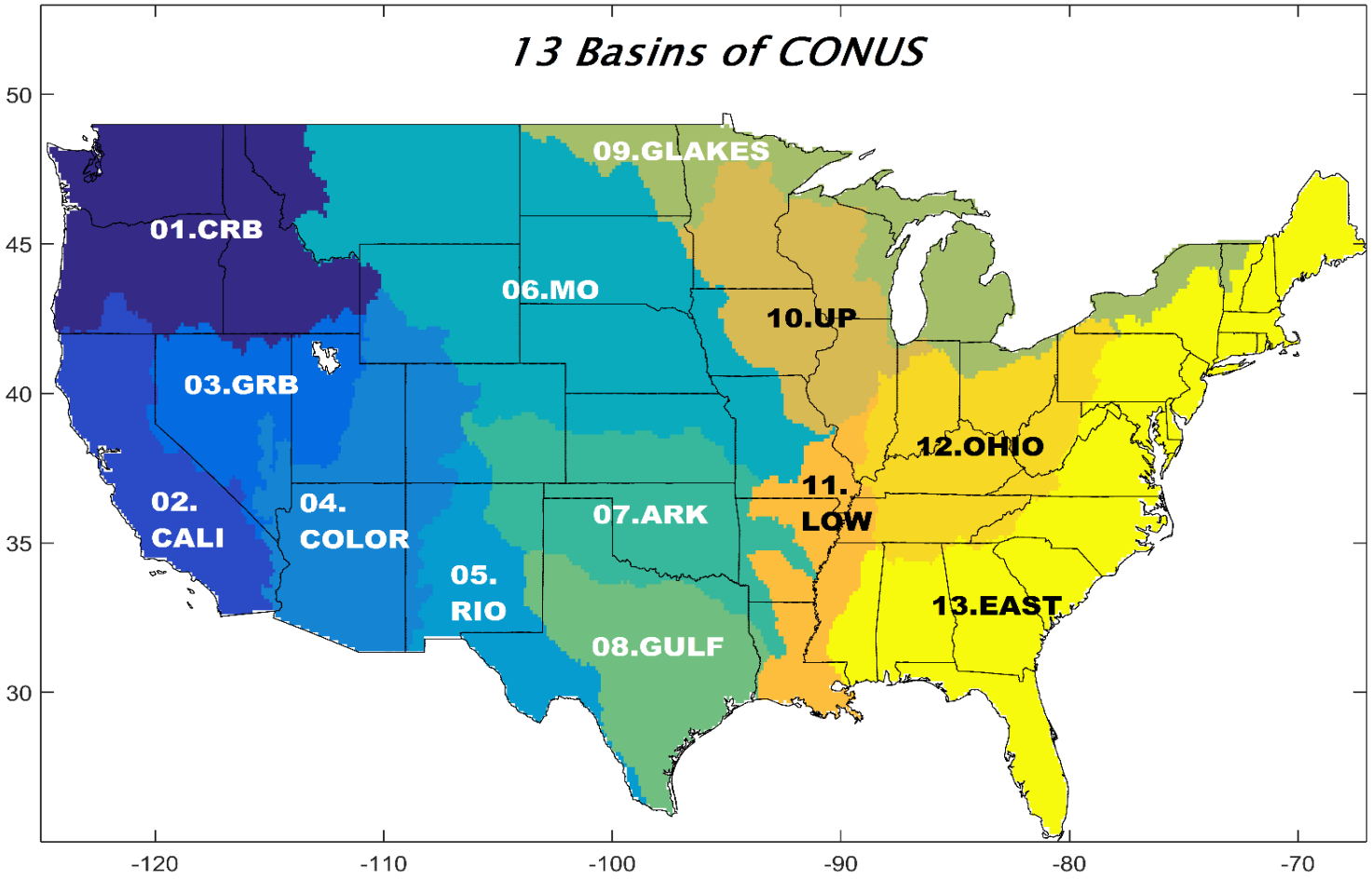

Figure 3-2. The CONUS domain and the 13 basins.

3.3 Meteorological Forcing Data

The precipitation, maximum and minimum temperature, and wind speed data (January 1, 1979 to present) are acquired from the Phase 2 of the North American Land Data Assimilation System (NLDAS-2) (Xia et al., 2014). The NLDAS-2 is originally from the first phase of NLDAS (NLDAS-1) project, which is initiated to generate reliable initial land surface states to coupled atmosphere-land models to improve weather predictions. The NLDAS is an interdisciplinary project with participants from the NOAA National Centers for Environmental Prediction (NCEP), the NOAA NWS Office of Hydrologic Development (OHD), the NOAA Environmental Satellite, Data, and Information Service (NESDIS), the NOAA Climate Prediction Center (CPC), the National Aeronautics and Space Administration (NASA) Goddard Space Flight Center (GSFC), and several universities including the University of Washington, the University of Maryland, the Princeton University, and Rutgers University.

The majority of NLDAS atmospheric forcing data is derived from the North American Regional Reanalysis (NARR) which features a 32-km spatial resolution and a 3-hour temporal resolution. Besides the precipitation, temperature, and wind speed, the NARR forcing data also include the specific humidity, surface pressure, incoming solar radiation, and incoming longwave radiation. The NLDAS software is used to interpolate the coarse-resolution NARR data to the finer-scale 1/8° NLDAS grid, and to the one-hour NLDAS temporal resolution (Xia et al., 2012). In this dissertation, the hourly NLDAS-2 primary forcing data are aggregated into daily time step for DA applications. Figure 3-3 shows an example of the daily 1/8° NLDAS-2 metrological forcing data (precipitation,

minimum and maximum temperature, and wind speed) over CONUS domain for December 31, 2015.

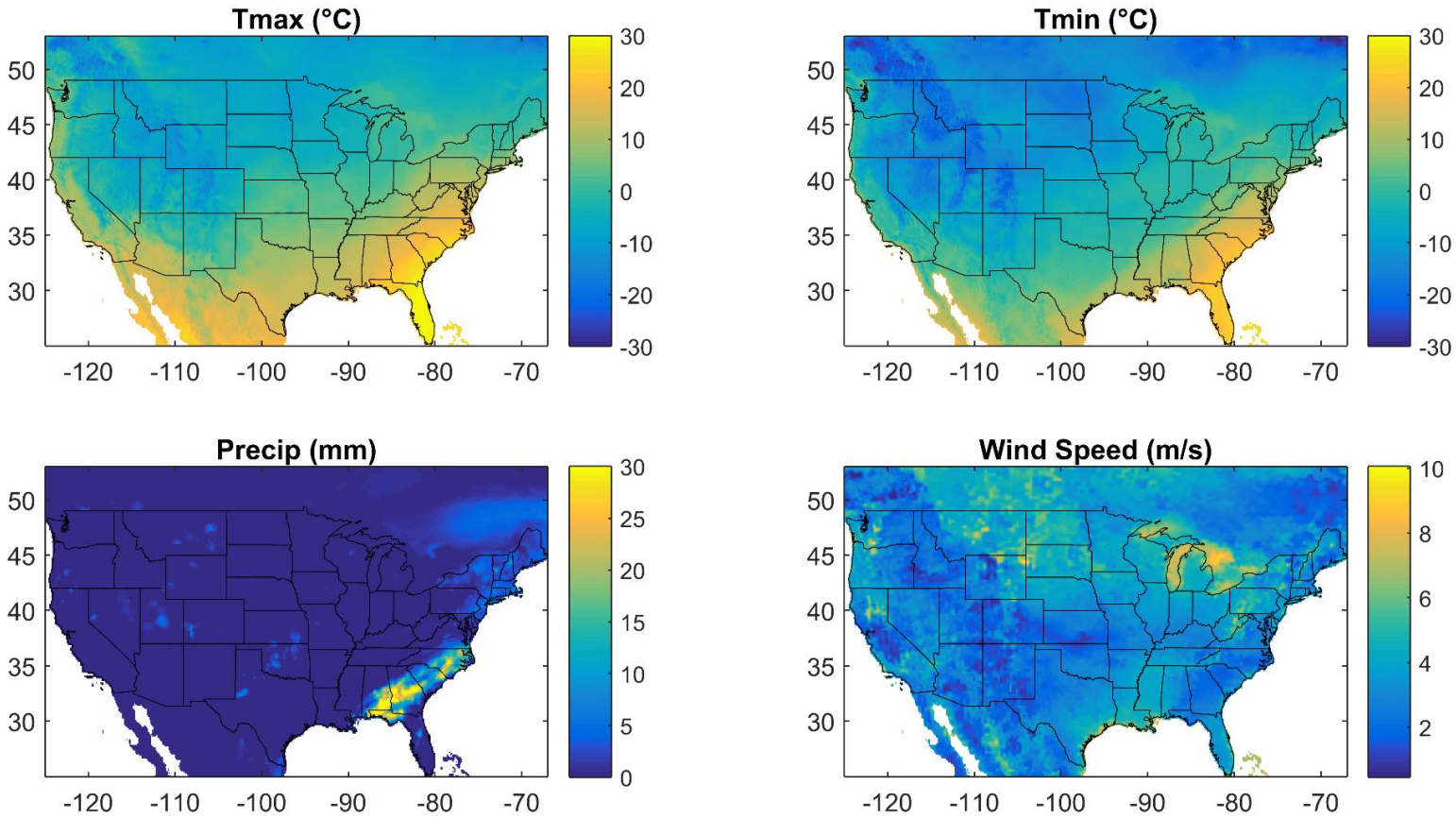

Figure 3-3. The daily 1/8° NLDAS-2 meteorological forcing data for December 31, 2015.

3.4 Remotely Sensed Surface Soil Moisture

The blended microwave soil moisture climate change initiative (CCI) products v02.2, which were released on February 2016 and the Advanced Microwave Scanning Radiometer2 (AMSR2) soil moisture products are used in this dissertation (Imaoka et al., 2010; Y. Y. Liu et al., 2012, 2011). The CCI soil moisture are merged from four passive and two active microwave products, including the Scanning Multichannel Microwave Radiometer (SMMR), Special Sensor Microwave Imager (SSM/I), Tropical Rainfall Measure Mission (TRMM) Microwave Imager (TMI), Advanced Microwave Scanning Radiometer for Earth Observing System (AMSR-E), Advanced Microwave Instrument (AMI), and Advanced Scatterometer (ASCAT). The AMSR2 is onboard the Global Change Observation Mission1-Water (GCOM-W1) satellite, which was launched in May 2012 by the Japan Aerospace Exploration Agency (JAXA).

According to Y.Y. Liu et al. (2012), the CCI merged soil moisture products are obtained by rescaling the active and passive retrievals into a common Noah simulated soil moisture climatology in the Global Land Data Assimilation System version 1 dataset (GLDAS-1-Noah) with the use of cumulative distribution function (CDF) matching approach (Madadgar et al., 2014; Reichle and Koster, 2004). This methodology consists of three steps: 1) merging the four passive products into one dataset from 1978 to 2014; 2) merging the two active products into one dataset from 1991 to 2014; 3) blending both merged products into one final dataset from 1978 to 2014. In the final blended soil moisture, passive and active merged products are used for sparsely and moderately vegetated regions, separately. The average of both products is taken for transition areas

where passive and active show similar performances. In this way, the blended soil moisture can take both the advantages of active and passive microwave sensors, as active products have higher accuracy over moderately vegetated regions while passive produces show better performance over sparsely vegetated regions (Albergel et al., 2009; Wagner et al., 2013, 2007).

The AMSR2 soil moisture products, generated by using the Land Parameter Retrieval Model (LPRM) developed by Vrije Universiteit Amsterdam and NASA Goddard Space Flight Center (GSFC) (Owe et al., 2008), are also employed in this dissertation to study the drought event in 2015. Both the CCI and AMSR2 products have a spatial resolution of 0.25° and a daily time step. Quality flags of both soil moisture is used to mask pixels affected by snow cover, temperatures below 0 °C, dense vegetation, and pixels where the soil moisture retrieval failed (Dorigo et al., 2015).

It is noted that the CCI and AMSR2 soil moisture products are selected in this study due to the data availability, since this dissertation focuses on the drought events in 2012 (case study 2), 2013, and 2015 (case study 1). In addition, the blended CCI product can have a greater number of observations than any single sensor product (higher temporal resolution), which leads to a better performance of DA application (Montzka et al., 2011; Yan et al., 2015). The latest SMAP L-band soil moisture products issued from March 31, 2015 will be used for future operational drought monitoring and forecasting. Figures 3-4 shows an example of the daily 0.25° CCI surface soil moisture for December 31, 2014.

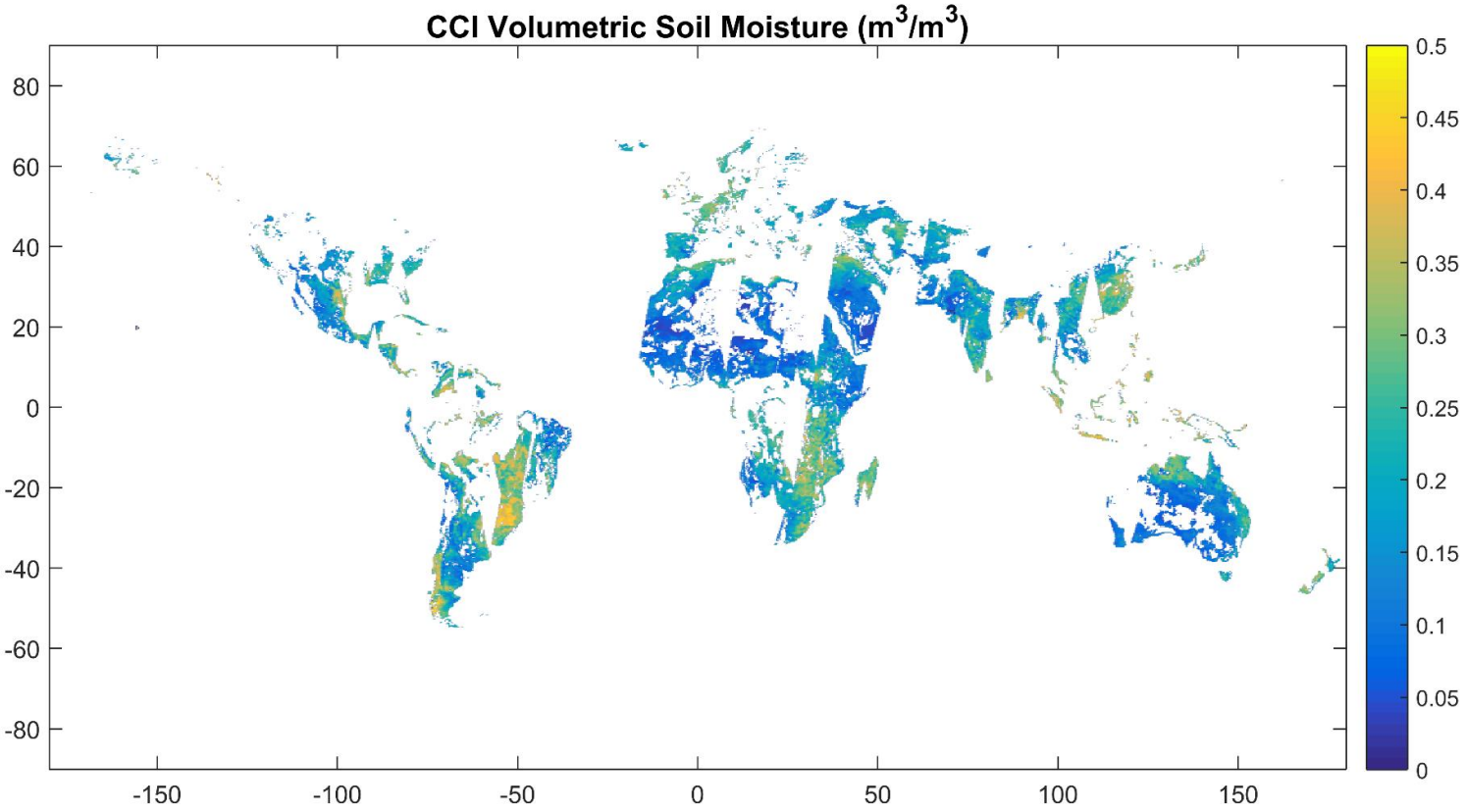

Figure 3-4. The daily 0.25° CCI soil moisture over global for December 31, 2014.

Chapter 4 Case Study 1: Synthetic Study

To objectively assess the potential benefit of assimilation of satellite surface soil moisture, a synthetic study is first conducted through a procedure called observing system simulation experiment (OSSE) or synthetic study (Moradkhani, 2008). The synthetic study includes the following four steps: 1) a "truth" run of the hydrologic model with the pre-calibrated model parameters; 2) simulated satellite surface soil moisture observations, which are generated from the truth run by incorporating the observation errors; 3) an open-loop (OL) run with the perturbed forcing data without DA; and 4) the DA step that assimilates the simulated surface soil moisture observations from step 2 to the model. Then the OL and DA results are compared against the truth simulation to evaluate the impact of satellite surface soil moisture assimilation.

It is noted that the definition of OL is slightly different in the synthetic study and real case study. In the synthetic study, the OL results are generated by running the model (after model calibration) using the perturbed forcing data without assimilation of satellite data. Therefore, OL is an ensemble run in the synthetic study. While in the real case study, the OL is defined as the model forward run (after model calibration) without assimilation of satellite data. In this time, the OL is a deterministic run since the perturbation of forcing data is not required. Figure 4-1 presents the flowchart of the synthetic study in this dissertation using the PRMS model.

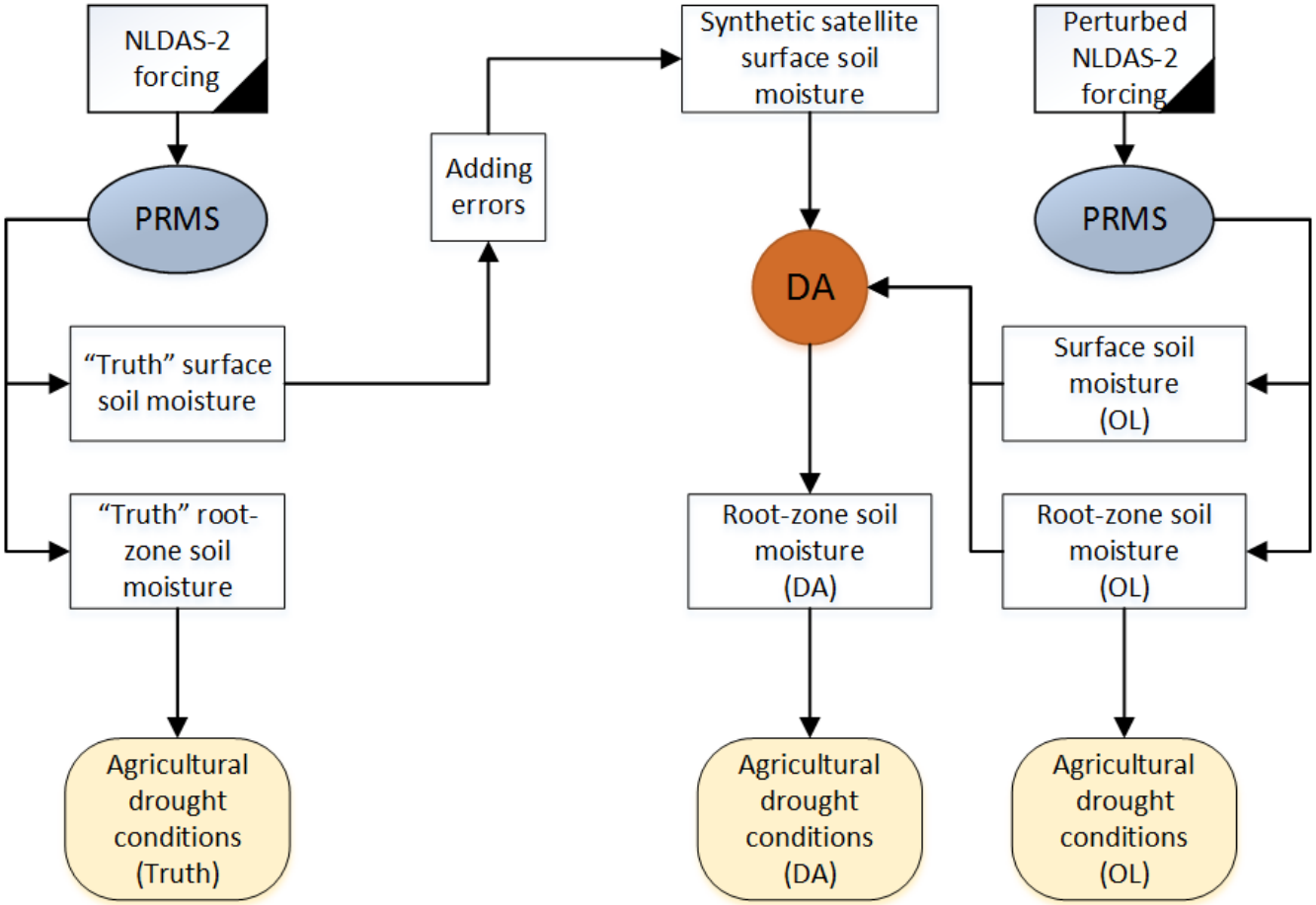

Figure 4-1. The flowchart of the synthetic study using PRMS model.

4.1 PRMS Model Calibration

Due to the CRB's significant extent into British Columbia, the HRU delineation is completed in two ways. The HRUs for the U.S. portion are provided by the PRMS Geospatial Fabric (Viger, 2014). For the area of the CRB inside British Columbia, the Environmental Systems Research Institute (ESRI) ArcMap 10.3.1 is used along with a digital elevation model to produce stream segment lines as well as watershed delineations. Due to a lack of data to calibrate the Canadian portion of the CRB, the HRUs are rather large, relative to the U.S. portion. The two spatial shapefiles (U.S. and Canadian) are then stitched together to ensure that there are no overlapping HRU areas, and to ensure the continuity between stream segments along the U.S. and Canadian border. As a result, a total of 7,739 HRUs and 4,019 stream segments are delineated for the CRB (Figure 4-2).

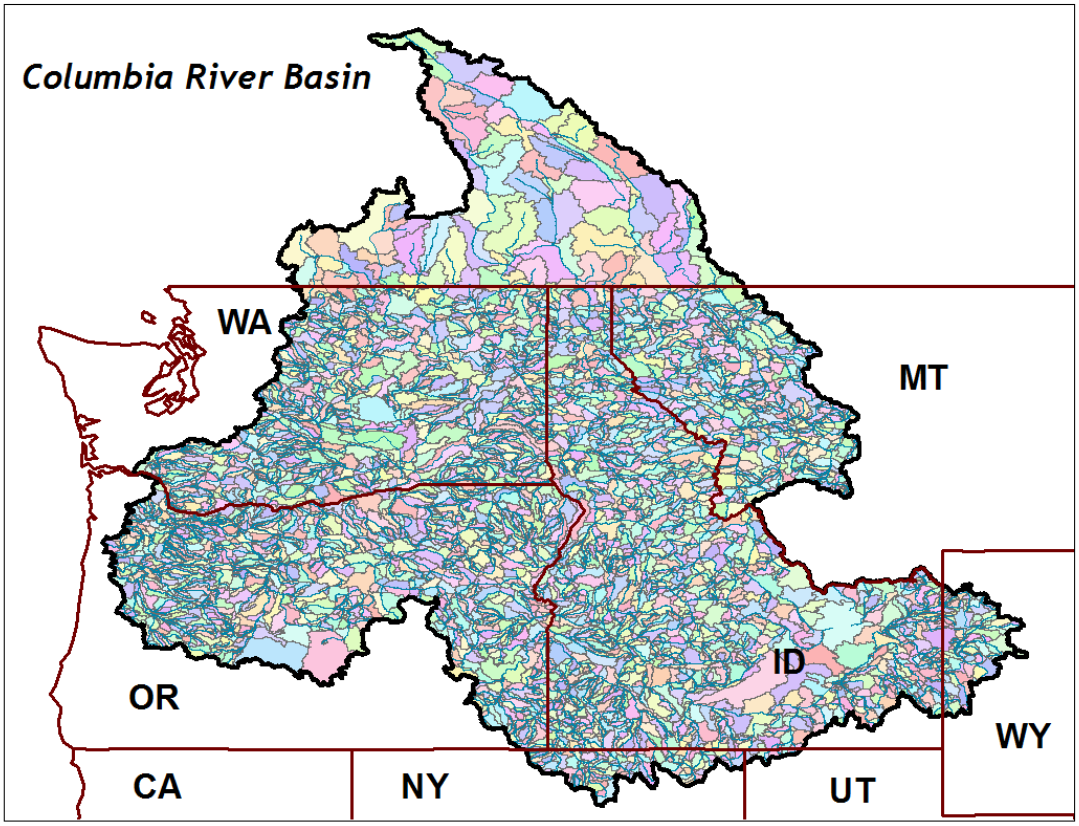

Figure 4-2. The location of the Columbia River Basin, the delineated 7,739 HRUs., and the delineated 4,019 stream segments.

Calibration of the PRMS is performed on a daily timescale utilizing a combination of unregulated U.S. Geological Survey (USGS) streamflow data, as well as No Regulation No Irrigation (NRNI) streamflow data provided by Bonneville Power Administration (BPA) (https://www.bpa.gov/power/streamflow/). The BPA-NRNI data cover daily streamflow from the period July 1, 1928 to September 30, 2008, and is generated in a joint effort between the U.S. Army Corps of Engineers (USACE) and the Bureau of Reclamation (BOR). The NRNI datasets emulate daily discharge gauges, typically at manmade control structures, where estimated and measured inputs and outputs can be summed to produce daily streamflow data.

In this study, 146 NRNI data sets are used as the primary control points for calibration along with over 300 selected USGS streamflow gauges. The NRNI data from January 1, 1979 to December 31, 2000 are used for calibration, and January 1, 2001 to September 30, 2008 for validation. Calibrations for USGS streamflow gauges vary in length due to lapsing streamflow gauge operation, however only data within the range of January 1, 1979 to December 31, 2010 are used for calibration/validation. Monthly averaged normal incident solar radiation atlas data (http://www.nrel.gov/gis/data_solar.html), and monthly averaged evaporation atlas (Farnsworth et al., 1982) are used for calibration of solar radiation (SR) and potential evapotranspiration (PET) parameters in the U.S. portion of the model. The SR and PET parameters for the Canadian portion of the CRB are extrapolated from the U.S. portion.

A combination of two programs created by the USGS is used in calibration, LUCA and LUMEN (Hay and Umemoto, 2006). LUMEN assists in model structure

during calibration so that the model can more easily be calibrated using a top-down approach. LUCA uses the Shuffled Complex Evolution (SCE) global search algorithm to calibrate the 31 model parameters (Duan et al., 1994). Figure 4-3 presents the Kling-Gupta efficiency (KGE) (Gupta et al., 2009) values for the 146 NRNI control points from January 1, 1984 to September 30, 2008. The majority of the gauges show the KGE values greater than 0.7, which indicates the good performance of the calibrated model.

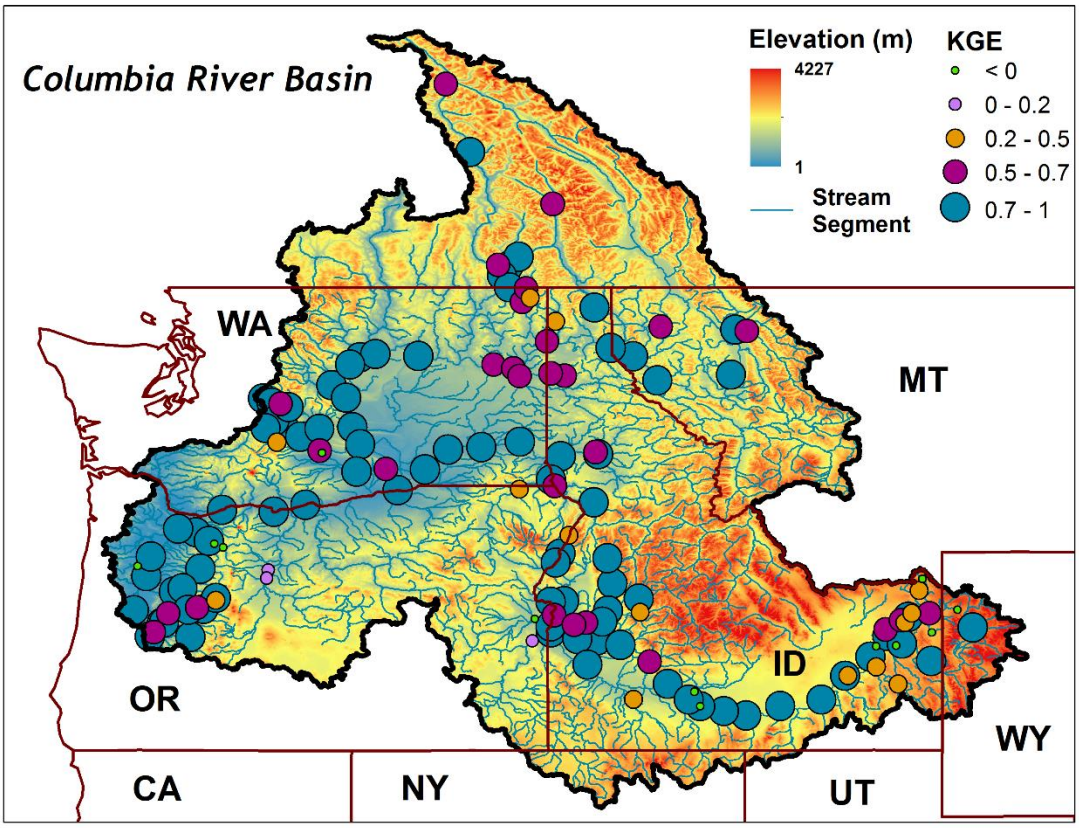

Figure 4-3. The location of the Columbia River Basin and the Kling-Gupta efficiency (KGE) values for the 146 No Regulation No Irrigation (NRNI) streamflow gauges.

4.2 Data Assimilation Implementation

The DA is performed by assimilation of the synthetic satellite surface soil moisture for the period of October 1, 2014 to September 30, 2015. This dissertation focuses on hindcasting the drought events in 2015 since the CRB received historically low snowpack in that year and drought emergences had been declared in Oregon and Washington states in spring 2015. Considering the satellite data availability, the CCI soil moisture products are used for DA in 2014, and AMSR2 retrievals are used for 2015. Contrary to the small ensemble size (12~20) used in the majority of previous satellite soil moisture DA studies (De Lannoy et al., 2012; Kumar et al., 2009; Pan and Wood, 2010; Reichle et al., 2010), a large ensemble size of 200 is used in this dissertation to fully quantify the soil moisture posteriors. For the purpose of better visualization, all PRMS simulation results are downscaled/upscaled into NLDAS $1/8^{th}$ degree grid cells. Results are presented only for the U.S. portion of CRB in this study. The PMCMC modular is written in Python script and all the simulations are run on the Linux Hydra Cluster (13 nodes, 208 processors) located at the Office of Information Technology (OIT), Portland State University (PSU).

In the DA implementation, the precipitation is perturbed with a lognormal distribution with a coefficient of variation of 0.25, and the minimum and maximum temperature are assumed to follow normal distribution with a coefficient of variation of 0.25. These values are suggested to account for errors in meteorological measurements due to spatial heterogeneity and sensor errors (Yan and Moradkhani, 2016a; Yan et al., 2015). The white noise (standard deviation) for the CCI and AMSR2 soil moisture are

0.04 and 0.08 m^3/m^3, respectively (Kumar et al., 2014b). Prior to DA, the CCI and AMSR2 satellite error standard deviations are scaled by the ratio of the soil moisture time series standard deviation of the PRMS model to that of the CCI and AMSR2 real data (separately for each HRU), as suggested by Reichle et al. (2007) and Q. Liu et al. (2011). After scaling, the synthetic satellite soil moisture observations are generated by perturbing the synthetic truths with a normal distribution with the scaled standard deviation.

In order to assess the DA performance on soil moisture prediction, the normalized information contribution (NIC) metric (Kumar et al., 2014a) is used in this dissertation. The NIC for root-mean-square-error (RMSE) is defined as follows:

$$NIC = \frac{RMSE_{OL} - RMSE_{DA}}{RMSE_{OL}} \tag{15}$$

where $RMSE_{OL}$ indicates the RMSE values between OL and synthetic truth, $RMSE_{DA}$ indicates the RMSE values between DA and synthetic truth. If NIC > 0, the DA improves the OL skill; if NIC = 0, the DA does not add any skill; if NIC < 0, the DA degrades the OL skill; and if NIC = 1, the DA achieves the maximum skill.

4.3 Drought Monitoring Results

Figure 4-4 presents the NIC values in the surface and root-zone soil moisture and their spatial distributions across the CRB. The majority of the grid cells show positive NIC values indicating the added-value of the DA. Generally, the improvements in the surface soil moisture field are consistent with the improvements in the root-zone soil moisture field. For surface soil moisture, the daily domain-averaged RMSE (m^3/m^3) for the OL is 0.021, and it decreases to 0.011with DA. Similarly, the daily domain-averaged root-zone soil moisture RMSE value decreases from 0.019 in the OL to 0.012 after DA. The improvements in surface field are higher than root-zone field, which is consistent with the previous soil moisture synthetic studies (Kumar et al., 2014a, 2009).

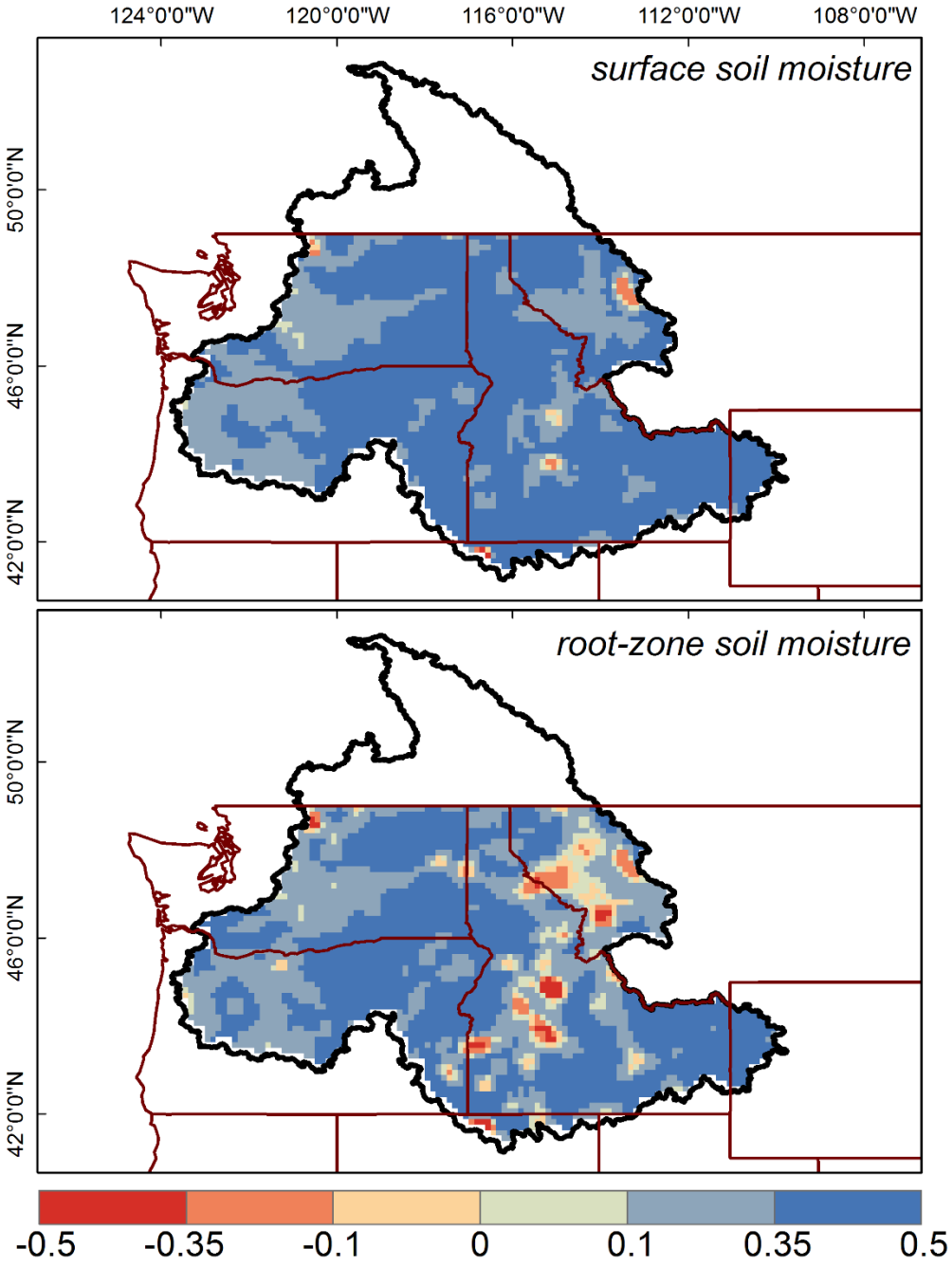

Figure 4-4. The normalized information contribution (NIC) value. The positive value indicates that the DA improves soil moisture prediction against OL; negative value indicates the degradation over the OL.

In Figure 4-4, it is also noted that several grid cells show negative NIC values. This may be caused by the inappropriate quantifications of the uncertainty in synthetic observations and model forecasts (Leisenring and Moradkhani, 2012, 2011). In the implementation of the DA, the identifications of model and observations errors are very unintuitive, and the experience estimates of forcing error may lead to over/under-confident soil moisture predictions (Y. Liu et al., 2012; Thiboult and Anctil, 2015). Properly quantifying the uncertainty in observations and forecast models is still the open question in the hydrologic DA community, and it is one of the major obstacles in operational hydrologic DA forecasting (Y. Liu et al., 2012). Especially for large-scale DA applications, it is not feasible to conclude on a single ideal manner to identify an optimal error implementation, and some degradation cells are always unavoidable (Kumar et al., 2014a).

In this study, drought is characterized with the soil moisture percentile and drought intensity is classified based on the National Drought Mitigation Center. Five categories are defined: D0 (abnormally dry, percentile $\leq$ 30%), D1 (moderate drought, percentile $\leq$ 20%), D2 (severe drought, percentile $\leq$ 10%), D3 (extreme drought, percentile $\leq$ 5%), and D4 (exceptional drought, percentile $\leq$ 2%). The root-zone soil moisture generated from the OL and DA seasonal integrations are compared against the corresponding synthetic truth percentiles. It is noted that the percentiles from the OL and DA in these comparisons are generated using the ensemble mean estimates. Figures 4-5 and 4-6 present the spatial distribution of drought intensities, and the drought extent bias (%) for five different drought (D0-D4) categories. The four seasons in the PNW (fall:

OND; winter: JFM; spring: AMJ; summer: JAS) are considered for the period of October 1, 2014 to September 30, 2015. The severe drought events in spring and summer of 2015 across the PNW can be seen in the synthetic truth. In all comparisons, the DA estimates show systematic improvements over the OL estimates. For fall 2014, the OL underestimates the intensity of drought across Washington and Idaho states whereas DA improves these representations. The drought extent bias (%) for D0-D4 between the OL and synthetic truth is 4.33%, and it decreases to 1.24% with DA. For winter and spring 2015, the OL underestimates the intensity of drought across PNW, and DA helps to reduce these large biases. Similarly, drought extent biases (%) decreases from 3.46% and 3.13% in the OL to 1.20% and 0.42% in the DA, respectively. Although the majority of grid cells in Washington and Oregon states show relatively high root-zone soil moisture values in summer 2015, the DA still helps reduce these biases. The drought extent bias (%) decreases from 20.13% to 13.71%. These results are consistent with the trends in Figure 4-4, which show the improvements obtained by data assimilation.

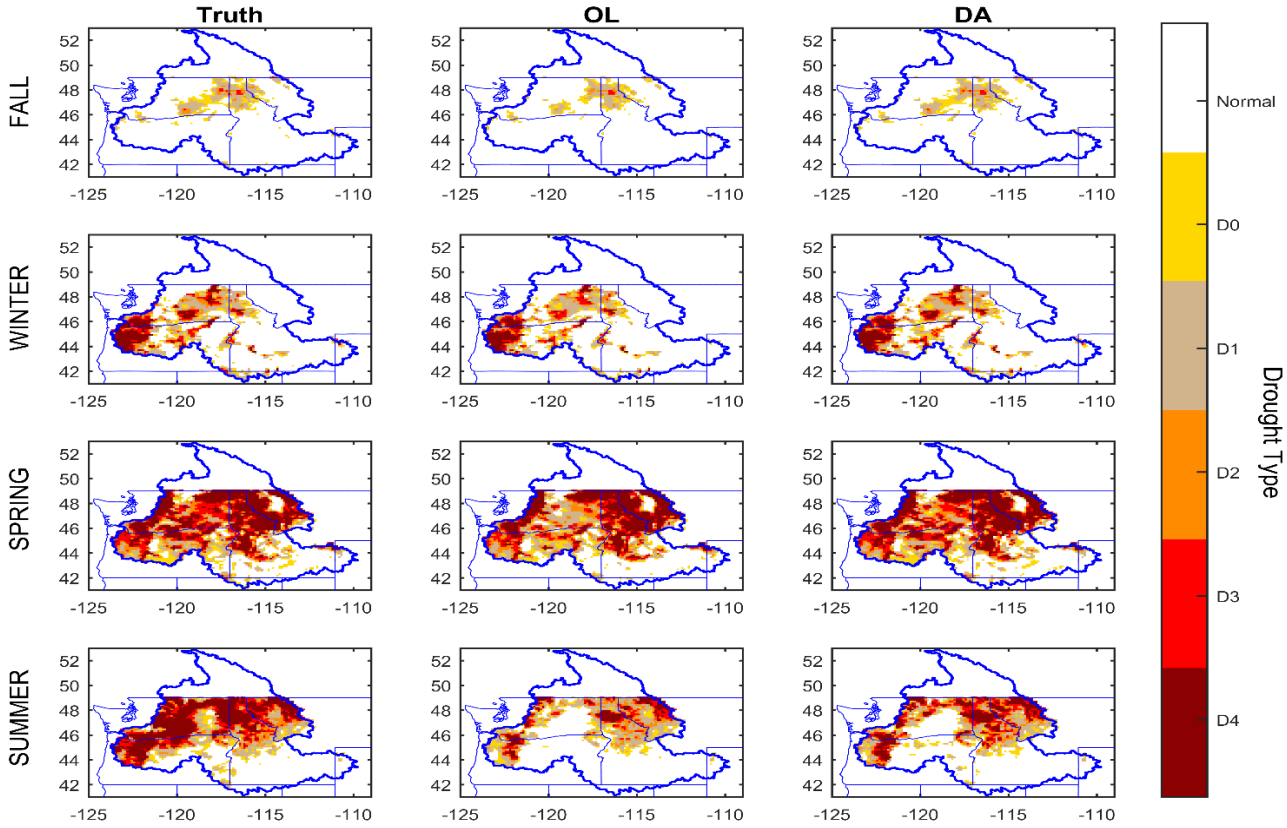

Figure 4-5. Comparison of the drought monitoring skill between the OL and DA for fall 2014 and winter/spring/summer 2015.

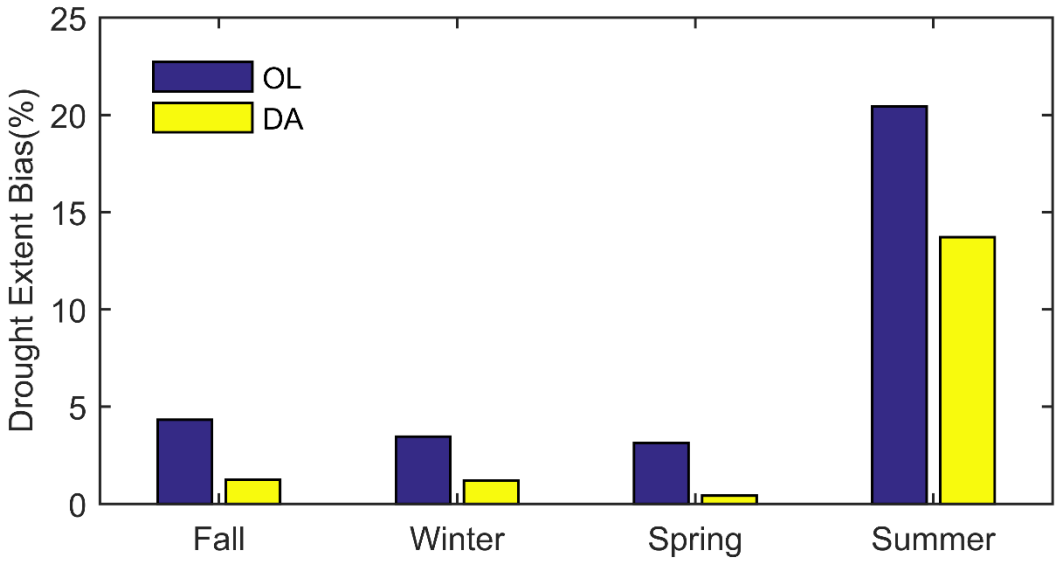

Figure 4-6. The absolute bias of drought extent (%) against the synthetic truth in the U.S. portion of the CRB.

4.4 Drought Forecasting Results

Prior to investigating the drought forecasting results, it is necessary to compare the initial conditions generated by the OL and DA. This comparison can be seen in Figure 4-7. In this figure, the initial conditions for seasonal drought forecasting beginning on January 1 (winter forecasting), April 1 (spring forecasting), July 1 (summer forecasting), and October 1, 2015 (fall forecasting) are presented. Each sub-plot contains the basin-averaged daily root-zone soil moisture for the synthetic truth, shown as a single value; the OL and the DA, shown as a distribution of values, which represent the probability distribution of initial root-zone soil moisture values. From Figure 4-7, it is observed that the OL and DA display very different behavior for each season. For all four seasons, the DA root-zone soil moisture reduce the uncertainty of OL estimations, and the mean root-zone soil moisture is closer to the synthetic truth for the DA.

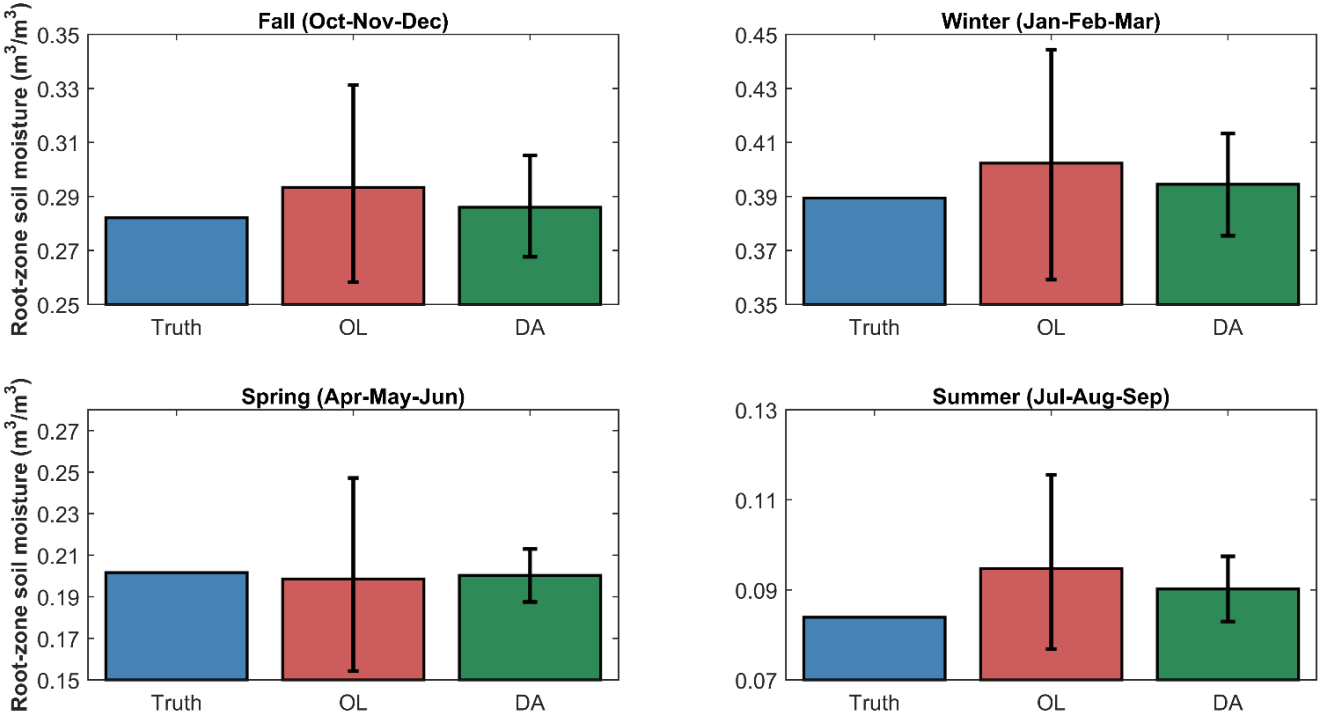

Figure 4-7. Comparison of the basin-averaged daily root-zone soil moisture (m^3/m^3) by the open-loop (OL) and data assimilation (DA) for fall 2014 and winter/spring/summer 2015 across the CRB. The error bars show the 95% prediction intervals.

Leaving out the first five years as model spin-up period, the copula drought forecasting model is developed based on the true simulations from January 1, 1984 to December 31, 2014. The probabilistic forecast of drought status in the following season given the drought condition in the current season is examined using root-zone soil moisture for each gird cell. The dependencies between aggregated root-zone soil moisture are modeled by a Gaussian copula while their marginal distributions are modeled with lognormal distributions as suggested by Madadgar and Moradkhani (2014b). It is noted that the OL and DA initial conditions are sampled as the posterior mean values.

Figure 4-8 presents the spatial distributions of seasonal drought forecasting probabilities of OL and DA for winter/spring/summer/fall 2015. The probabilistic drought conditions in each season are forecasted using the root-zone soil moisture in the previous season. The absolute drought extent bias (%) between the synthetic truth and MLE forecasted droughts are shown in Figure 4-9. Generally, compared with the synthetic truth, both OL and DA seasonal forecasting products show high probabilities (>30%) for the major drought locations in the following seasons. These results indicate the efficiency of the copula model in seasonal drought forecasting. Based on the drought extent bias for the four seasons, the DA estimates show systematic improvements over the OL estimates. For instances, the drought extent bias between the MLE-OL and synthetic truth is 29.87% for winter 2015 forecasting, and it decreases to 20.71% with MLE-DA. Similarly, drought extent bias decreases from 4.73% with MLE-OL to 0.95% with MLE-DA for 2015 summer.

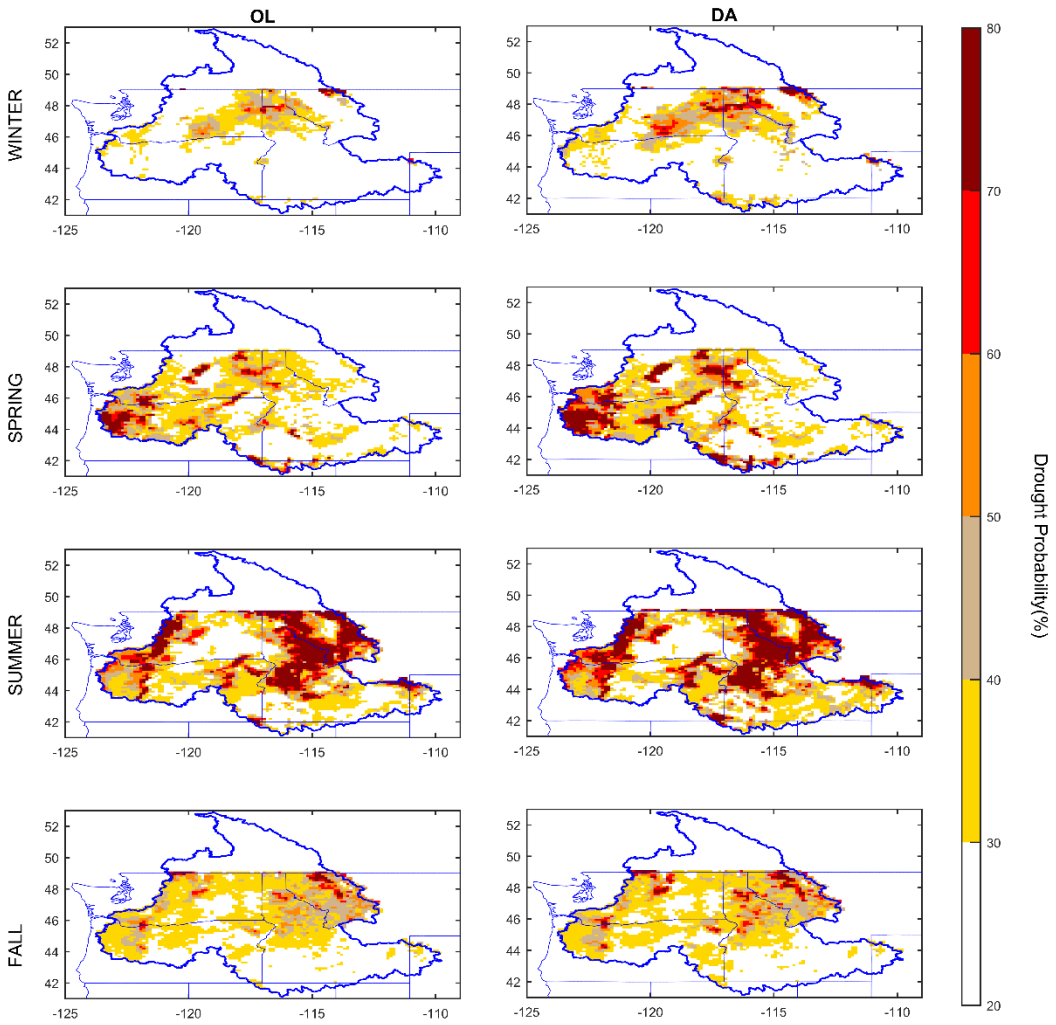

Figure 4-8. Seasonal probabilistic drought forecasting for both OL and DA for different seasons in 2015 given the drought status in each of the previous seasons.

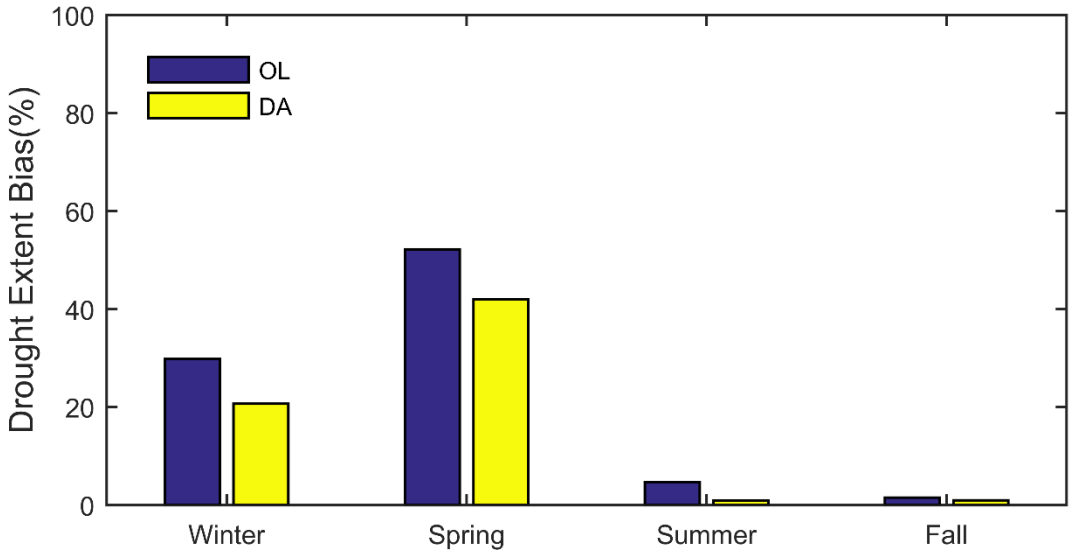

Figure 4-9. The absolute drought extent bias between the OL/DA and synthetic truth for the seasonal forecasting for winter/spring/summer/fall 2015.

Chapter 5 Case Study 1: Real Case Study

When assimilating the real satellite soil moisture data, the systematic biases between the satellite-based and model-based soil moisture cannot be avoided (Reichle and Koster, 2004). Proper treatment of these systematic biases is important, as the DA algorithm is designed to work with errors that are strictly random (Dee and Da Silva, 1998; Doucet and Johansen, 2011; Evensen, 1994). The most common approach, the CDF-matching (Reichle and Koster, 2004), is implemented in this dissertation to rescale the satellite observations to the model's climatology. The CDF-matching approach can correct all the moments of the distribution regardless of its shape. Leaving out the first five years as the model spin-up period, the CCI soil moisture products are rescaled from 1984-2014. The AMSR2 soil moisture products are rescaled from 2012-2015. For real data study, the perturbation errors are the same as the synthetic study except for the model error. The model error is normally distributed with a coefficient of variation of 0.15 (Yan et al., 2015).

Since no "true" drought data exist for real case study, the state drought declarations are used as the references to assess the drought forecasting skill (Shukla et al., 2011). Two case studies are presented here to indicate the added-value of DA for improving drought forecasting skill. (1) In spring 2013, drought declarations were issued for nine counties in the southern Idaho. Three months later, a total of 19 counties in Idaho issued drought emergence. (2) In winter 2015, the PNW received historically low snowpack conditions. In June 2015, the Washington State Governor Jay Inslee declared the statewide drought and Oregon State Governor Kate Brown declared drought

emergencies for 19 out of 36 Oregon counties (about 80% of the state's landmass). As a result, the DA is performed by assimilating the real satellite surface soil moisture over a six-month period until the forecast initialization date (July 1, 2013 and April 1, 2015).

5.1 Drought Monitoring Results

Figures 5-1 and 5-2 present the drought conditions in spring 2013 and winter 2015 and the detected drought areas with OL and DA. For spring 2013, the OL misses the drought events in parts of southeast Idaho, however, the DA helps to correct these biases. The detected drought areas of CRB for OL and DA are 73.17% and 81.43%, respectively. For winter 2015, the OL underestimates the drought events in parts of Oregon and Idaho whereas DA improves these representations. The detected drought areas increase from 36.37% in the OL to 58.85% after the DA, respectively. The DA provides a more accurate estimate of drought areas, and is more consistent with the state drought conditions. In summary, compared with the OL, the DA improves the drought monitoring skill for both 2013 and 2015. These results demonstrate the added-value of DA to facilitate the state drought response actions.

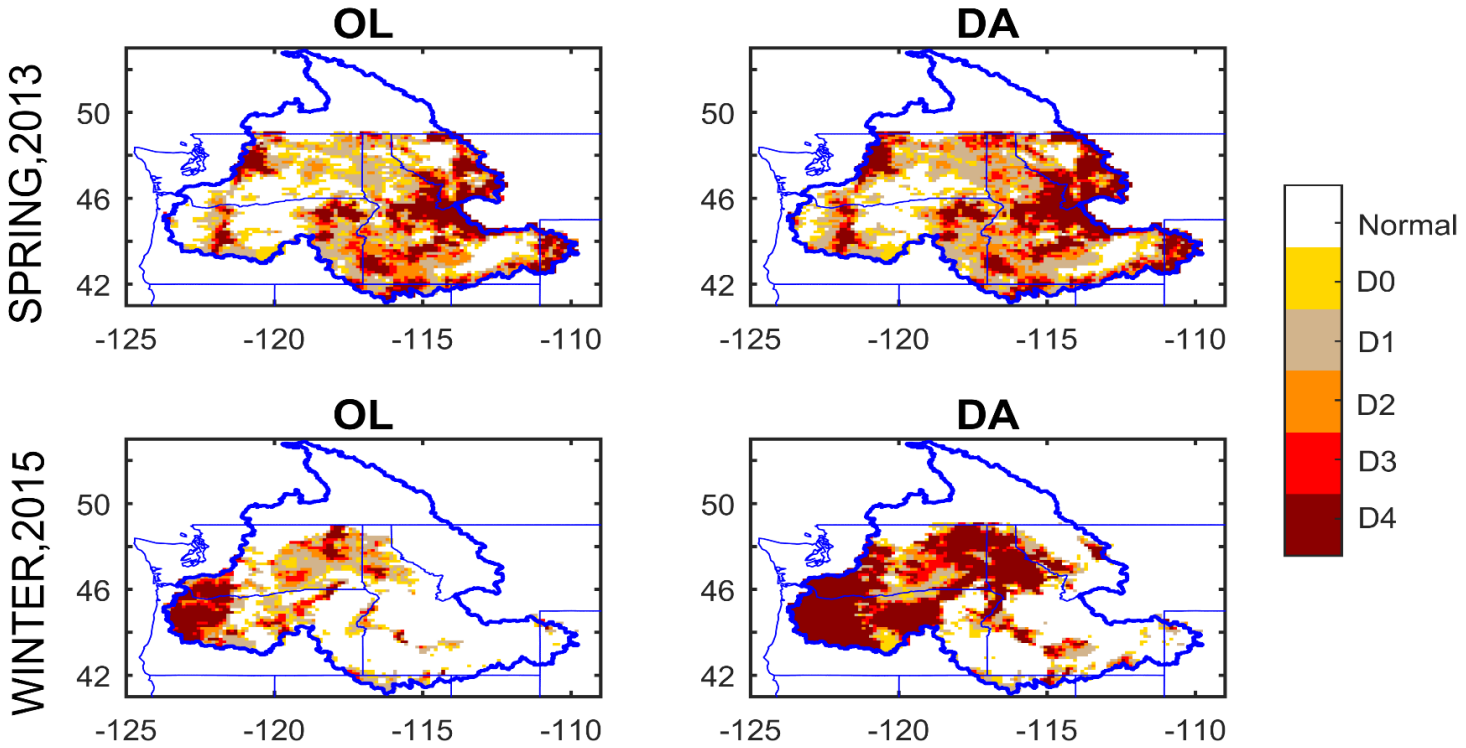

Figure 5-1. Spatial assessment of drought for 2013 and 2015 before and after DA.

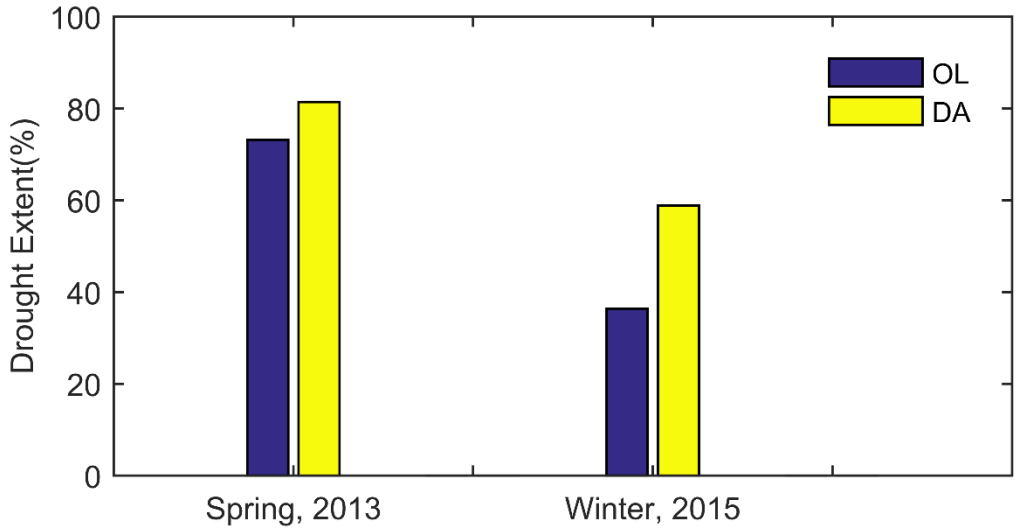

Figure 5-2. Drought extent for spring 2013 and winter 2015 drought events before and after data assimilation.

5.2 Drought Forecasting Results

With the copula-based seasonal drought forecasting system, the drought conditions of the PNW in summer 2013 and spring 2015 can be predicted based on the drought conditions in spring 2013 and winter 2015. The DA can further improve the drought forecasting skill as demonstrated in the synthetic study. Similarly to the synthetic study, and prior to investigating the seasonal drought forecasting results, it is necessary to compare the initial conditions of OL and DA. In Figure 5-3, the initial conditions for seasonal drought forecasting beginning on July 1, 2013 (summer forecasting) and April 1, 2015 (spring forecasting) are presented. Each sub-plot contains the basin-averaged daily root-zone soil moisture for the OL, shown as a single value; and the DA, shown as a distribution of values, which represent the probability distribution of initial root-zone soil moisture values. For both seasons, the DA root-zone soil moisture shows lower values, which is more consistent with the real drought situations.

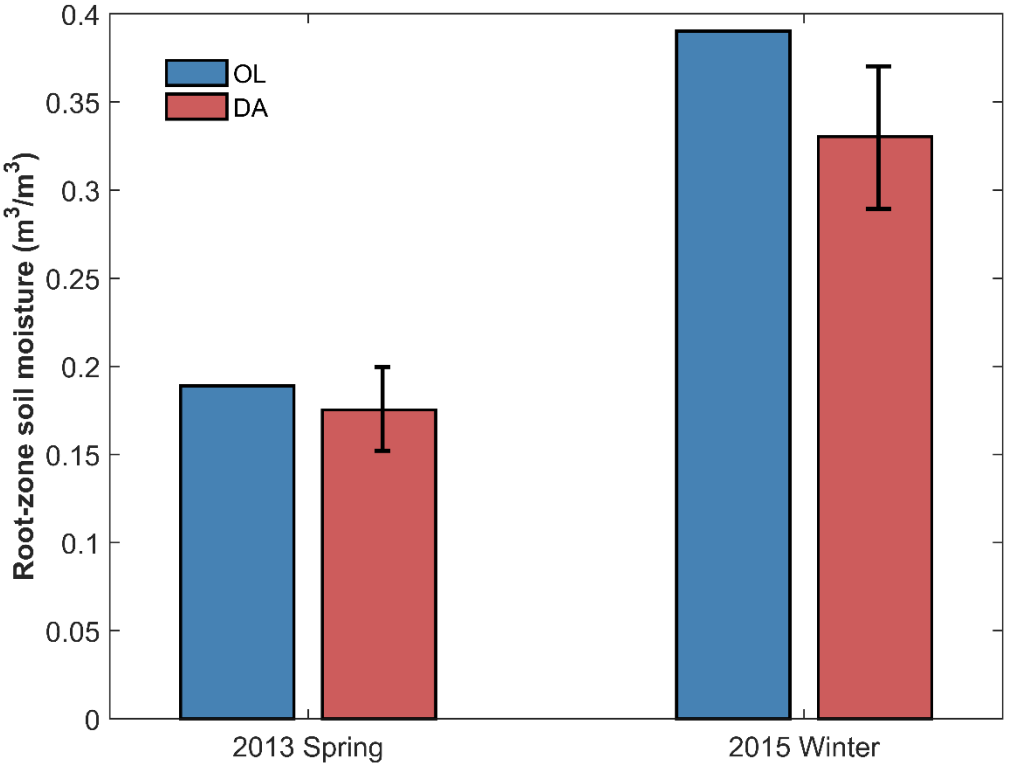

Figure 5-3. Comparison of the basin-averaged daily root-zone soil moisture (m^3/m^3) by the open-loop (OL) and data assimilation (DA) for spring 2013 and winter 2015 across the CRB. The error bars show the 95% prediction intervals.

Figure 5-4 presents the spatial distributions of seasonal drought forecasting probabilities and MLE forecasted droughts for summer 2013 and spring 2015, respectively. The MLE forecasted drought extent (%) over the U.S. portion of the CRB between the OL and DA is shown in Figure 5-5. Given the initial conditions in spring 2013, the basin-averaged forecasted drought probabilities for summer 2013 are 51.80% and 54.64% for OL and DA, respectively. The forecasting drought probabilities for spring 2015 are 32.86% and 49.58% for OL and DA, respectively. For both cases, the DA suggests a higher probability of drought in summer 2013 and spring 2015, which is more consistent with the state declaration. The MLE forecasted drought extents increase from 64.67% and 25.85% in the OL to 70.57% and 52.83% in the DA for summer 2013 and spring 2015, respectively. Especially for the spring 2015, the OL forecasts underestimate the severe drought conditions for Washington and Oregon. In terms of both forecasted probabilities and MLE forecasted drought extents, the DA is much more consistent with the state declaration. In summary, compared with the OL, the DA improves the drought forecasting skill for both summer 2013 and spring 2015. These results demonstrate the added-value of DA to facilitate the state drought preparation and declaration at least three months before the official state drought declaration.

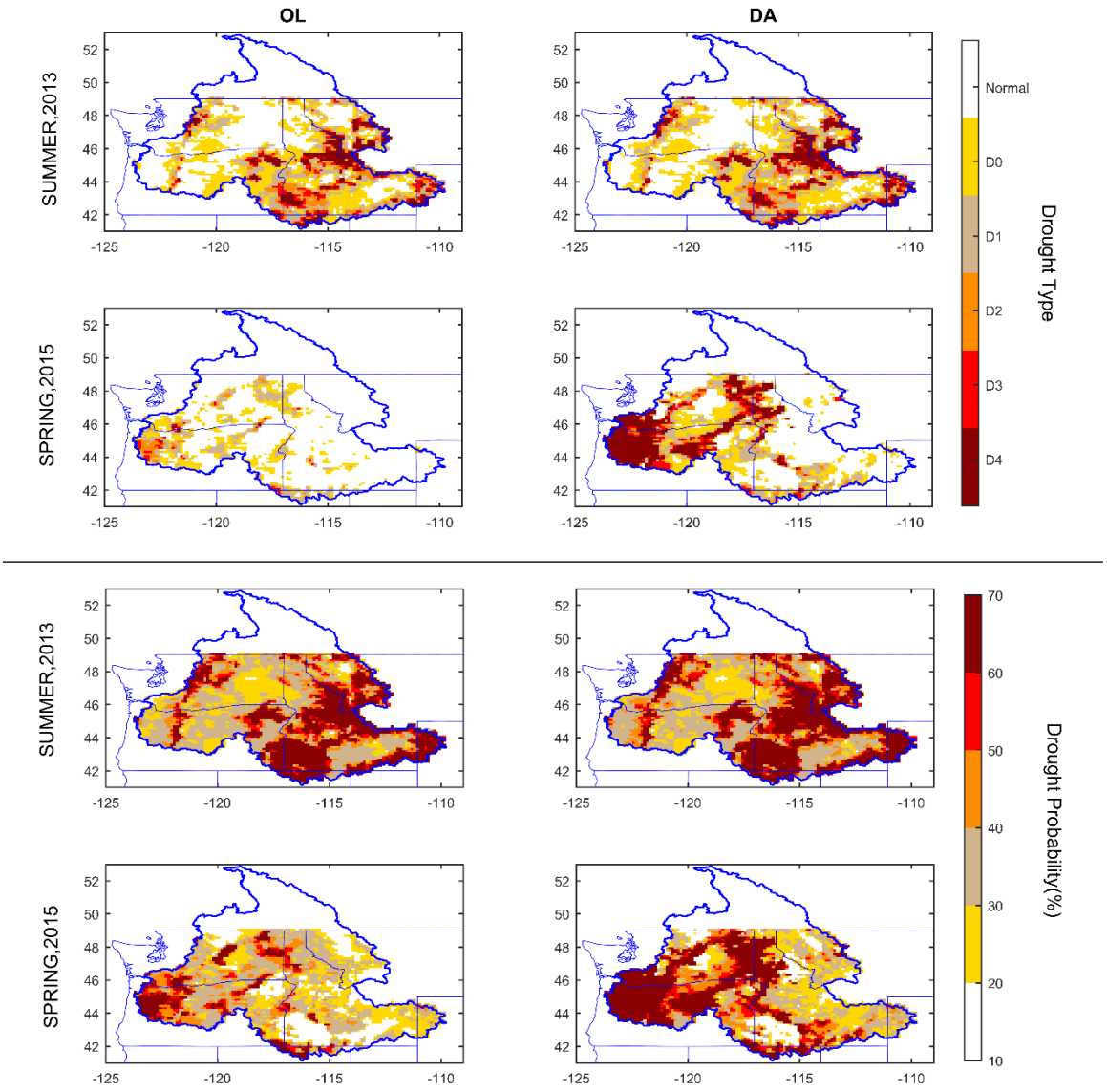

Figure 5-4. The seasonal probabilistic drought forecasts for summer 2013 and spring 2015 given the drought status in spring 2013 and winter 2015, respectively. The top-panel shows the forecasted drought areas based on MLE and the bottom-panel indicates the forecasted drought probabilities.

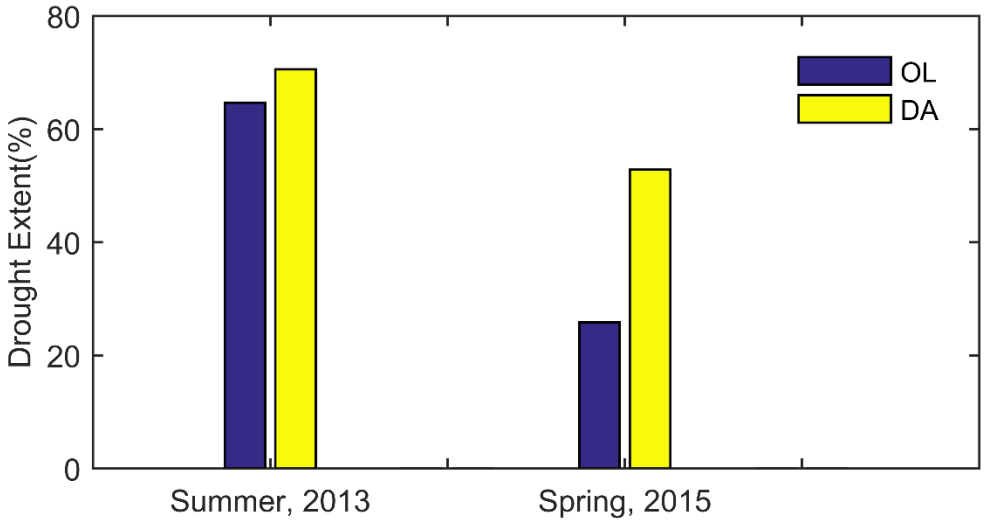

Figure 5-5. The forecasted drought extent between the OL and DA based on MLE across the CRB.

Chapter 6 Case Study 2: Synthetic Study

To objectively assess the potential benefit of the assimilation of satellite surface soil moisture, a synthetic study is first conducted through a procedure called observing system simulation experiment (OSSE) or synthetic study (Moradkhani, 2008). The synthetic study includes the following four steps: 1) a "truth" run of hydrologic model with the pre-calibrated model parameters; 2) simulated satellite surface soil moisture observations, which are generated from the truth run by incorporating the observation errors; 3) an open-loop (OL) run with the perturbed forcing data without DA; and 4) the DA step that assimilates the simulated surface soil moisture observations from step 2 to the model. Then the OL and DA results are compared against the truth simulation to evaluate the impact of satellite surface soil moisture assimilation. Figure 6-1 presents the flowchart of the synthetic study in this dissertation using VIC model.

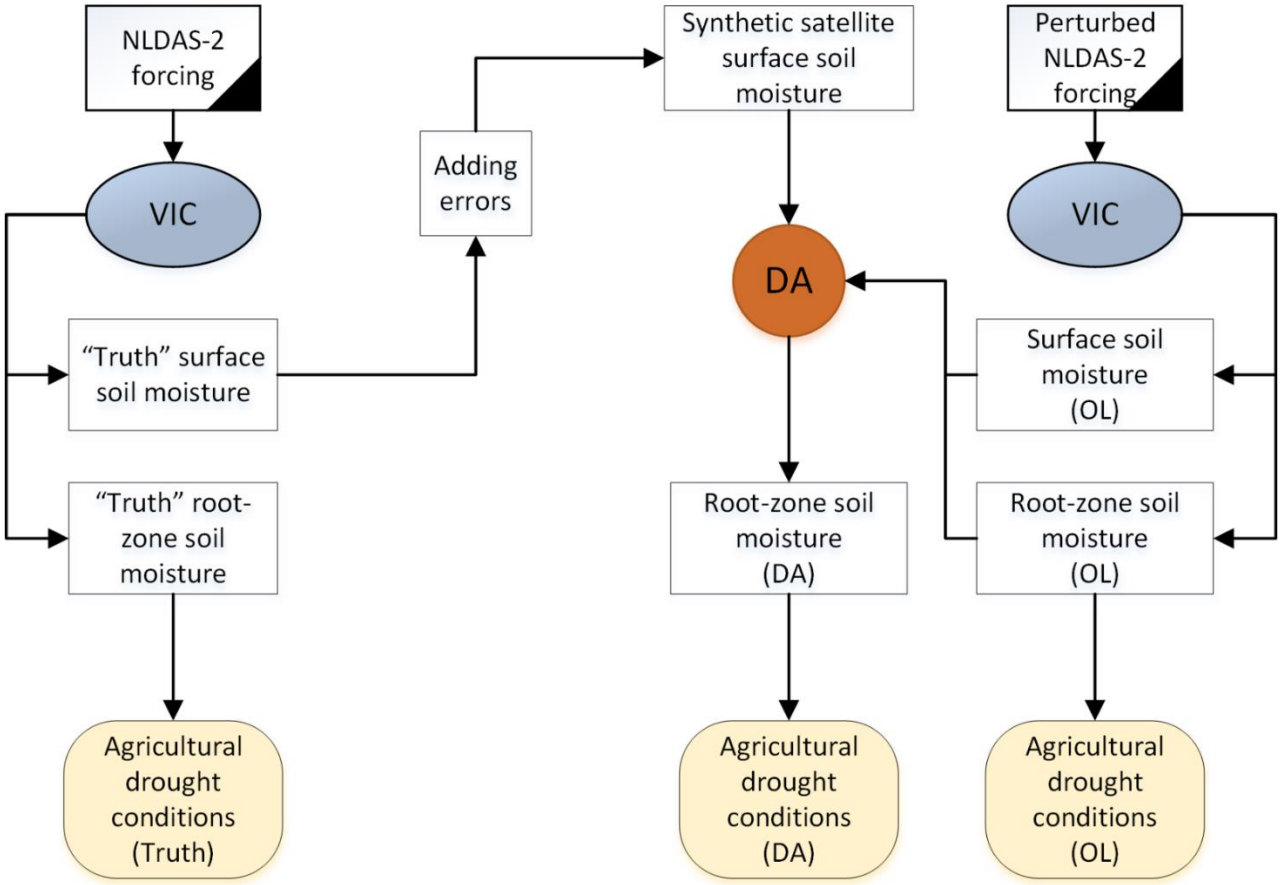

Figure 6-1. The flowchart of the synthetic study using VIC model.

6.1 Retrospective Simulation

In this dissertation, the VIC model is performed to simulate the soil moisture and reconstruct the 2012 drought conditions over the CONUS domain, at a 1/8° spatial resolution. The model parameter files, including the elevations, soil properties, and vegetation cover, are acquired from the VIC retrospective land surface dataset (http://www.hydro.washington.edu/SurfaceWaterGroup/Data/VIC_retrospective/index.html) (Maurer et al., 2002). For instance, Figure 6-2 presents the spatial distribution of mean cell elevation across CONUS.

For synthetic truth simulation, the VIC model is run using the NLDAS-2 forcing data from January 1, 1979 to December 31, 2015 to produce long-term girded surface and root-zone soil moisture. In this dissertation, the VIC model is run in water balance mode, which means that the surface temperature is set equal to the surface air temperature rather than iteratively solving the surface energy budget. The OL simulation is run with the perturbed NLDAS-2 forcing data for the period of January 1, 2012 to December 31, 2012. The ensemble size and perturbation errors in the OL simulation are the same as the DA, which is discussed in the following section.

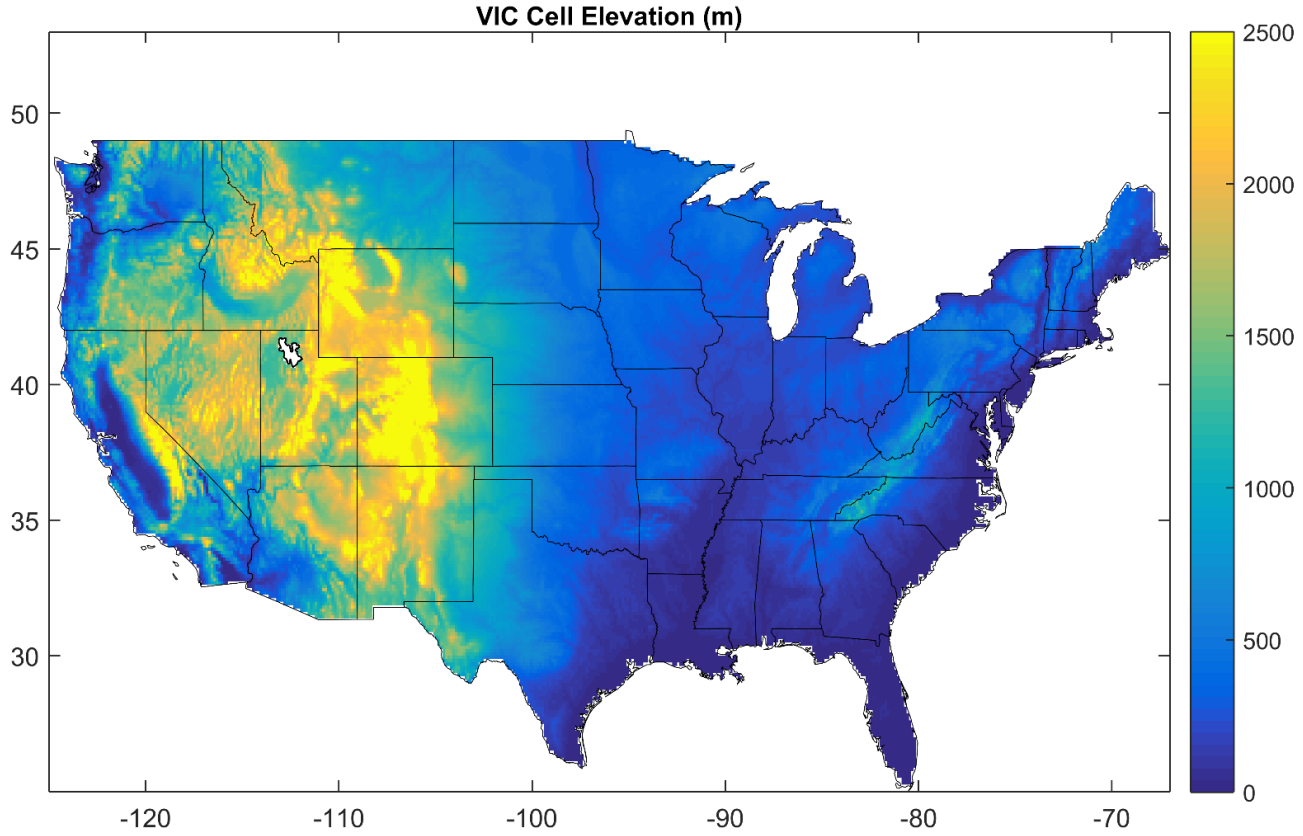

Figure 6-2. The mean elevation of each grid cell cross CONUS.

6.2 Data Assimilation Implementation

The DA is performed by assimilating the synthetic satellite surface soil moisture for the period of January 1, 2012 to December 31, 2012. Contrary to the small ensemble size (12~20) used in the majority of previous satellite soil moisture DA studies (De Lannoy et al., 2012; Kumar et al., 2009; Pan and Wood, 2010; Reichle et al., 2010), a large ensemble size of 100 is used in this dissertation, in order to fully quantify the soil moisture posteriors. The PMCMC modular is written in Python script, and all the simulations are run on the Linux Hydra Cluster (13 nodes, 208 processors) located at the Office of Information Technology (OIT), Portland State University (PSU).

In the DA implementation, zero-mean, normally distributed with a coefficient of variation of 0.35 additive perturbations are applied to the minimum and maximum temperature. The precipitation and wind speed are perturbed with a lognormal distribution with a coefficient of variation of 0.35. These values are suggested by DeChant and Moradkhani (2014b) to account for errors in the forcing data due to the sensor errors and spatial heterogeneity. The white noise (standard deviation) for the CCI satellite soil moisture is set to 0.04 m^3/m^3 (Kumar et al., 2014b). Prior to DA, the CCI satellite error standard deviations are scaled by the ratio of the soil moisture time series standard deviation of the VIC model to that of the CCI real data (separately for each grid cell), as suggested by Reichle et al. (2007) and Q. Liu et al. (2011). After scaling, the synthetic CCI soil moisture is generated by incorporating the scaled observation errors.

6.3 Drought Monitoring Results

Figure 6-3 presents the NIC values in the surface and root-zone soil moisture and their spatial distributions across the CONUS. The majority of the grid cells show the positive NIC values indicating the added-value of the DA. Generally, the improvements in the surface soil moisture field are consistent with the improvements in the root-zone soil moisture field, with more prominent improvements in the surface soil moisture field. The improvements in surface field are higher than root-zone field, which is mainly caused by the weak and highly non-linear cross covariance between the two layers. This finding is also consistent with the previous synthetic soil moisture DA studies (Kumar et al., 2014a, 2009). For surface soil moisture, the daily domain-averaged RMSE (m^3/m^3) for the OL is 0.0042, and it decreases to 0.0027 with DA. Similarly, the daily domain-averaged root-zone soil moisture RMSE (m^3/m^3) value decreases from 0.0034 in the OL to 0.0024 after DA.

In Figure 6-3, it is also noted that several grid cells show negative NIC values. This may be caused by the inappropriate quantifications of the uncertainty in synthetic observations and model forecasts (Leisenring and Moradkhani, 2012, 2011). In the implementation of the DA, the identifications of model and observations errors are very unintuitive and the experience estimates of forcing error may lead to over/under-confident soil moisture predictions (Y. Liu et al., 2012; Thiboult and Anctil, 2015). Properly quantifying the uncertainty in observations and forecast models is still the open question in hydrologic DA community, and it is one of the major obstacles in operational hydrologic DA forecasting (Y. Liu et al., 2012). Especially for large-scale DA

applications, it is not feasible to conclude on a single ideal manner to identify an optimal error implementation, and some degradation cells are always unavoidable (Kumar et al., 2014a).

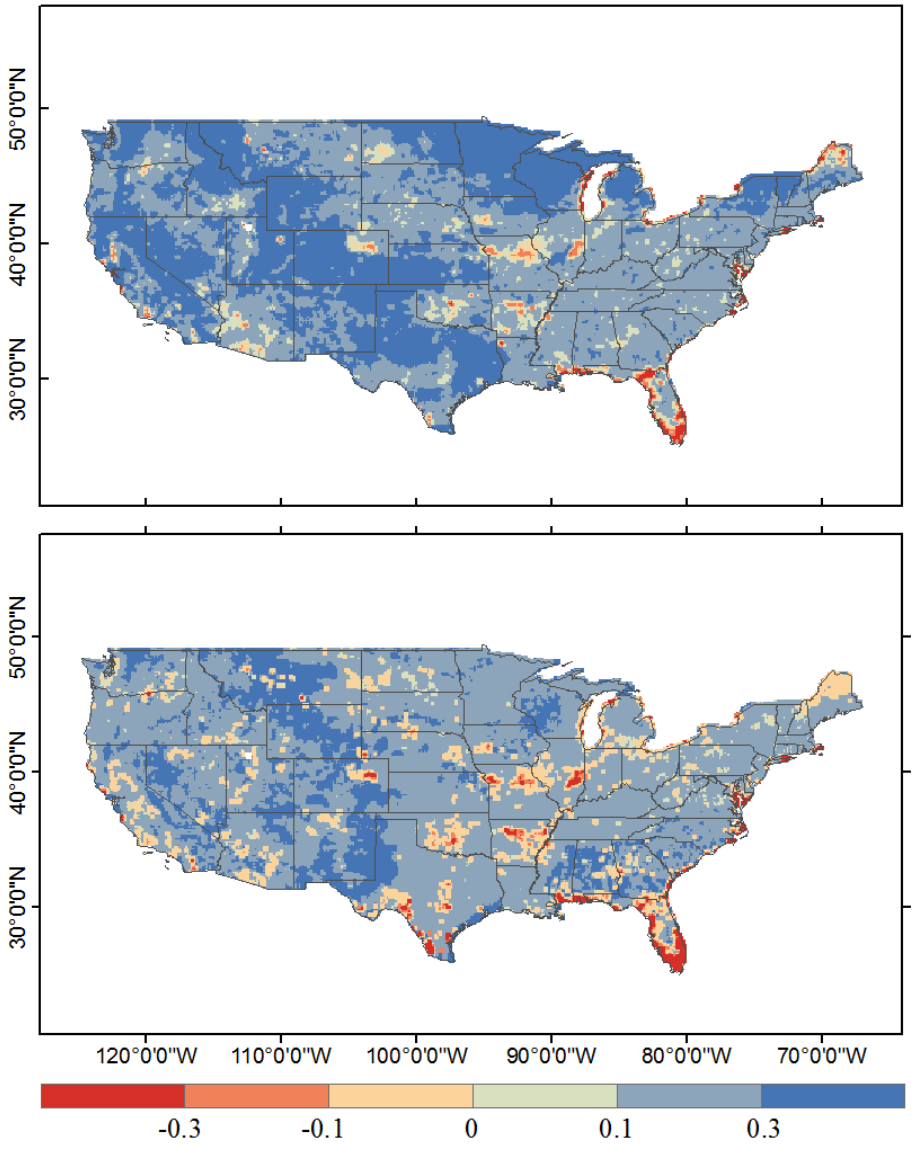

Figure 6-3. The normalized information contribution (NIC) value between the OL and DA (Eq. 15). The positive value indicates that the DA improves soil moisture prediction against OL; negative value indicates the degradation over the OL. Top: surface soil moisture filed. Bottom: root-zone soil moisture filed.

In this dissertation, drought is characterized with the soil moisture percentile and the drought intensity is classified based on the five categories from NDMC: D0, D1, D2, D3, and D4. Leaving the first year as the model spin-up period, the soil moisture climatology is the truth soil moisture simulations from January 1, 1980 to December 31, 2015. Then, the soil moisture percentiles generated from the OL and DA monthly integrations are compared against the corresponding synthetic truth. For instance, to estimate the monthly soil moisture percentile in October 2010, one must first take all soil moisture October values over 1980-2015 to construct the climatological distribution for each grid cell. Then, for any specific grid cell soil moisture value in October 2010, the corresponding soil moisture percentile can be estimated from the climatological distribution.

Figures 6-4 and 6-5 present the spatial distribution of drought intensities and the drought extent bias (%) for five drought categories (D0-D4) over CONUS. The severe drought events from May-August 2012 across the Central U.S. can be clearly seen in the synthetic truth. In all comparisons, the DA estimates show systematic improvement over the OL estimates. For the May 2012 case, the OL underestimates the intensity of drought across the Nevada, Utah, Colorado, and New Mexico states whereas DA improves these representations. The drought extent bias (%) for D0-D4 between the OL and synthetic truth is 5.11%, and it decreases to 1.28% with DA. For the June and July 2012 cases, the OL underestimates the intensity of drought across the Central U.S. (i.e., the Kansas, Nebraska, and Colorado states), and DA helps to reduce these large biases. Similarly, drought extent biases (%) decrease from 5.25% and 4.69% in the OL to 1.02% and 0.53%

in the DA, respectively. Although several grid cells in the Central U.S. show relatively high soil moisture values in August 2012, the DA still helps reduce these biases. The drought extent bias (%) decreases from 3.02% to 0.34%. Overall, these results are consistent with the trends in Figure 6-3, which show the improvements obtained by data assimilation.

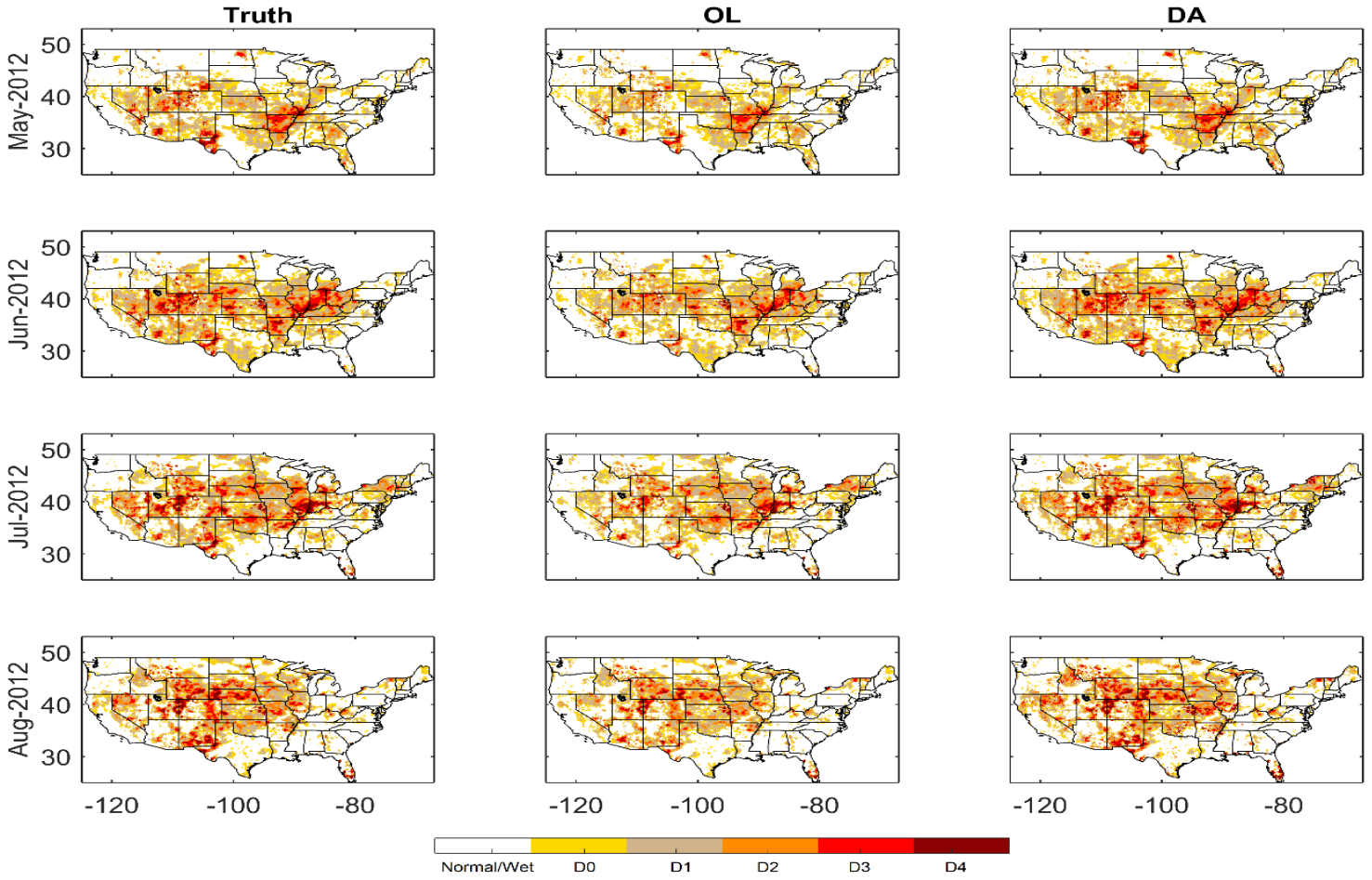

Figure 6-4. Comparison of the drought monitoring skill between OL and DA for May-August 2012.

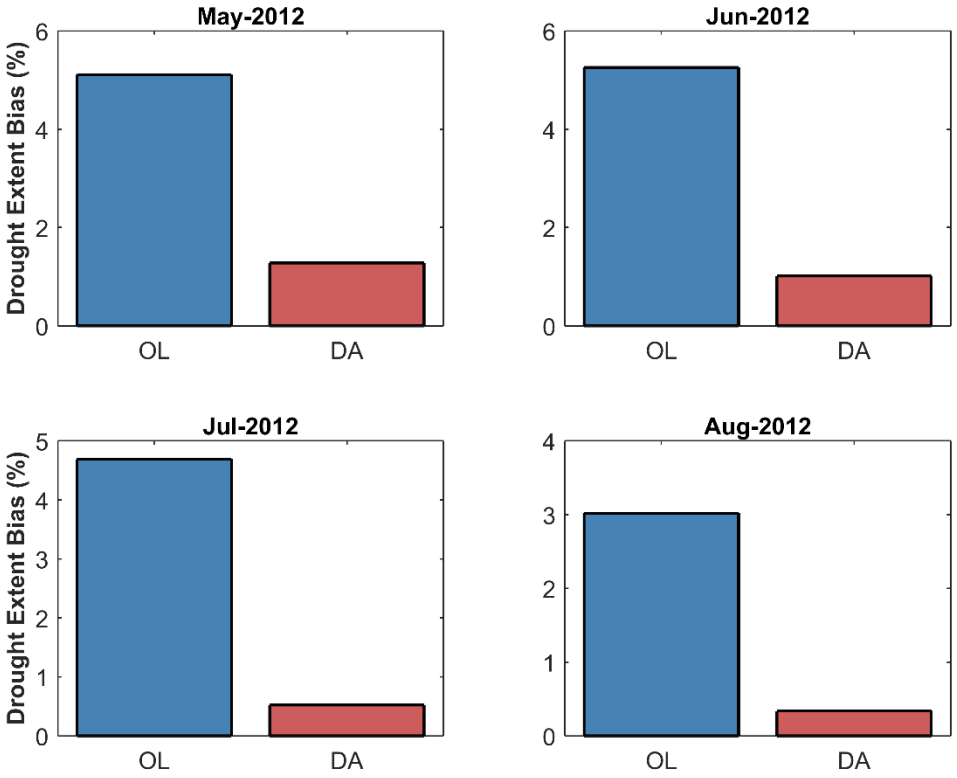

Figure 6-5. The absolute bias of drought extent (%) against the synthetic truth over the CONUS.

6.4 Drought Forecasting Results

Prior to investigating the drought forecasting results, it is necessary to compare the initial conditions generated by the OL and DA. This comparison can be seen in Figure 6-6. In this figure, the average initial conditions (May-August) for monthly drought forecasting beginning on May 1, June 1, July 1, and August 1, 2012 are presented. Each sub-plot represents the initial conditions in one grid cell of each basin, including the cell-averaged daily soil moisture for the synthetic truth (shown as a single value); the OL and the DA (shown as a distribution of values) represent the probability distribution of initial soil moisture values. From Figure 6-6, it is observed that the OL and DA display very different behavior for each basin. In general, for all basins, the DA soil moisture reduces the uncertainty of OL estimations, and the mean soil moisture is closer to the synthetic truth for the DA.

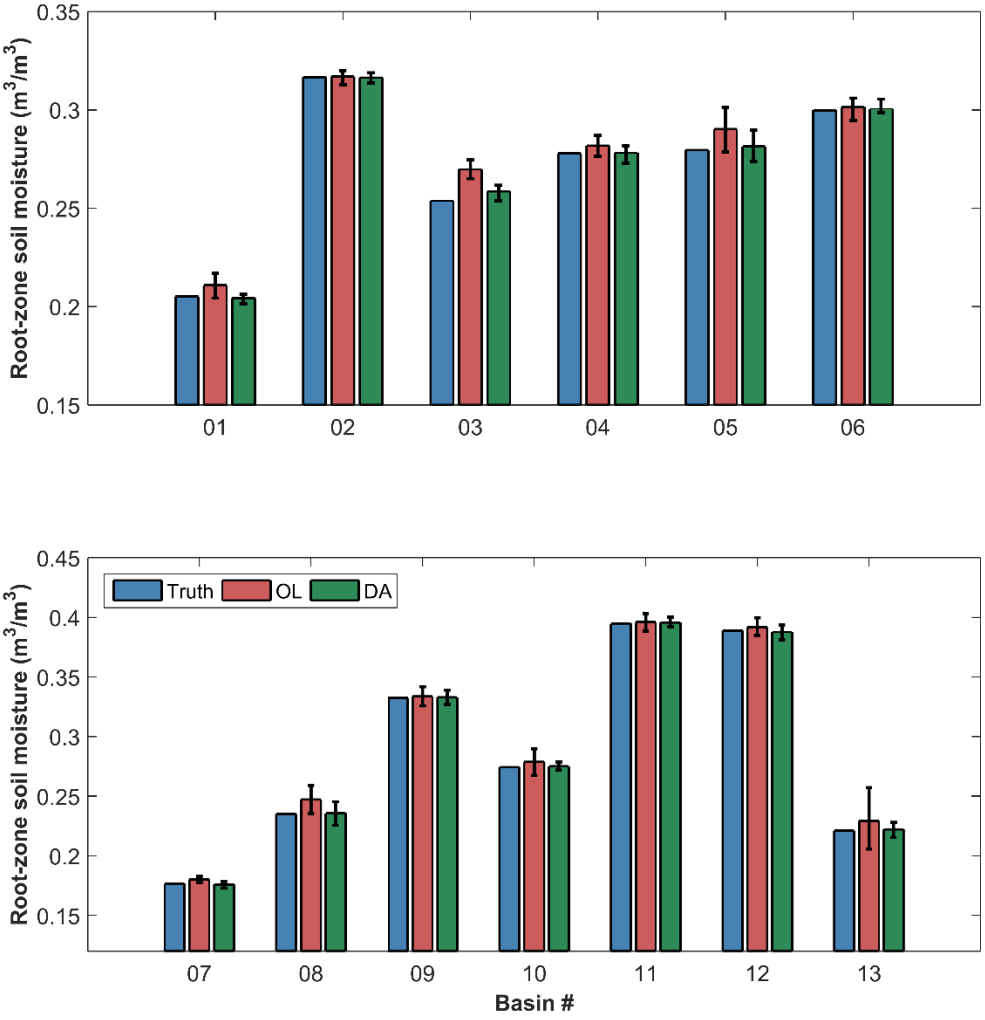

Figure 6-6. Comparison of the cell-averaged daily root-zone soil moisture (m^3/m^3) by the OL and DA for May-August 2012. The error bars show the 95% prediction intervals.

Leaving out the first year as model spin-up period, the copula drought forecasting model is developed based on the truth simulations from January 1, 1980 to December 31, 2015. Given the drought condition in the current month/season, the probabilistic forecast of drought status in the following month/season is examined using soil moisture for each grid cell. The dependencies between monthly/seasonal aggregated soil moisture are modeled by a Gaussian copula while their marginal distributions are modeled with lognormal distributions as suggested by Madadgar and Moradkhani (2014a). For each forecast initialization date, the initial condition uncertainty through DA is characterized by estimating the PDF through the ensemble members, while the initial condition of OL is treated as deterministic values (posterior mean).

In this dissertation, the PDF of initial condition is assumed to be Gaussian, and is estimated by using the first two moments, mean and variance. It is noted that the Gaussian distribution is used here for its efficiency to represent the ensemble distribution and its simplicity for sampling algorithm (Hut et al., 2015); other non-parametric PDF estimation methods, such as kernel density, can also be applied. After the estimation of the PDF, the initial condition of the DA is sampled and the monthly to seasonal drought forecasts are generated. Then, the copula forecasted monthly/seasonal drought conditions are compared against the corresponding synthetic truths.

Figure 6-7 presents the spatial distributions of monthly drought forecasting probabilities of OL and DA for May-August 2012. The probabilistic drought conditions in each month are forecasted using the soil moisture in the previous month. Generally, compared with the synthetic truth, both OL and DA monthly forecasting products show

high probabilities (>30%) for the Central U.S. in the following months. These results indicate the efficiency of the multivariate copula model in forecasting the summer drought of 2012. In the July 2012 case, the OL-based drought forecasts underestimate the severity of drought in the Central U.S. such as the Kansas, Oklahoma, Arkansas, Missouri, and Nebraska states, and DA helps to correct these biases. Similarly, in the August 2012 where the drought event achieves the peak intensity, the OL underestimates the intensity of drought over areas of the Central U.S. whereas DA improves these representations. The absolute drought extent bias (%) between the synthetic truth and MLE forecasted droughts are shown in the top panel of Figure 6-8. Based on the drought extent bias, the DA estimates show systematic improvement over the OL estimates over the four months. For instances, the drought extent bias between the OL and the synthetic truth is 15.89% for May 2012, and it decreases to 13.05% with DA. Similarly, drought extent bias decreases from 16.10% with OL to 4.21% with DA for August 2012.

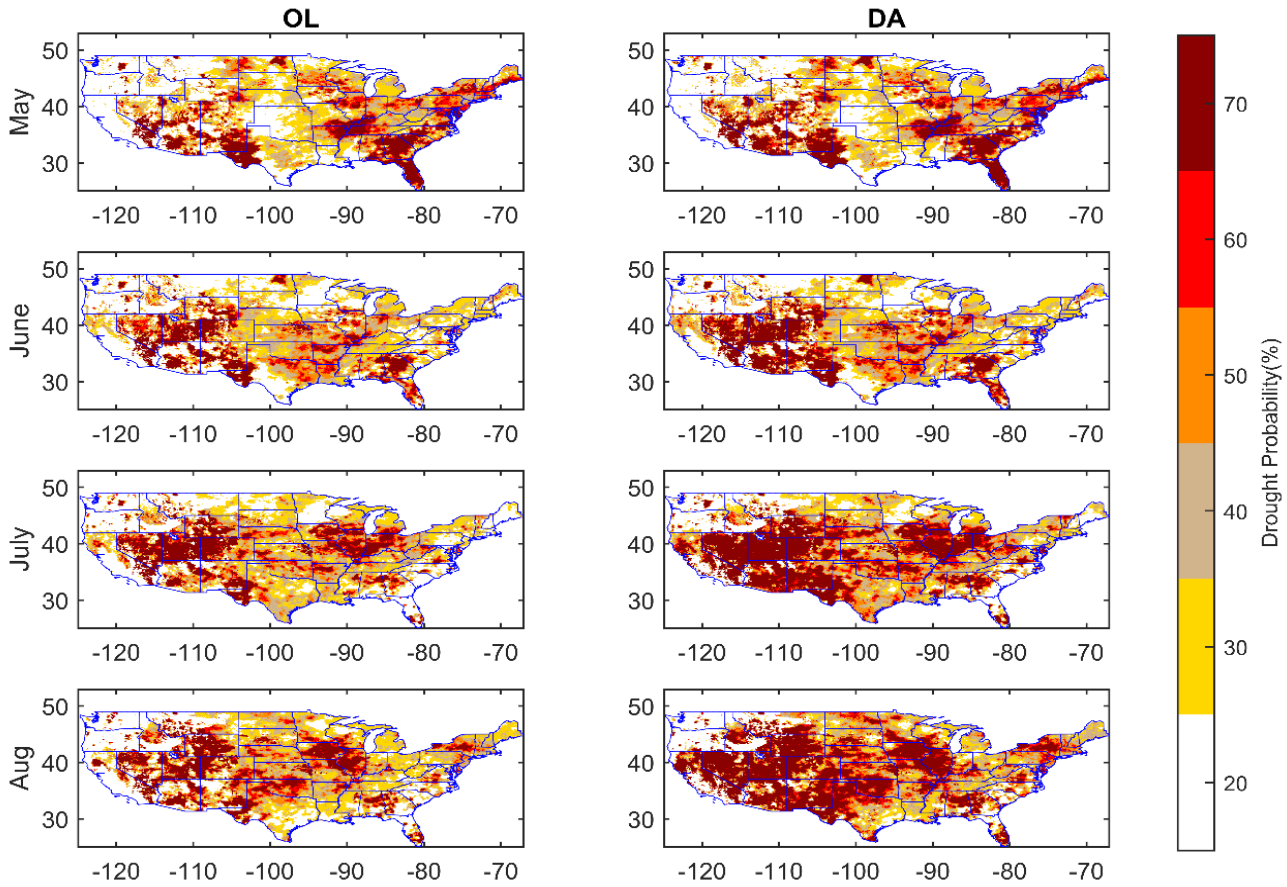

Figure 6-7. Monthly probabilistic drought forecasts between OL and DA for May-August 2012.

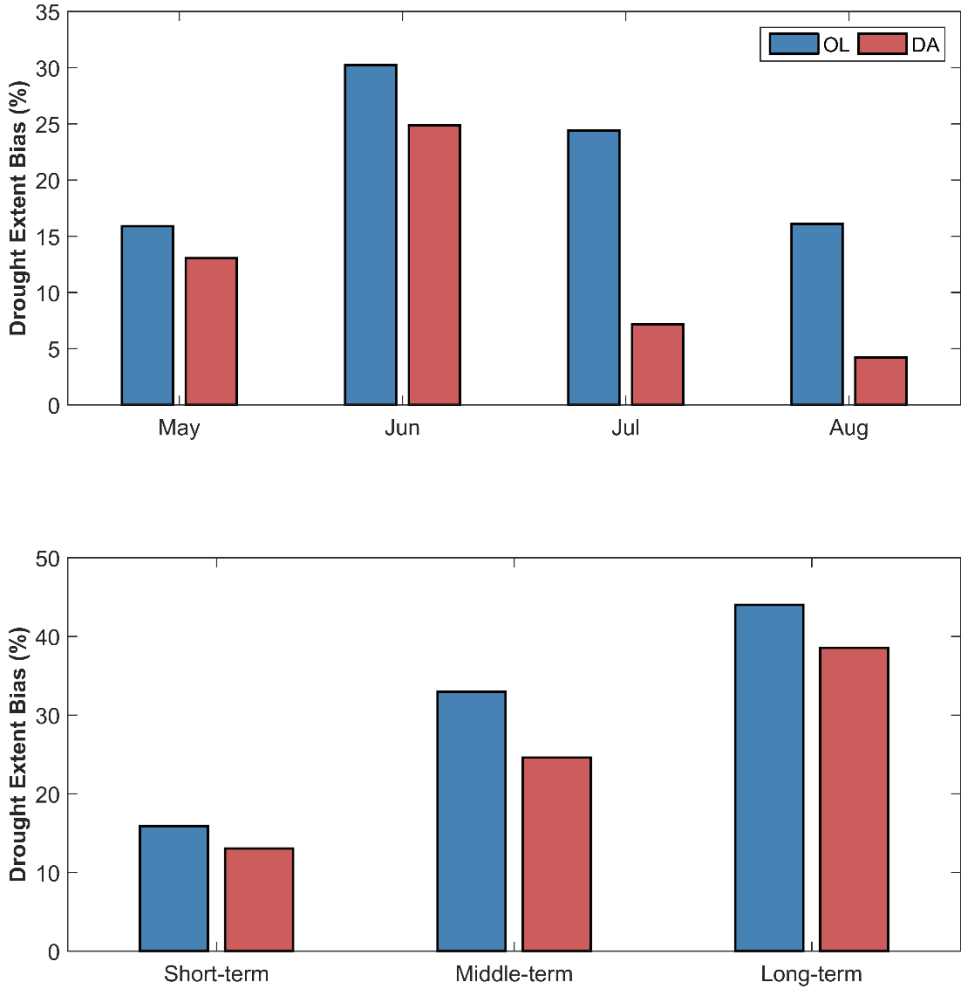

Figure 6-8. The forecasted drought extent bias between OL and DA based on MLE across the CONUS. Top: monthly drought forecasting bias for May/June/July/August 2012. Bottom: monthly to seasonal drought forecasting bias for May (short-term)/May-June (middle-term) /May-July (long-term) 2012 (according to the framework shown in Figure 2-7).

Besides the monthly drought forecasts, Figure 6-9 also shows the spatial distributions of bimonthly to seasonal drought forecasting probabilities of OL and DA for May-June/May-July, 2012. Similar to the monthly drought forecasts, both of the bimonthly and seasonal drought forecasts issued on May 1 based on DA show higher drought probabilities in the Central U.S. than the forecasts based on OL. These results can demonstrate the added value of DA to forecast the drought event across the Central U.S. in summer, providing early warning and drought preparedness time for decision makers.

The absolute drought extent bias (%) between the synthetic truth and MLE forecasted droughts are shown in the bottom panel of Figure 6-8. Similar to monthly drought forecasts in Figure 6-7, the DA forecasts show systematic improvements over the OL forecasts. For OL, the drought extent bias for the short- (monthly), middle- (bimonthly), and long-term (seasonal) forecasts are 15.89%, 32.97%, and 44.10%, respectively. While for the DA-based drought forecasts the drought extent bias decreases to 13.05%, 24.59%, and 38.55%, respectively. It is also noted that the drought extent bias between OL and DA decreases from short- to long-term, indicating that the drought forecast skills are dominated by initial conditions in short lead times (monthly), and become less sensitive to initial conditions in long lead times (seasonal). This finding is also consistent with other previous studies (DeChant and Moradkhani, 2015b; Koster et al., 2010; Yuan et al., 2016).

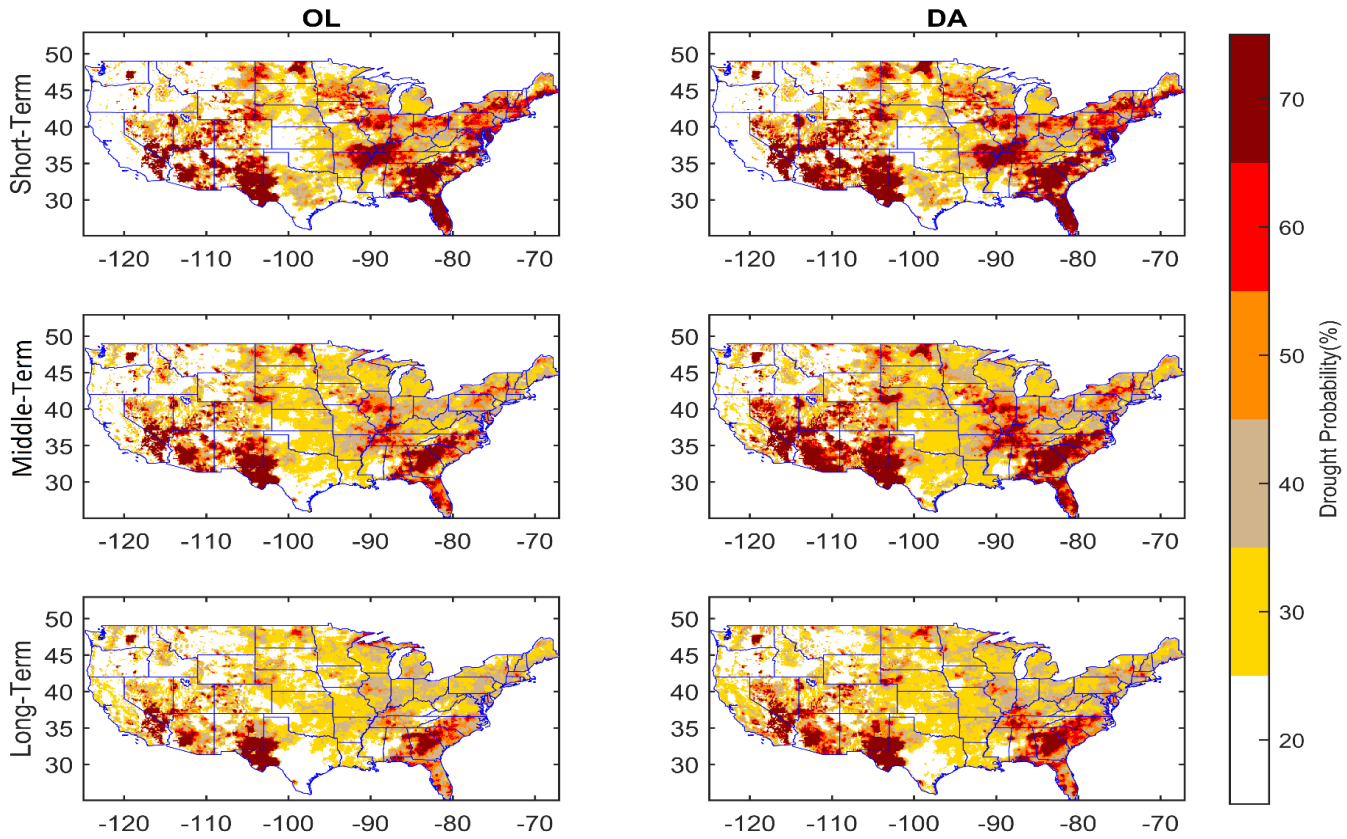

Figure 6-9. The monthly (short-term), bimonthly (middle-term), and seasonal (long-term) drought forecasts between OL and DA for May/May-June/May-July 2012 (according to the framework shown in Figure 2-7).

Chapter 7 Case Study 2: Real Case Study

When assimilating the real satellite soil moisture data, the systematic biases between the satellite-based and model-based soil moisture cannot be avoided (Reichle and Koster, 2004). Proper treatment of these systematic biases is important, as the DA algorithm is designed to work with errors that are strictly random (Dee and Da Silva, 1998; Doucet and Johansen, 2011; Evensen, 1994). The most common approach, the CDF-matching (Reichle and Koster, 2004), is implemented in this dissertation to rescale the satellite observations to the model's climatology. The CDF-matching approach can correct all the moments of the distribution regardless of its shape. Leaving out the first year as the model spin-up period, the CCI soil moisture products are rescaled from 1980-2014. For real data study, the perturbation errors are the same as the synthetic study except for the model error. The model error is normally distributed with a coefficient of variation of 0.1 (Yan and Moradkhani, 2016a; Yan et al., 2015).

The DA is performed by assimilating the rescaled real satellite surface soil moisture from February 1 to August 31, 2012. This DA period can be divided into two parts: 1) The DA from February 1 to April 31 is used to characterize the soil moisture initial condition uncertainty until the monthly/bimonthly/seasonal forecast initialization date on May 1, 2012. Since the NOAA CPC's SDO issued on 17 May 2012 failed to forecast this event, it is important to examine whether the proposed monthly/seasonal drought forecasting products can successfully forecast this drought event. 2) The DA from May 1 to August 31 is used to improve the soil moisture prediction, which translates into a drought monitoring skill. Since the USDM did not capture this event until late

June, it is important to investigate whether the proposed monthly drought monitoring products can better capture this drought event, especially in May.

Since no "true" drought data exist for the real case study, the state-of-the-art USDM and drought economic loss are used as the references to assess the OL and DA drought monitoring and forecasting skill. According to the USDM, during May-August 2012, over three-quarters of CONUS experienced at least D0 drought conditions and the Central U.S. experienced D2-D4 drought conditions (Figures 7-1, 7-2, 7-3, 7-4). During the same period of time, the summer drought intensity can be classified as D4 since it resulted in major curtailment of crop yields, and caused about $12 billion economic loss (Hoerling et al., 2014).

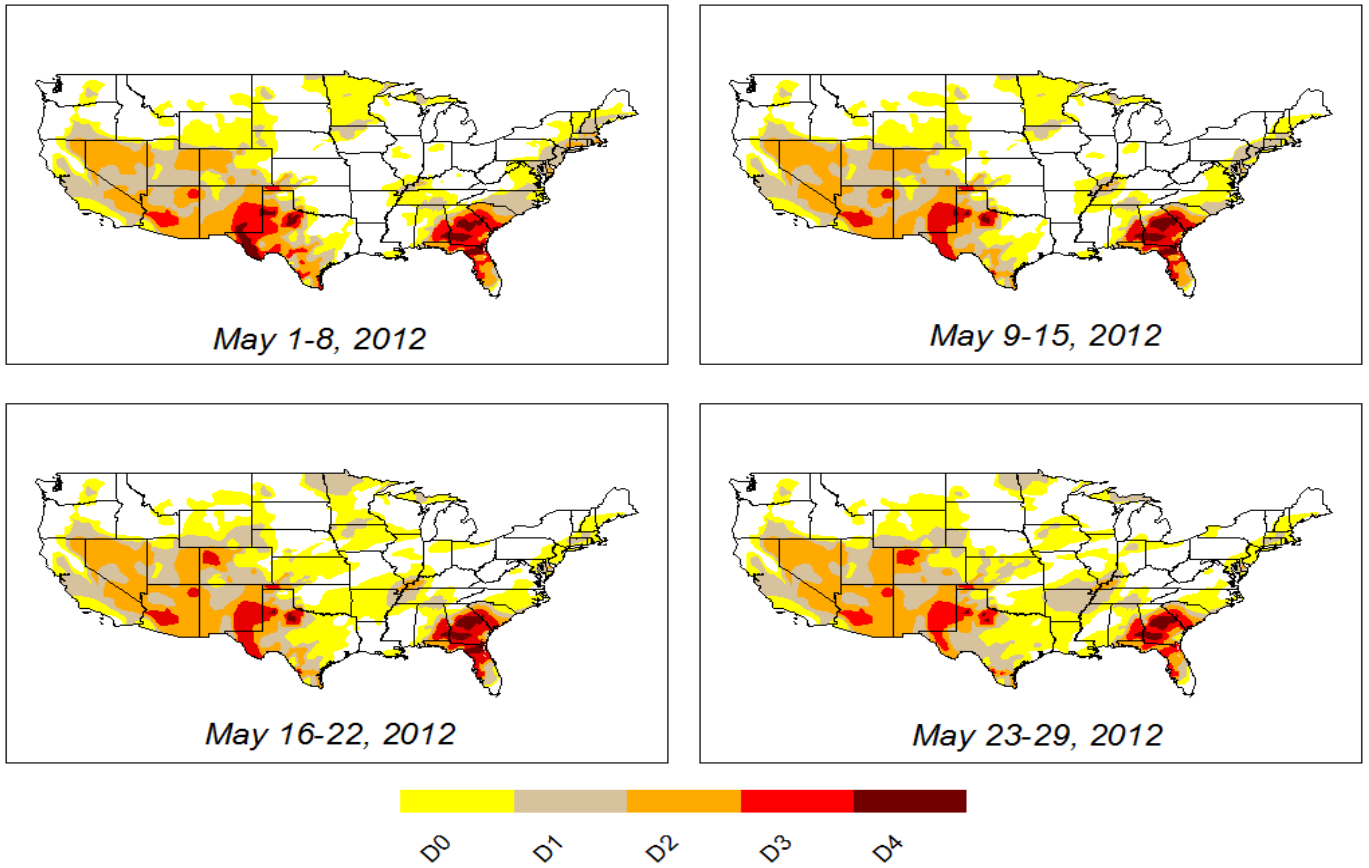

Figure 7-1. The USDM weekly drought monitoring for May 2012. The drought in Central U.S. is missed.

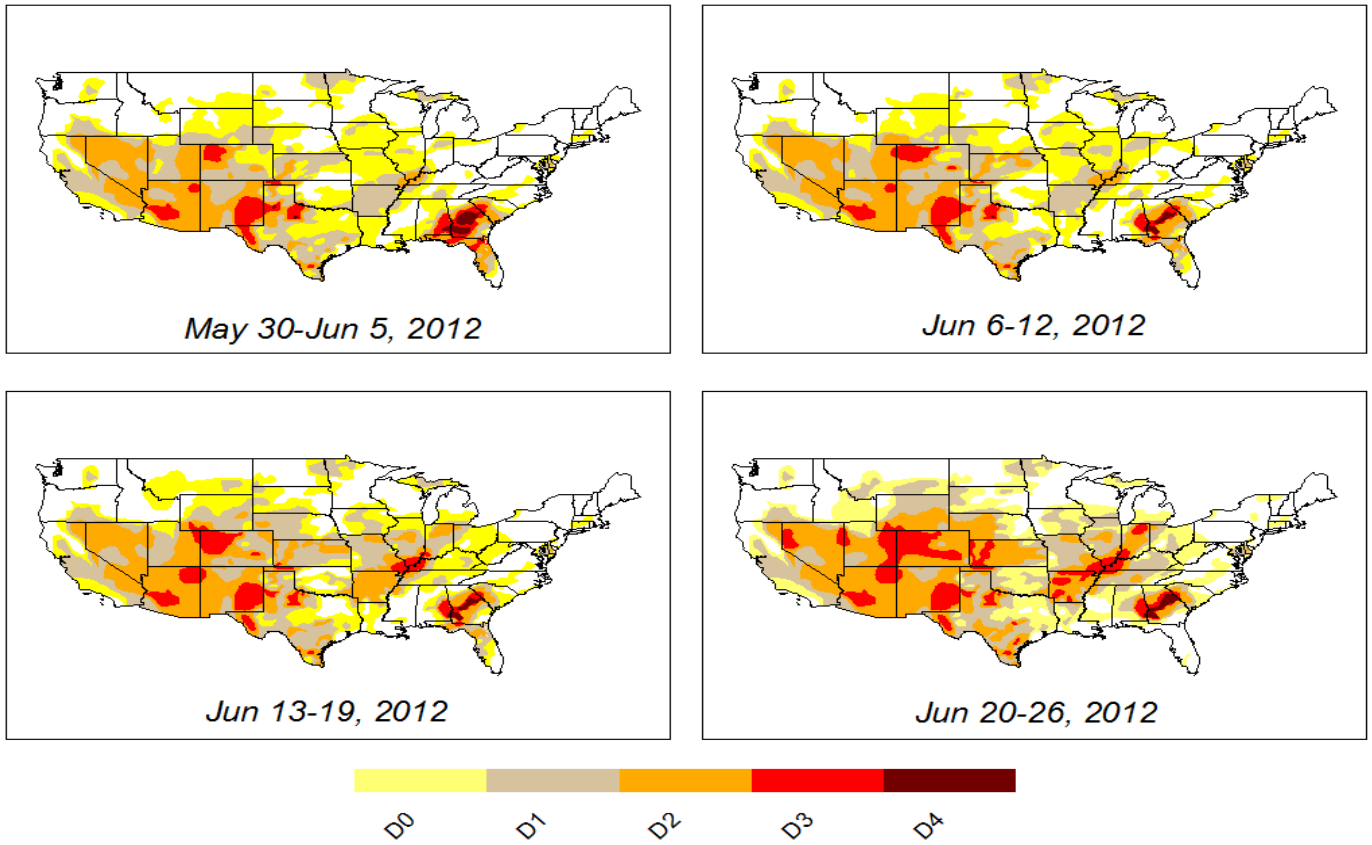

Figure 7-2. The USDM weekly drought monitoring for June 2012. The severe drought in Central U.S. is captured since June 26.

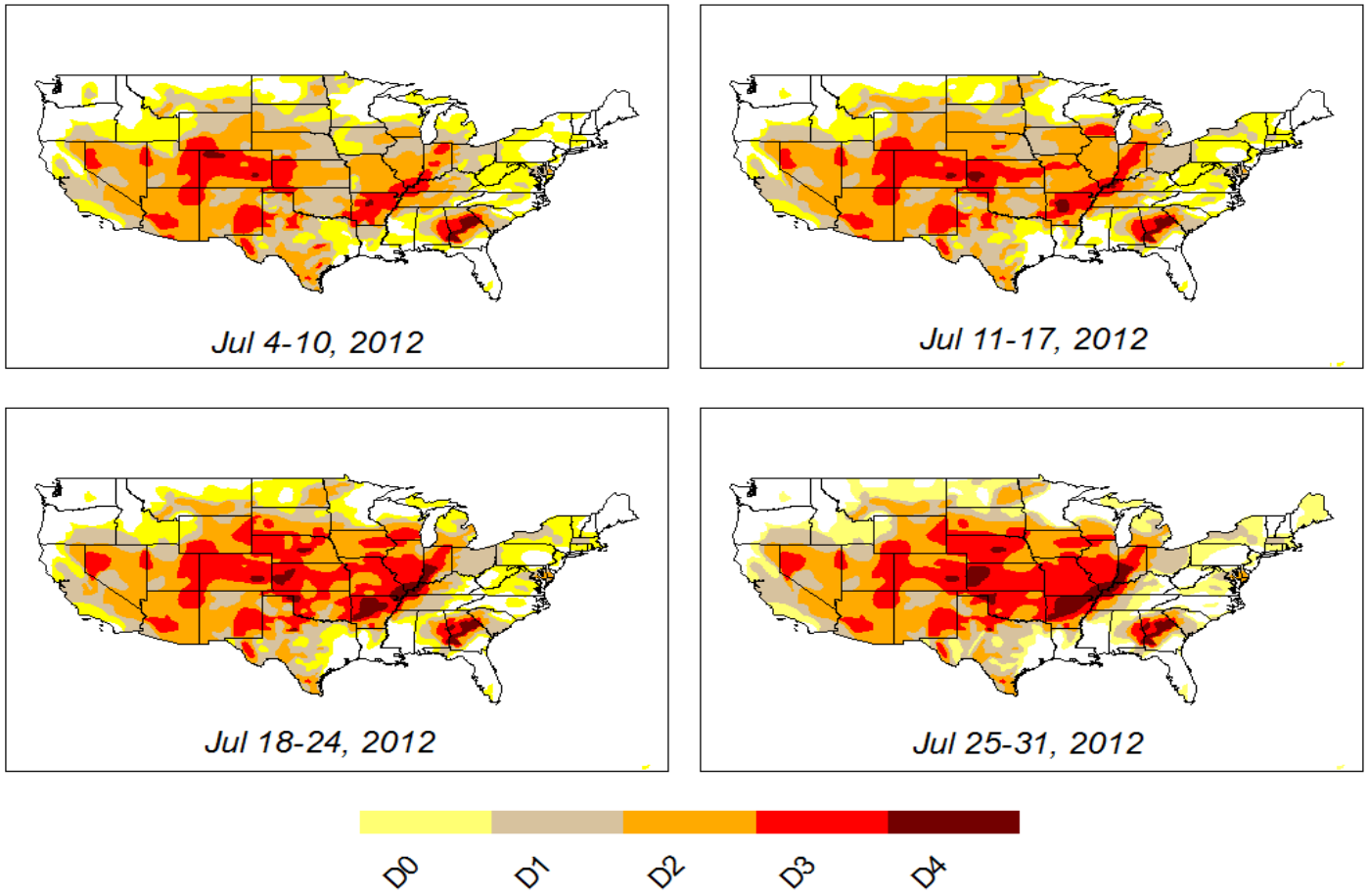

Figure 7-3. The USDM weekly drought monitoring for July 2012.

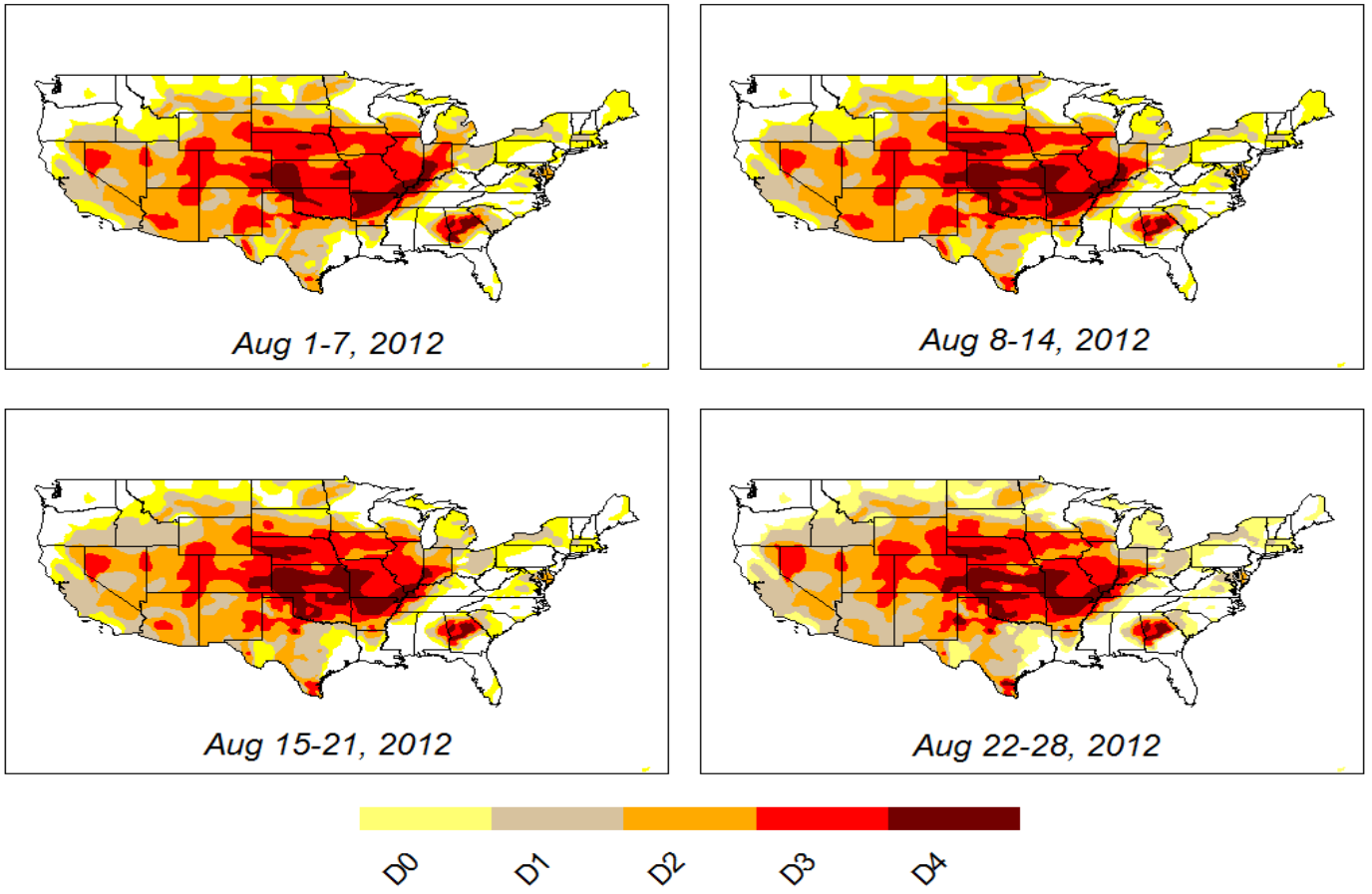

Figure 7-4. The USDM weekly drought monitoring for August 2012.

7.1 Drought Monitoring Results

Figure 7-5 presents the OL and DA monthly drought monitoring results across CONUS in May/June/July/August 2012. Note that the drought monitoring from the DA in these comparisons is generated using the posterior means. For the purpose of comparing drought intensity, the USDM weekly monitoring results are also presented in Figure 7-5. It is noted that the USDM results are not the "truth", since they are largely based on subjective information and did not capture the 2012 Central U.S. drought event until June 26, 2012 (Mo and Lettenmaier, 2015; Xiao et al., 2016).

Figure 7-5 illustrates the added impact of assimilation of remotely sensed soil moisture for improving drought monitoring skill. For the May 2012 case (the onset of the 2012 summer drought), the USDM completely missed the drought onset in the Central U.S. (such as Arkansas, Missouri, Oklahoma, and Kansas). Although the OL shows some improvements over the USDM, the soil moisture DA provides a better estimate of drought severity, especially for D0 and D1 categories (over Nebraska and Tennessee). For the August 2012 case (the 2012 drought event reached peak intensity in August), the USDM successfully captures this severe drought events in the Central U.S. whereas the OL underestimates the drought intensity and DA provides similar results as the USDM. Similar results can also be found in June and July 2012 cases. Overall, the DA estimation predicts more intense drought over the Central U.S. and does capture very well the spatial pattern of the intense drought relative to the OL.

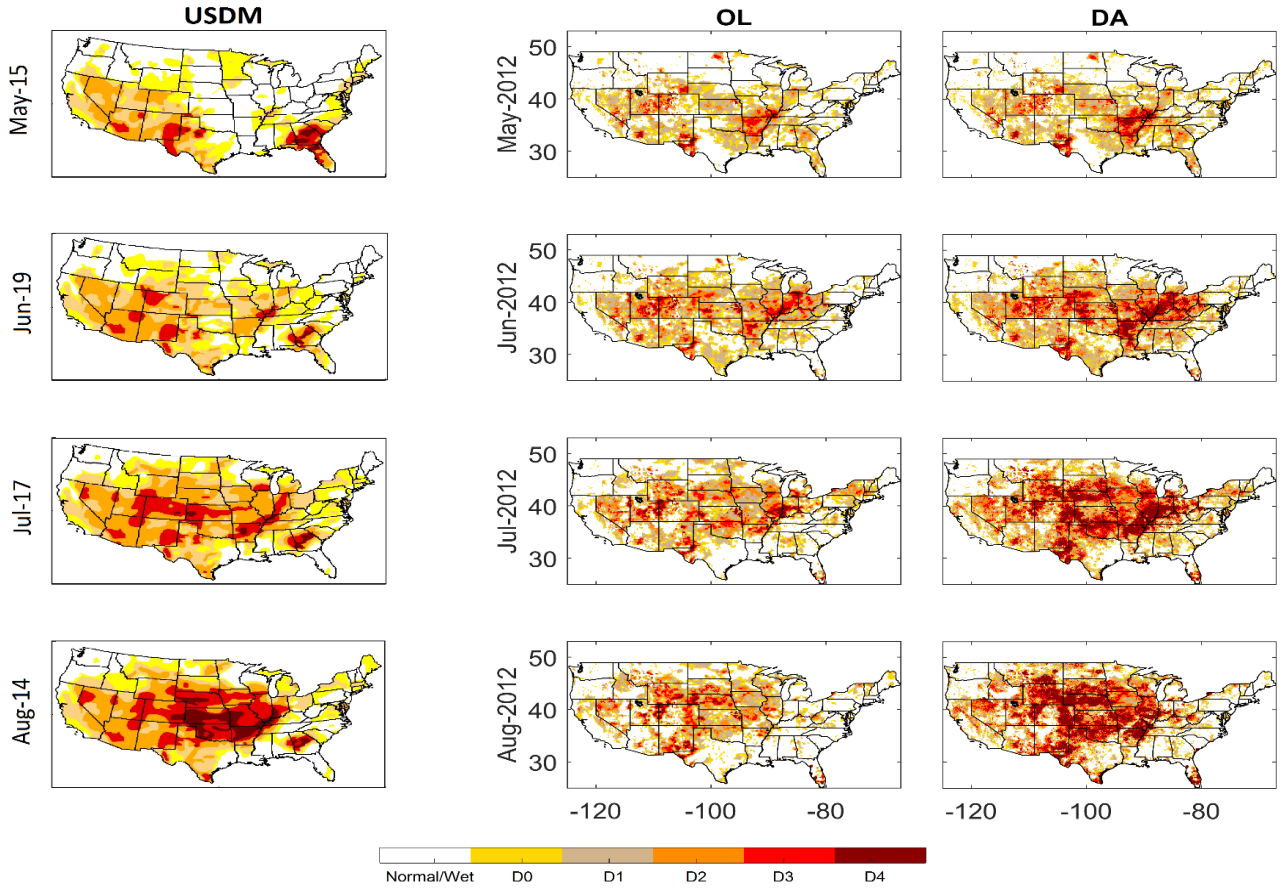

Figure 7-5. Comparison of the drought intensity over CONUS from OL, DA, and USDM.

Figure 7-6 summarizes the detected drought areas over CONUS based on OL, DA, and USDM. For the May 2012 case, the USDM missed the drought events in parts of the Central U.S., however, the DA helps to correct these biases. The detected drought areas over CONUS for OL and DA are 43.82% and 47.91%, respectively. For the August 2012 case, the OL underestimates the drought intensity whereas DA improves these representations. The detected drought areas increase from 48.17% in the OL to 62.66% after the DA, respectively. Similarly, the DA adds the drought monitoring skills for the June and July 2012 cases, from 55.27% and 54.45% by OL to 62.49% and 65.73% by DA. As a result, the DA provides a more accurate estimate of drought areas, more consistent with the USDM map, and the significant economic loss of this drought event.

In summary, compared with the OL, the DA systematically improves the drought monitoring skill for 2012 drought event from May to August. Compared with the USDM, the DA can better capture the drought onset in May and provide similar results in August. These results demonstrate the added-value of DA to facilitate the state drought preparation and effective response actions.

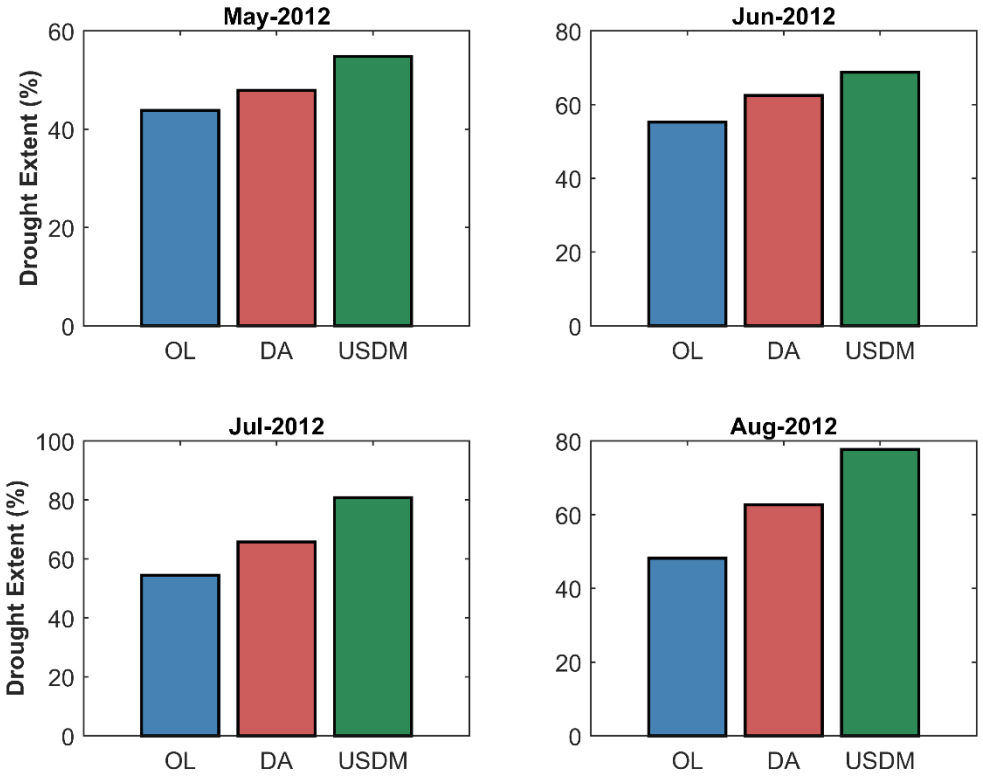

Figure 7-6. Comparison of the drought extent (%) over CONUS from OL, DA, and USDM.

7.2 Drought Forecasting Results

Since the NOAA CPC's SDO issued on 17 May 2012 failed to forecast the 2012 summer drought event, it is necessary to examine whether the proposed monthly/seasonal drought forecasting products can successfully forecast this drought event. Similar to the synthetic study, prior to investigating the monthly/seasonal drought forecasting results, it is necessary to compare the initial conditions of OL and DA. It is noted that the OL simulation in real case study is the synthetic truth in the synthetic study.

In Figure 7-7, the initial conditions (from February to April 2012) of the 13 basins for seasonal drought forecasting beginning on 1 May 2012 are presented. Each sub-plot contains the basin-averaged daily soil moisture for the OL, shown as a single value; and the DA, shown as a distribution of values, which represent the probability distribution of initial soil moisture values. Compared with the OL, the DA ensemble mean soil moisture mainly show lower values in basin 3 (GRB), basin 4 (COLOR), basin 6 (MO), basin 7 (ARK), basin 11 (LOW), and basin 13 (EAST), leading to higher drought risk in the Central U.S. and the Southeast in May-August 2012, which is more consistent with the real drought situations (Figures 7-1, 7-2, 7-3, 7-4).

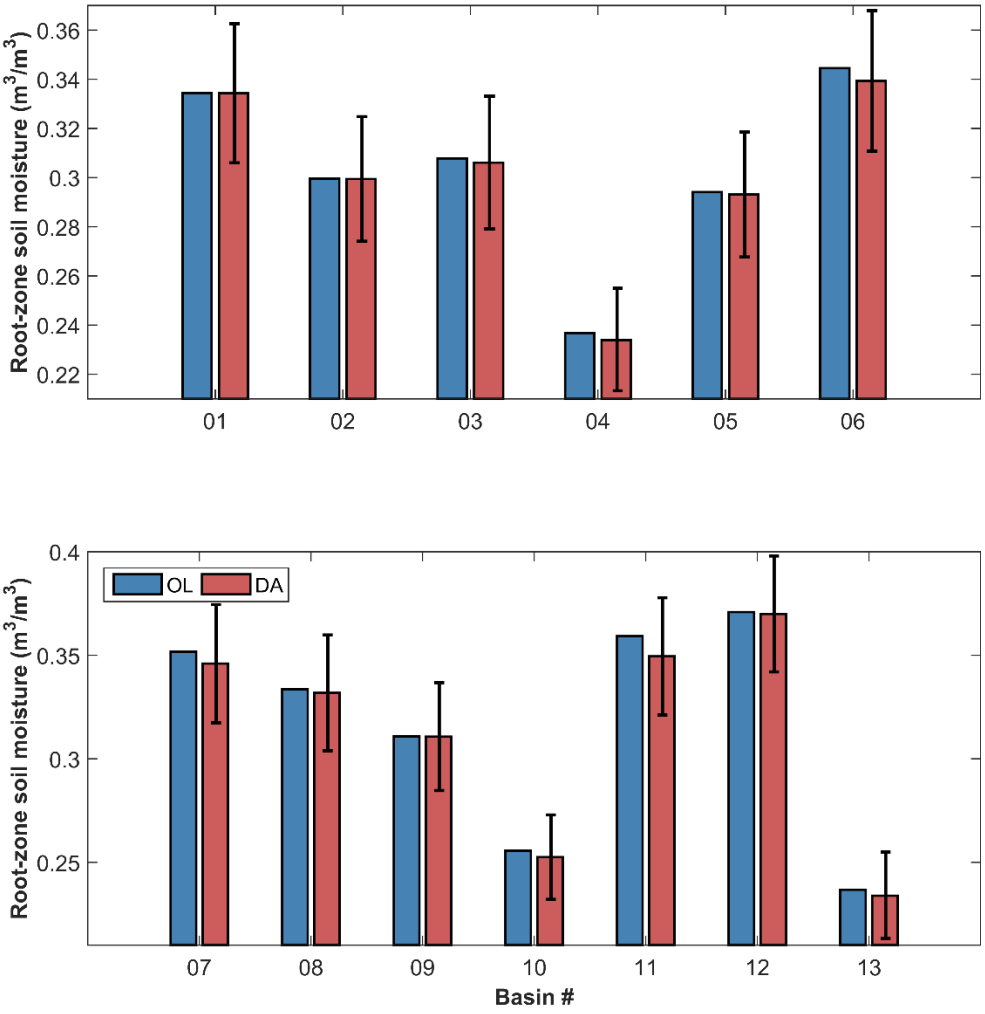

Figure 7-7. Comparison of the 13 basin-averaged daily root-zone soil moisture (m^3/m^3) by the open-loop (OL) and data assimilation (DA) for February to April 2012. The error bars show the 95% prediction intervals.

The same as the synthetic study, the multivariate copula model is developed based on the OL soil moisture simulation from 1 January 1980 to 31 December 2015. Given the drought condition in the current month/season, the probabilistic forecast of drought status in the following month/season is examined using soil moisture for each grid cell. The dependencies between monthly/seasonal aggregated soil moisture are modeled by a Gaussian copula while their marginal distributions are modeled with lognormal distributions. The method of sampling initial conditions from the estimated PDF is the same as in the synthetic study. Figures 7-8, 7-9, 7-10 present the spatial distributions of monthly (short-term), bimonthly (middle-term), and seasonal (long-term) drought forecasting probabilities, and the corresponding MLE forecasted drought types for May/May-June/May-July 2012, respectively. The MLE forecasted drought extent (%) over the CONUS between the OL and DA is shown in Figure 7-11.

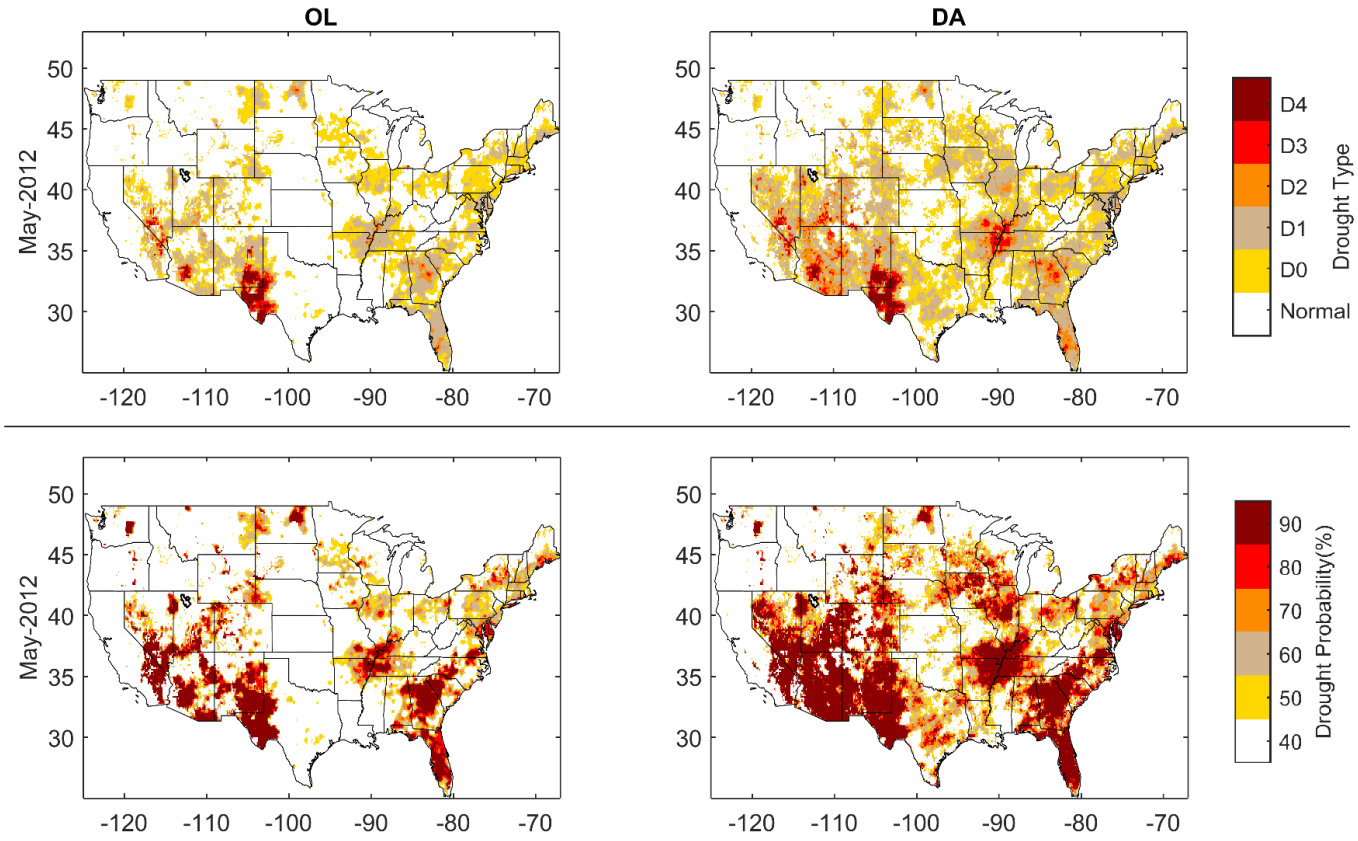

Figure 7-8. The monthly probabilistic drought forecast between OL and DA for May 2012. Top: the drought forecasting types based on MLE. Bottom: the probabilities under drought.

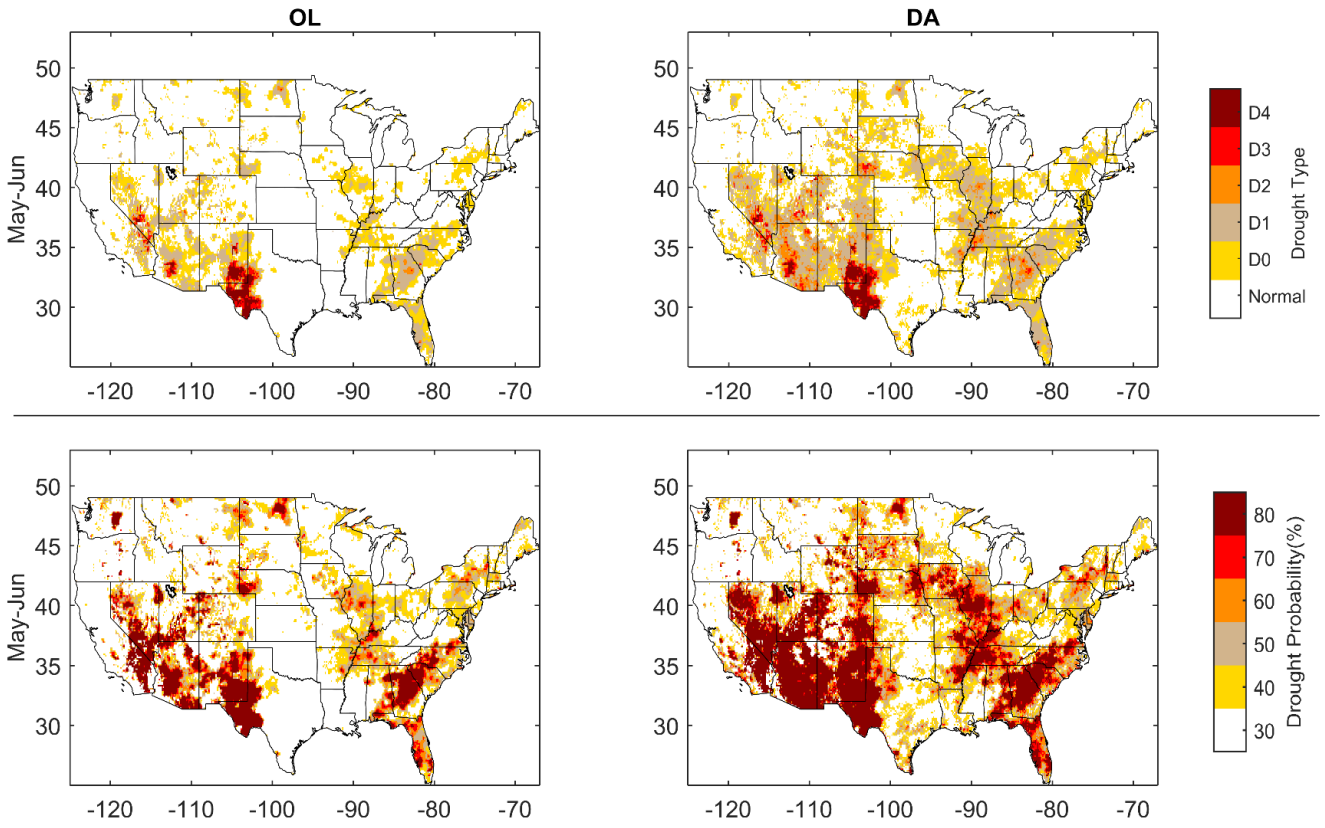

Figure 7-9. The bimonthly probabilistic drought forecast between OL and DA for May-June 2012. Top: the drought forecasting types based on MLE. Bottom: the probabilities under drought.

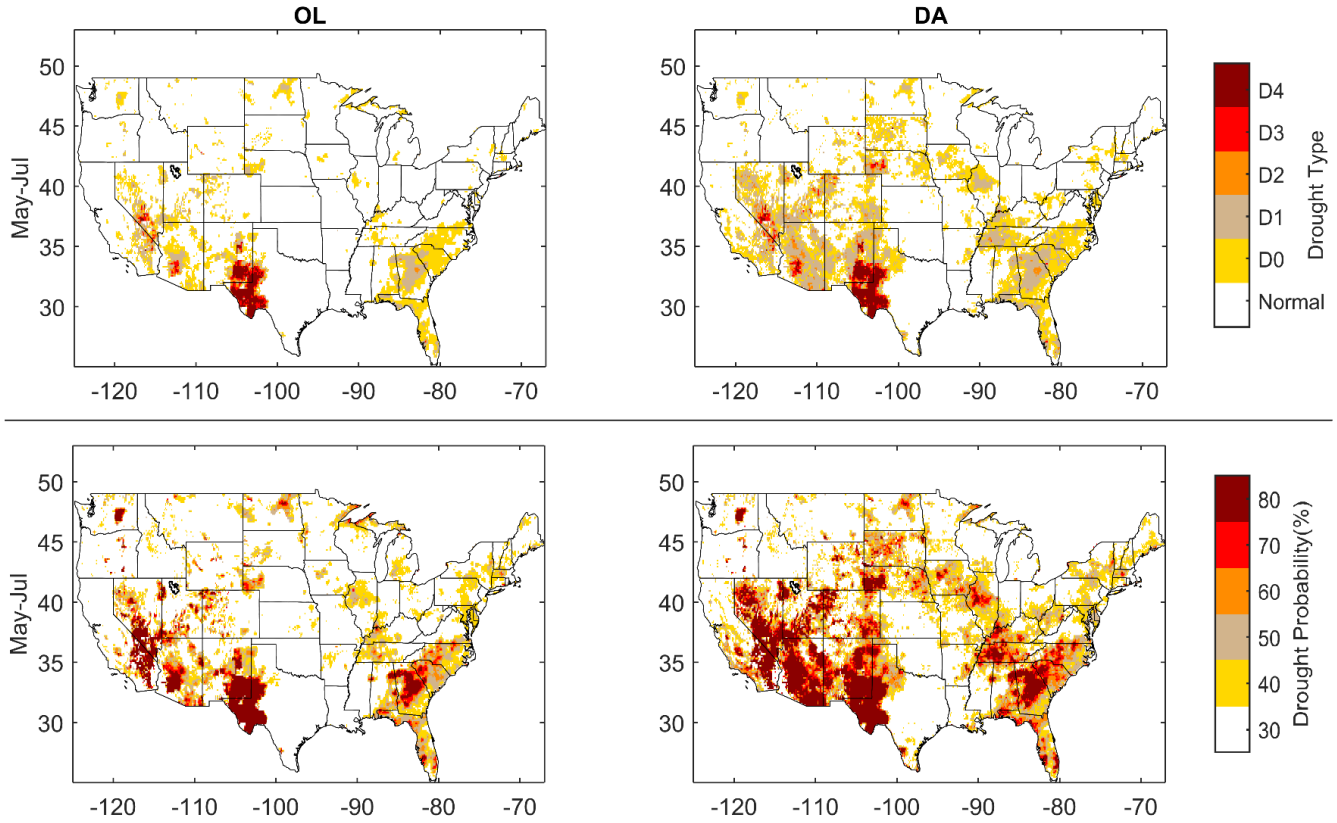

Figure 7-10. The seasonal probabilistic drought forecast between OL and DA for May-July 2012. Top: the drought forecasting types based on MLE. Bottom: the probabilities under drought.

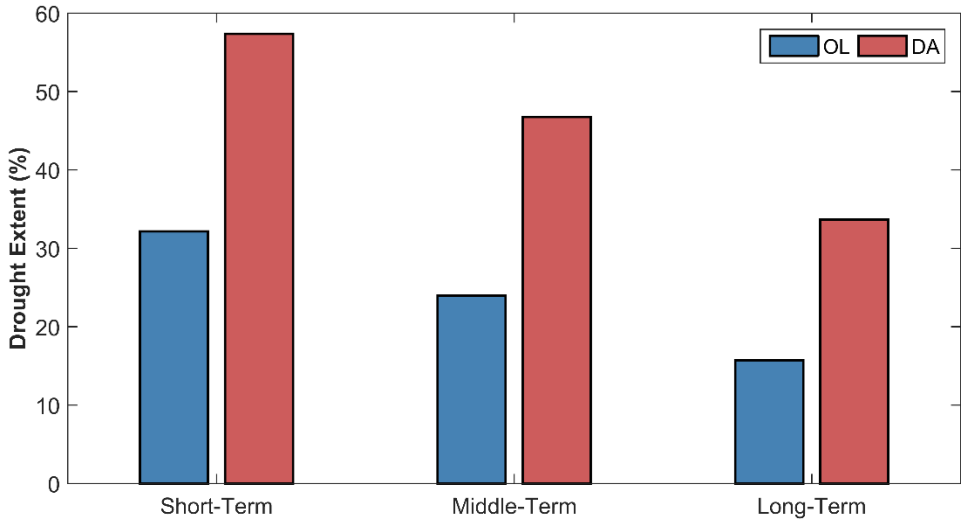

Figure 7-11. The forecasted drought extent between OL and DA based on MLE across CONUS for monthly (short-term), bimonthly (middle-term), and seasonal (long-term) forecast (according to the framework shown in Figure 2-7).

Based on Figure 7-8, for the May 2012 case, the DA suggests a high probability of drought across the Southwest (over Nevada, Utah, Arizona, and New Mexico) and the Central U.S. (over Colorado, Kansas, Iowa, Nebraska, and Arkansas). The OL forecasts underestimate the drought conditions over these regions whereas DA improves these representations. The Arkansas-Tennessee belt shows a probability of drought around 90% in May, indicating a higher risk of drought events. Therefore, the DA-based drought forecasts can improve the detection of the 2012 summer drought onset in May. In Figure 7-11, the MLE forecasted drought extents increase from 32.16% in the OL to 57.36% in the DA for May 2012. Similar patterns of improvements can also be observed in the bimonthly and seasonal drought forecasts in Figures 7-9 and 7-10. For the May-June 2012 case, the OL forecasted drought probability around the Arkansas-Tennessee belt is round 40%, and it increases to about 80% with DA. For the May-July 2012 case, the forecasted drought probability around the Arkansas-Tennessee belt increases from about 40% in the OL to 70% in the DA.

Based on these figures, it is also noted that several drought events in parts of the Central U.S. are also missed in the DA based MLE forecasted products, such as the Oklahoma and Kansas. This is mainly due to the model structure deficiency of the copula model, which means that the persistence of the soil moisture cannot predict the summer drought event in these regions. Although the drought events in Oklahoma and Kansas are underestimated among the monthly, bimonthly, and seasonal MLE forecasts, the DA still suggested higher drought probabilities (about 40%) in these regions than the OL forecasts (around 30%). From the Figure 7-11, the MLE bimonthly and seasonal forecasted

drought extents increase from 23.98% and 15.73% in the OL to 46.76% and 33.65% in the DA. It is also noted that both the OL and DA forecasted drought extents decrease from short- (monthly) to long-term (seasonal), indicating that the forecasting uncertainty increases from a short lead times (monthly) to a long lead times (seasonal).

Lastly, the comparison of the proposed DA seasonal drought forecast and the NOAA CPC's SDO is presented in Figure 7-12. From Figure 7-12, it is observed that both the SDO and the proposed drought forecast capture well the drought events in the Southwest (over south California, Nevada, Utah, Arizona, New Mexico, and parts of Texas) and the Southeast (over Florida, Georgia, North and South Carolina). However, there are three key differences between these two forecasts.

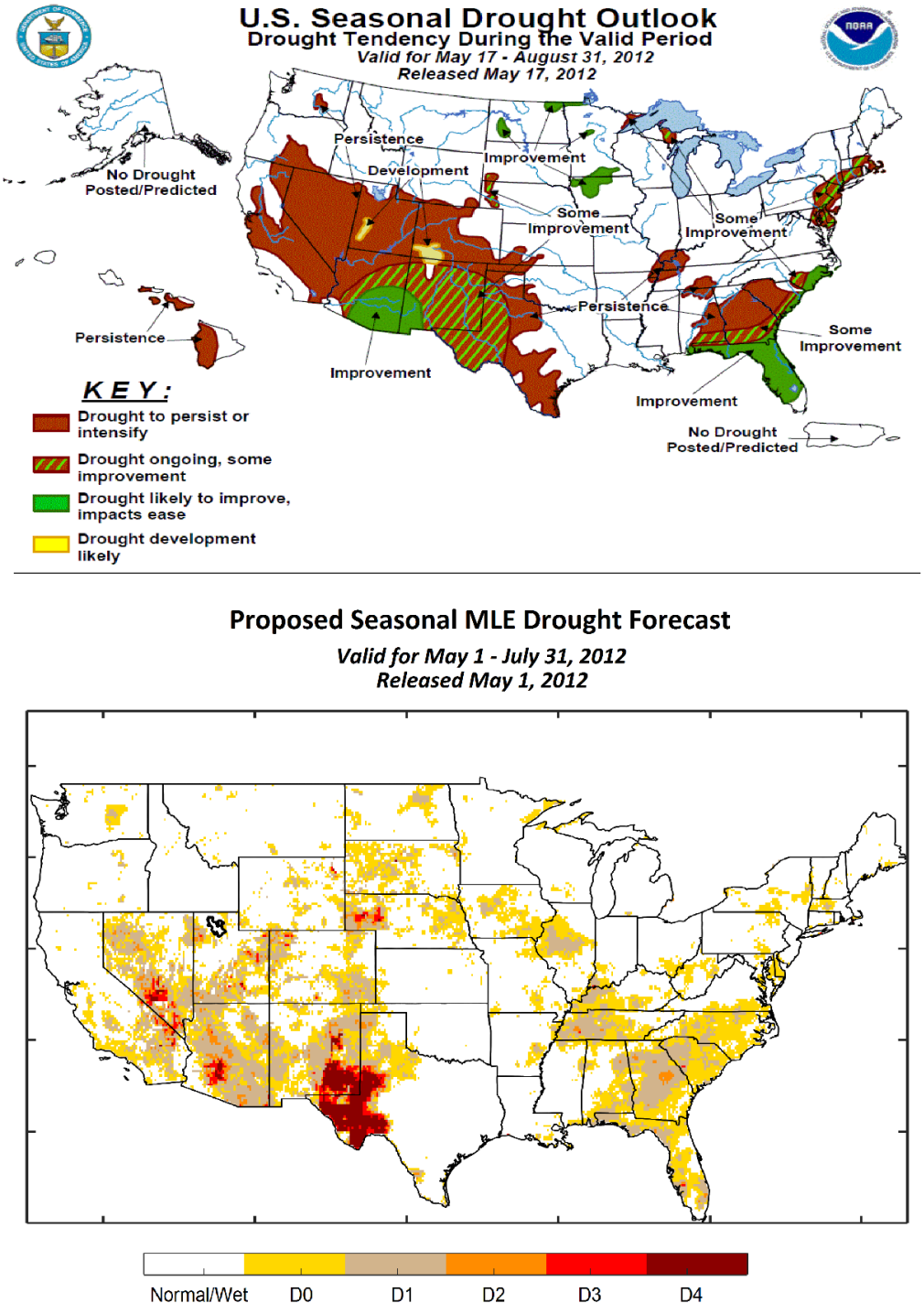

Figure 7-12. Comparison of the NOAA CPC's SDO and the proposed seasonal drought forecast based on MLE.

1). The SDO only forecasts drought persistent areas and drought ongoing areas, and does not provide the probability of under drought and the maximum likelihood drought intensity. The proposed drought forecast system can generate both the probabilities for areas under drought and the possible severity of future drought events. These two drought products can provide much more flexibility and information for decision makers and water resource managers. For instance, while the SDO forecasted the drought event in Arizona in summer 2012, decision makers did not have any more information about this future drought event. How much water should be cut from the reservoir release is still a question. However, this question can be better answered from the proposed drought forecast. The probability of under drought in Arizona in summer 2012 ranges from 40% to 80%, and the MLE forecasted drought event is classified as D1 category in most parts of Arizona. If the drought emergence plan of a reservoir can be classified into five categories (level 1 to level 5), then the decision maker can select the level 2 drought emergence plan.

2). The SDO completely misses the summer drought event in the Central U.S., while the proposed seasonal drought forecast partially captures this drought event. It is observed SDO forecasts normal/wet conditions in South Dakota, Nebraska, Kansas, Oklahoma, Iowa, Missouri, Arkansas, Tennessee, and Illinois, whereas DA improves these representations. Especially over the South Dakota, Nebraska, Iowa, Illinois, and Tennessee, the proposed system forecasts the D0 to D1 drought events in these regions. Although the seasonal forecast still does not capture the drought events in Kansas, Oklahoma, Missouri, and Arkansas, the predicted drought probabilities for these regions

are about 30%-40%, which still can give an early warning for decision makers to some extent.

3). The SDO was issued on May 17 where the drought event had already occurred and was developing, while the seasonal MLE drought forecast was issued on May 1 where the drought event had not occurred. Therefore, it is more difficult to forecast the summer drought event on May 1 than May 17, which demonstrates the efficiency of the proposed drought forecasting system from another perspective. In addition, only the seasonal MLE drought forecast is presented in Figure 7-12, however, there are other two drought forecasting products: monthly and bimonthly. Due to the persistence of soil moisture, the forecasting uncertainty is reduced from a seasonal product to a monthly product and the accuracy is in reverse (Figure 7-11). As discussed in the above paragraphs, the monthly drought forecasting products can detect the severe drought condition in most parts of the Central U.S. in May. Further, the three drought forecasting products can be used for three different purposes as mentioned in Section 2.6. The monthly forecasting products can be used for irrigation, reservoir operations, and water supply plans. The bimonthly and seasonal forecasting products offer the seasonal drought information in an earlier time manner (up to three-month preparation time), and can be used for drought risk assessment and drought preparation.

In summary, in terms of both forecasted probabilities and MLE forecasted drought extents, the DA forecasts show the improved estimation of drought onset in the Central U.S. and are more consistent with the USDM map and the significant economic loss. Compared to OL forecasts, the DA monthly, bimonthly, and seasonal drought

forecasts show higher drought extents across the Central U.S. DA systematically improves the probability of detection for the onset of drought and the severity of the drought event. Compared to the CPC's SDO, the proposed DA-based drought forecasting products can better capture the drought events in the Central U.S., and they also allow for greater flexibility in the decision making process. These results demonstrate the added-value of DA to facilitate the drought detection, preparation, and effective response, at least one month before the severe damage occurs.

Lastly, there exists one issue which should be paid attention. The "false alarm" or "false positive", which indicates that the system over-forecasts the drought severity or forecasts a drought event while the drought event does not occur. Considering the huge negative impact of a "false negative" in the 2012 summer drought case, it is therefore that the primary objective of this dissertation is to investigate whether the proposed system can successfully forecast this drought event. However, since the study region is the CONUS, the "false positive" issue can also be examined at the same time. For instance, the 2012 summer drought did not cover the PNW Region. From Figure 7-10, it is noted that the Oregon, Washington, and Idaho States are forecasted to have very few drought regions in May-July 2012, and both OL and DA generate similar drought forecasts. From Figure 7-12, it is also noted that the NOAA SDO and the proposed system provide similar drought forecast in PNW and almost all the areas in PNW are forecasted to have non-droughts. These results further support the efficiency of the proposed system in drought forecasting. It is also noted that in this dissertation, the proposed system is only

examined using two drought case studies. Obviously, more studies are need to further verify the drought forecasting skills.

Chapter 8 Conclusions and Future Study

In this dissertation, a land data assimilation based drought monitoring system and a hybrid dynamical-statistical drought forecasting system are proposed to improve the drought monitoring and forecasting skill. Besides the drought monitoring system, the hybrid drought forecasting system is a combination of dynamical and statistical framework. The dynamical hydrologic modeling is coupled with the copula-based statistical forecasting. Moreover, the ensemble data assimilation technique is used to improve state initialization in the copula-based probabilistic forecasting framework by allowing for uncertainty in the initial condition. These proposed drought monitoring and forecasting systems are implemented over the Columbia River Basin and Contiguous United States. The impact of assimilating remotely sensed surface soil moisture on improving soil moisture predictions and drought monitoring; quantifying the initial condition uncertainty; and their subsequent contributions toward an improved forecasting of agricultural droughts are examined. Results from both synthetic and real case studies suggest that the proposed drought monitoring and forecasting system significantly improve agricultural drought monitoring and the seasonal agricultural drought forecasting skills, and can facilitate the state drought preparation and declaration. Similar to what has been explained here, other satellite or in-situ data, e.g. precipitation and total water storage, can also be assimilated in the same way to improve the forecasting of meteorological and hydrological droughts.

One limitation of this study is the multiscale issue, where the spatial resolution of the assimilated satellite observations (coarse resolution ~25 km) is different from the

model output resolution (fine resolution ~10 km). To further improve the DA performance and the drought forecasting skill, a machine learning technique can be incorporated in the system to downscale the satellite data from coarse resolution to fine resolution (Piles et al., 2011; Rodriguez-Fernandez et al., 2015). Another improvement that can be added to the proposed system is to use vine copula model in the drought forecasting model (Kurowicka, 2010). The advantage of vine copula is the capability to establish a high-dimensional multivariate probabilistic model. In this way, the drought statuses in the future can be inferred from the current drought statuses from multi-aspects, such as precipitation anomaly and soil moisture, leading to a higher drought forecasting skill.

References

Ahmadalipour, A., Moradkhani, H., Svoboda, M., 2016. Centennial drought outlook over the CONUS using NASA-NEX downscaled climate ensemble. Int. J. Climatol. doi:10.1002/joc.4859

Ahmadalipour, A., Moradkhani, H., Yan, H., Zarekarizi, M., 2017. Remote sensing of drought: vegetation, soil moisture, and data assimilation, in: Lakshmi, V. (Ed.), Remote Sensing of Hydrological Extremes. Springer International Publishing Switzerland, pp. 121–149. doi:10.1007/978-3-319-43744-6_7

Albergel, C., Rüdiger, C., Carrer, D., Calvet, J.-C., Fritz, N., Naeimi, V., Bartalis, Z., Hasenauer, S., 2009. An evaluation of ASCAT surface soil moisture products with in-situ observations in Southwestern France. Hydrol. Earth Syst. Sci. 13, 115–124. doi:10.5194/hess-13-115-2009

Andrieu, C., Doucet, A., Holenstein, R., 2010. Particle Markov chain Monte Carlo methods. J. R. Stat. Soc. Ser. B (Statistical Methodol. 72, 269–342. doi:10.1111/j.1467-9868.2009.00736.x

Beven, K.J., 2006. A manifesto for the equifinality thesis. J. Hydrol. 320, 18–36. doi:10.1016/j.jhydrol.2005.07.007

Brocca, L., Moramarco, T., Melone, F., Wagner, W., Hasenauer, S., Hahn, S., 2012. Assimilation of surface- and root-zone ASCAT soil moisture products into rainfall-runoff modeling. IEEE Trans. Geosci. Remote Sens. 50, 2542–2555. doi:10.1109/TGRS.2011.2177468

Champagne, C., McNairn, H., Berg, A. a., 2011. Monitoring agricultural soil moisture

extremes in Canada using passive microwave remote sensing. Remote Sens. Environ. 115, 2434–2444. doi:10.1016/j.rse.2011.04.030

Cheng, L., Hoerling, M., AghaKouchak, A., Livneh, B., Quan, X.-W., Eischeid, J., 2016. How has human-induced climate change affected California drought risk? J. Clim. 29, 111–120. doi:10.1175/JCLI-D-15-0260.1

Clark, M.P., Fan, Y., Lawrence, D.M., Adam, J.C., Bolster, D., Gochis, D.J., Hooper, R.P., Kumar, M., Leung, L.R., Mackay, D.S., Maxwell, R.M., Shen, C., Swenson, S.C., Zeng, X., 2015. Improving the representation of hydrologic processes in Earth System Models. Water Resour. Res. 51, 5929–5956. doi:10.1002/2015WR017096

Crow, W.T., Kustas, W.P., Prueger, J.H., 2008. Monitoring root-zone soil moisture through the assimilation of a thermal remote sensing-based soil moisture proxy into a water balance model. Remote Sens. Environ. 112, 1268–1281. doi:10.1016/j.rse.2006.11.033

Dai, A., Trenberth, K.E., Qian, T., 2004. A global dataset of Palmer Drought Severity Index for 1870–2002: Relationship with soil moisture and effects of surface warming. J. Hydrometeorol. 5, 1117–1130. doi:10.1175/JHM-386.1

Day, G.N., 1985. Extended streamflow forecasting using NWSRFS. J. Water Resour. Plan. Manag. 111, 157–170. doi:10.1061/(ASCE)0733-9496(1985)111:2(157)

De Lannoy, G.J.M., Reichle, R.H., Arsenault, K.R., Houser, P.R., Kumar, S., Verhoest, N.E.C., Pauwels, V.R.N., 2012. Multiscale assimilation of Advanced Microwave Scanning Radiometer–EOS snow water equivalent and Moderate Resolution Imaging Spectroradiometer snow cover fraction observations in northern Colorado.

Water Resour. Res. 48, W01522. doi:10.1029/2011WR010588

DeChant, C.M., and H. Moradkhani, 2015a. On the Assessment of Reliability in Probabilistic Hydro-meteorological Event Forecasting, Water Resources Research, 51(6), 3867-3883, doi: 10.1002/2014WR016617

DeChant, C.M., Moradkhani, H., 2015b. Analyzing the sensitivity of drought recovery forecasts to land surface initial conditions. J. Hydrol. 526, 89–100. doi:10.1016/j.jhydrol.2014.10.021

DeChant, C.M., Moradkhani, H., 2014a. Hydrologic prediction and uncertainty quantification, in: Eslamian, S. (Ed.), Handbook of Engineering Hydrology. CRC press, pp. 387–414.

DeChant, C.M., Moradkhani, H., 2014b. Toward a reliable prediction of seasonal forecast uncertainty: Addressing model and initial condition uncertainty with ensemble data assimilation and sequential Bayesian combination. J. Hydrol. 519, 2967–2977. doi:10.1016/j.jhydrol.2014.05.045

DeChant, C.M., Moradkhani, H., 2012. Examining the effectiveness and robustness of sequential data assimilation methods for quantification of uncertainty in hydrologic forecasting. Water Resour. Res. 48, W04518. doi:10.1029/2011WR011011

DeChant, C.M., Moradkhani, H., 2011a. Improving the characterization of initial condition for ensemble streamflow prediction using data assimilation. Hydrol. Earth Syst. Sci. 15, 3399–3410. doi:10.5194/hess-15-3399-2011

DeChant, C.M., Moradkhani, H., 2011b. Radiance data assimilation for operational snow and streamflow forecasting. Adv. Water Resour. 34, 351–364.

doi:10.1016/j.advwatres.2010.12.009

Dee, D.P., Da Silva, A.M., 1998. Data assimilation in the presence of forecast bias. Q. J. R. Meteorol. Soc. 124, 269–295. doi:10.1002/qj.49712454512

Demirel, M.C., Moradkhani, H., 2016. Assessing the impact of CMIP5 climate multi-modeling on estimating the precipitation seasonality and timing. Clim. Change 135, 357–372. doi:10.1007/s10584-015-1559-z

Dong, J., Steele-Dunne, S.C., Judge, J., van de Giesen, N., 2015. A particle batch smoother for soil moisture estimation using soil temperature observations. Adv. Water Resour. 83, 111–122. doi:10.1016/j.advwatres.2015.05.017

Dorigo, W.A., Gruber, A., De Jeu, R.A.M., Wagner, W., Stacke, T., Loew, A., Albergel, C., Brocca, L., Chung, D., Parinussa, R.M., Kidd, R., 2015. Evaluation of the ESA CCI soil moisture product using ground-based observations. Remote Sens. Environ. 162, 380–395. doi:10.1016/j.rse.2014.07.023

Doucet, A., Johansen, A., 2011. A tutorial on particle filtering and smoothing: fifteen years later, in: The Oxford Handbook of Nonlinear Filtering. Oxford University Press, pp. 656–704.

Duan, Q., Sorooshian, S., Gupta, V.K., 1994. Optimal use of the SCE-UA global optimization method for calibrating watershed models. J. Hydrol. 158, 265–284. doi:10.1016/0022-1694(94)90057-4

Dutra, E., Viterbo, P., Miranda, P.M.A., 2008. ERA-40 reanalysis hydrological applications in the characterization of regional drought. Geophys. Res. Lett. 35, L19402. doi:10.1029/2008GL035381

Entekhabi, D., Njoku, E.G., O'Neill, P.E., Kellogg, K.H., Crow, W.T., Edelstein, W.N., Entin, J.K., Goodman, S.D., Jackson, T.J., Johnson, J., Kimball, J., Piepmeier, J.R., Koster, R.D., Martin, N., McDonald, K.C., Moghaddam, M., Moran, S., Reichle, R., Shi, J.C., Spencer, M.W., Thurman, S.W., Tsang, L., Van Zyl, J., 2010. The soil moisture active passive (SMAP) mission. Proc. IEEE 98, 704–716. doi:10.1109/JPROC.2010.2043918

Evensen, G., 1994. Sequential data assimilation with a nonlinear quasi-geostrophic model using Monte Carlo methods to forecast error statistics. J. Geophys. Res. 99, 10143–10162. doi:10.1029/94JC00572

Farnsworth, R.K., Thompson, E.S., Peck, E.L., 1982. Evaporation Atlas for the Contiguous 48 United States. NOAA Technical Report NWS 33.

Griffin, D., Anchukaitis, K.J., 2014. How unusual is the 2012-2014 California drought? Geophys. Res. Lett. 41, 9017–9023. doi:10.1002/2014GL062433

Gupta, H. V., Kling, H., Yilmaz, K.K., Martinez, G.F., 2009. Decomposition of the mean squared error and NSE performance criteria: Implications for improving hydrological modelling. J. Hydrol. 377, 80–91. doi:10.1016/j.jhydrol.2009.08.003

Gupta, H. V., Wagener, T., Liu, Y., 2008. Reconciling theory with observations: Elements of a diagnostic approach to model evaluation. Hydrol. Process. 22, 3802–3813. doi:10.1002/hyp.6989.

Halmstad, A., M.R. Najafi, and H. Moradkhani, 2012. Analysis of Precipitation Extremes with the Assessment of Regional Climate Models over the Willamette River Basin-U.S., Hydrological Processes, 27, 2579–2590, doi: 10.1002/hyp.937.

Hamlet, A.F., Lettenmaier, D.P., 1999. Effects of climate change on hydrology and water resources in the Columbia River basin. J. Am. Water Resour. Assoc. 35, 1597–1623. doi:10.1111/j.1752-1688.1999.tb04240.x

Han, X., Franssen, H.J.H., Montzka, C., Vereecken, H., 2014. Soil moisture and soil properties estimation in the Community Land Model with synthetic brightness temperature observations. Water Resour. Res. 50, 6081–6105. doi:10.1002/2013WR014586

Hao, Z., AghaKouchak, A., 2013. Multivariate standardized drought index: A parametric multi-index model. Adv. Water Resour. 57, 12–18. doi:10.1016/j.advwatres.2013.03.009

Hay, L.E., Umemoto, M., 2006. Multiple-objective stepwise calibration using Luca. US Geological Survey.

Hayes, M., Svoboda, M., Le Comte, D., Redmond, K.T., Pasteris, P., 2005. Drought monitoring: New tools for the 21st century, in: Wihite, D.A. (Ed.), Drought and Water Crises: Science, Technology, and Management Issues. CRC Press, pp. 53–69.

Hey, T., Tansley, S., Tolle, K., 2009. The fourth paradigm: data-intensive scientific discovery, 1st ed, Microsoft Research.

Hillier, D., Dempsey, B., 2012. A dangerous delay: The cost of late response to early warnings in the 2011 drought in the Horn of Africa. Oxfam Policy Pract. Agric. Food L. 12, 1–34.

Hoerling, M., Eischeid, J., Kumar, A., Leung, R., Mariotti, A., Mo, K., Schubert, S., Seager, R., 2014. Causes and predictability of the 2012 Great Plains drought. Bull.

Am. Meteorol. Soc. 95, 269–282. doi:10.1175/BAMS-D-13-00055.1

Howitt, R., MacEwan, D., Medellín-Azuara, J., Lund, J., Sumner, D., 2015. Economic analysis of the 2015 drought for California agriculture. Univ. California, Davis.

Hut, R., Amisigo, B.A., Steele-Dunne, S., van de Giesen, N., 2015. Reduction of used memory ensemble Kalman filtering (RumEnKF): A data assimilation scheme for memory intensive, high performance computing. Adv. Water Resour. 86, 273–283. doi:10.1016/j.advwatres.2015.09.007

Imaoka, K., Kachi, M., Kasahara, M., Ito, N., Nakagawa, K., Oki, T., 2010. Instrument performance and calibration of AMSR-E and AMSR2. Int. Arch. Photogramm. Remote Sens. Spat. Inf. Sci. - ISPRS Arch. 38, 13–16.

Jackson, T.J., Cosh, M.H., Bindlish, R., Starks, P.J., Bosch, D.D., Seyfried, M., Goodrich, D.C., Moran, M.S., Du, J., 2010. Validation of advanced microwave scanning radiometer soil moisture products. IEEE Trans. Geosci. Remote Sens. 48, 4256–4272. doi:10.1109/TGRS.2010.2051035

Jaeger, W.K., A. Platinga, H. Chang, J. McDonnell H. Moradkhani, D. Hulse, R. Hagerty, et al. (2013), Toward a formal definition of water scarcity in natural-human systems, *Water Resources Research*, vol. 49, 1–12, doi:10.1002/wrcr.20249.

Kerr, Y.H., Waldteufel, P., Wigneron, J.-P., Delwart, S., Cabot, F., Boutin, J., Escorihuela, M.-J., Font, J., Reul, N., Gruhier, C., Juglea, S.E., Drinkwater, M.R., Hahne, A., Martín-Neira, M., Mecklenburg, S., 2010. The SMOS mission: new tool for monitoring key elements of the global water cycle. Proc. IEEE 98, 666–687. doi:10.1109/JPROC.2010.2043032

Keyantash, J., Dracup, J.A., 2002. The quantification of drought: An evaluation of drought indices. Bull. Am. Meteorol. Soc. 83, 1167–1180. doi:10.1175/1520-0477(2002)083<1191:TQODAE>2.3.CO;2

Koster, R.D., Mahanama, S.P.P., Yamada, T.J., Balsamo, G., Berg, A.A., Boisserie, M., Dirmeyer, P.A., Doblas-Reyes, F.J., Drewitt, G., Gordon, C.T., Guo, Z., Jeong, J.-H., Lawrence, D.M., Lee, W.-S., Li, Z., Luo, L., Malyshev, S., Merryfield, W.J., Seneviratne, S.I., Stanelle, T., van den Hurk, B.J.J.M., Vitart, F., Wood, E.F., 2010. Contribution of land surface initialization to subseasonal forecast skill: First results from a multi-model experiment. Geophys. Res. Lett. 37, L02402. doi:10.1029/2009GL041677

Kumar, S. V., Harrison, K.W., Peters-Lidard, C.D., Santanello, J. a., Kirschbaum, D., 2014a. Assessing the impact of L-band observations on drought and flood risk estimation: A decision-theoretic approach in an OSSE environment. J. Hydrometeorol. 15, 2140–2156. doi:10.1175/JHM-D-13-0204.1

Kumar, S. V., Peters-Lidard, C.D., Mocko, D., Reichle, R., Liu, Y., Arsenault, K.R., Xia, Y., Ek, M., Riggs, G., Livneh, B., Cosh, M., 2014b. Assimilation of remotely sensed soil moisture and snow depth retrievals for drought estimation. J. Hydrometeorol. 15, 2446–2469. doi:10.1175/JHM-D-13-0132.1

Kumar, S. V., Reichle, R.H., Koster, R.D., Crow, W.T., Peters-Lidard, C.D., 2009. Role of subsurface physics in the assimilation of surface soil moisture observations. J. Hydrometeorol. 10, 1534–1547. doi:10.1175/2009JHM1134.1

Kumar, S. V., Zaitchik, B.F., Peters-Lidard, C.D., Rodell, M., Reichle, R., Li, B.,

Jasinski, M., Mocko, D., Getirana, A., De Lannoy, G., Cosh, M.H., Hain, C.R., Anderson, M., Arsenault, K.R., Xia, Y., Ek, M., 2016. Assimilation of gridded GRACE terrestrial water storage estimates in the North American Land Data Assimilation System. J. Hydrometeorol. 17, 1951–1972. doi:10.1175/JHM-D-15-0157.1

Kurowicka, D., 2010. Dependence modeling: vine copula handbook. World Scientific Publishing Company.

Kurtz, W., He, G., Kollet, S.J., Maxwell, R.M., Vereecken, H., Franssen, H.J.H., 2016. TerrSysMP-PDAF (version 1.0): A modular high-performance data assimilation framework for an integrated land surface-subsurface model. Geosci. Model Dev. 9, 1341–1360. doi:10.5194/gmd-9-1341-2016

Leavesley, G.H., Lichty, R.W., Thoutman, B.M., Saindon, L.G., 1983. Precipitation-runoff modeling system: User's manual. US Geological Survey Colorado, CO.

Leisenring, M., Moradkhani, H., 2012. Analyzing the uncertainty of suspended sediment load prediction using sequential data assimilation. J. Hydrol. 468-469, 268–282. doi:10.1016/j.jhydrol.2012.08.049

Leisenring, M., Moradkhani, H., 2011. Snow water equivalent prediction using Bayesian data assimilation methods. Stoch. Environ. Res. Risk Assess. 25, 253–270. doi:10.1007/s00477-010-0445-5

Li, F., Crow, W.T., Kustas, W.P., 2010. Towards the estimation root-zone soil moisture via the simultaneous assimilation of thermal and microwave soil moisture retrievals. Adv. Water Resour. 33, 201–214. doi:10.1016/j.advwatres.2009.11.007

Li, H., Luo, L., Wood, E.F., Schaake, J., 2009. The role of initial conditions and forcing uncertainties in seasonal hydrologic forecasting. J. Geophys. Res. 114, D04114. doi:10.1029/2008JD010969

Liang, X., Lettenmaier, D.P., Wood, E.F., Burges, S.J., 1994. A simple hydrologically based model of land surface water and energy fluxes for general circulation models. J. Geophys. Res. 99, 14415–14428. doi:10.1029/94JD00483

Liang, X., Xie, Z., 2001. A new surface runoff parameterization with subgrid-scale soil heterogeneity for land surface models. Adv. Water Resour. 24, 1173–1193. doi:10.1016/S0309-1708(01)00032-X

Liu, Q., Reichle, R.H., Bindlish, R., Cosh, M.H., Crow, W.T., de Jeu, R., De Lannoy, G.J.M., Huffman, G.J., Jackson, T.J., 2011. The contributions of precipitation and soil moisture observations to the skill of soil moisture estimates in a land data assimilation system. J. Hydrometeorol. 12, 750–765. doi:10.1175/JHM-D-10-05000.1

Liu, X., Luo, Y., Yang, T., Liang, K., Zhang, M., Liu, C., 2015. Investigation of the probability of concurrent drought events between the water source and destination regions of China's water diversion project. Geophys. Res. Lett. 42, 8424–8431. doi:10.1002/2015GL065904

Liu, Y., Weerts, a. H., Clark, M., Hendricks Franssen, H.J., Kumar, S., Moradkhani, H., Seo, D.J., Schwanenberg, D., Smith, P., Van Dijk, a. I.J.M., Van Velzen, N., He, M., Lee, H., Noh, S.J., Rakovec, O., Restrepo, P., 2012. Advancing data assimilation in operational hydrologic forecasting: Progresses, challenges, and emerging

opportunities. Hydrol. Earth Syst. Sci. 16, 3863–3887. doi:10.5194/hess-16-3863-2012

Liu, Y.Y., Dorigo, W.A., Parinussa, R.M., De Jeu, R.A.M., Wagner, W., McCabe, M.F., Evans, J.P., Van Dijk, A.I.J.M., 2012. Trend-preserving blending of passive and active microwave soil moisture retrievals. Remote Sens. Environ. 123, 280–297. doi:10.1016/j.rse.2012.03.014

Liu, Y.Y., Parinussa, R.M., Dorigo, W. a., De Jeu, R. a M., Wagner, W., M. Van Dijk, a. I.J., McCabe, M.F., Evans, J.P., 2011. Developing an improved soil moisture dataset by blending passive and active microwave satellite-based retrievals. Hydrol. Earth Syst. Sci. 15, 425–436. doi:10.5194/hess-15-425-2011

Lloyd-Hughes, B., 2014. The impracticality of a universal drought definition. Theor. Appl. Climatol. 117, 607–611. doi:10.1007/s00704-013-1025-7

Lohmann, D., Raschke, E., Nijssen, B., Lettenmaier, D.P., 1998. Regional scale hydrology: I. Formulation of the VIC-2L model coupled to a routing model. Hydrol. Sci. J. 43, 131–141. doi:10.1080/02626669809492107

Luo, L., Wood, E.F., 2007. Monitoring and predicting the 2007 U.S. drought. Geophys. Res. Lett. 34, L22702. doi:10.1029/2007GL031673

Madadgar, S., Moradkhani, H., 2016. Copula function and drought, in: Handbook of Drought and Water Scarcity, Vol. 1: Principles of Drought and Water Scarcity. Francis and Taylor.

Madadgar, S., Moradkhani, H., 2014a. Spatio-temporal drought forecasting within Bayesian networks. J. Hydrol. 512, 134–146. doi:10.1016/j.jhydrol.2014.02.039

Madadgar, S., Moradkhani, H., 2014b. Improved Bayesian multimodeling: Integration of copulas and Bayesian model averaging. Water Resour. Res. 50, 9586–9603. doi:10.1002/2014WR015965

Madadgar, S., Moradkhani, H., 2013a. A Bayesian framework for probabilistic seasonal drought forecasting. J. Hydrometeorol. 14, 1685–1705. doi:10.1175/JHM-D-13-010.1

Madadgar, S., Moradkhani, H., 2013b. Drought analysis under climate change using copula. J. Hydrol. Eng. 18, 746–759. doi:10.1061/(ASCE)HE.1943-5584.0000532

Madadgar, S., Moradkhani, H., Garen, D., 2014. Towards improved post-processing of hydrologic forecast ensembles. Hydrol. Process. 28, 104–122. doi:10.1002/hyp.9562

Mao, Y., Nijssen, B., Lettenmaier, D.P., 2015. Is climate change implicated in the 2013–2014 California drought? A hydrologic perspective. Geophys. Res. Lett. 42, 2805–2813. doi:10.1002/2015GL063456

Markstrom, S.L., Niswonger, R.G., Regan, R.S., Prudic, D.E., Barlow, P.M., 2008. GSFLOW-coupled ground-water and surface-water FLOW model based on the integration of the Precipitation-Runoff Modeling System (PRMS) and the Modular Ground-Water Flow Model (MODFLOW-2005). US Geological Survey.

Markstrom, S.L., Regan, R.S., Hay, L.E., Viger, R.J., Webb, R.M., Payn, R.A., LaFontaine, J.H., 2015. PRMS-IV, the precipitation-runoff modeling system, version 4. US Geological Survey.

Massari, C., Brocca, L., Tarpanelli, A., Moramarco, T., 2015. Data assimilation of satellite soil moisture into rainfall-runoff modelling: A complex recipe? Remote

Sens. 7, 11403–11433. doi:10.3390/rs70911403

Maurer, E.P., Wood, A.W., Adam, J.C., Lettenmaier, D.P., Nijssen, B., 2002. A long-term hydrologically based dataset of land surface fluxes and states for the Conterminous United States*. J. Clim. 15, 3237–3251. doi:10.1175/1520-0442(2002)015<3237:ALTHBD>2.0.CO;2

Mendoza, P.A., Clark, M.P., Barlage, M., Rajagopalan, B., Samaniego, L., Abramowitz, G., Gupta, H., 2015. Are we unnecessarily constraining the agility of complex process-based models? Water Resour. Res. 51, 716–728. doi:10.1002/2014WR015820

Milly, P.C.D., Betancourt, J., Falkenmark, M., Hirsch, R.M., Kundzewicz, Z.W., Lettenmaier, D.P., Stouffer, R.J., 2008. Stationarity is dead: whither water management? Science (80-.). 319, 573–574. doi:10.1126/science.1151915

Mishra, A.K., Desai, V.R., 2005. Drought forecasting using stochastic models. Stoch. Environ. Res. Risk Assess. 19, 326–339. doi:10.1007/s00477-005-0238-4

Mishra, A.K., Singh, V.P., 2011. Drought modeling – A review. J. Hydrol. 403, 157–175. doi:10.1016/j.jhydrol.2011.03.049

Mishra, A.K., Singh, V.P., 2010. A review of drought concepts. J. Hydrol. 391, 202–216. doi:10.1016/j.jhydrol.2010.07.012

Mishra, V., Cherkauer, K.A., 2010. Retrospective droughts in the crop growing season: Implications to corn and soybean yield in the Midwestern United States. Agric. For. Meteorol. 150, 1030–1045. doi:10.1016/j.agrformet.2010.04.002

Mo, K.C., Lettenmaier, D.P., 2015. Heat wave flash droughts in decline. Geophys. Res.

Lett. 42, 2823–2829. doi:10.1002/2015GL064018

Montzka, C., Moradkhani, H., Weihermüller, L., Franssen, H.-J.H., Canty, M., Vereecken, H., 2011. Hydraulic parameter estimation by remotely-sensed top soil moisture observations with the particle filter. J. Hydrol. 399, 410–421. doi:10.1016/j.jhydrol.2011.01.020

Moradkhani, H., 2008. Hydrologic remote sensing and land surface data assimilation. Sensors 8, 2986–3004. doi:10.3390/s8052986

Moradkhani, H., Dechant, C.M., Sorooshian, S., 2012. Evolution of ensemble data assimilation for uncertainty quantification using the particle filter-Markov chain Monte Carlo method. Water Resour. Res. 48, W12520. doi:10.1029/2012WR012144

Moradkhani, H., Hsu, K.-L., Gupta, H., Sorooshian, S., 2005a. Uncertainty assessment of hydrologic model states and parameters: Sequential data assimilation using the particle filter. Water Resour. Res. 41, W05012. doi:10.1029/2004WR003604

Moradkhani, H., Sorooshian, S., 2008. General review of rainfall-runoff modeling: model calibration, data assimilation, and uncertainty analysis, in: Hydrological Modelling and the Water Cycle. Springer Berlin Heidelberg, pp. 1–24.

Moradkhani, H., Sorooshian, S., Gupta, H. V., Houser, P.R., 2005b. Dual state-parameter estimation of hydrological models using ensemble Kalman filter. Adv. Water Resour. 28, 135–147. doi:10.1016/j.advwatres.2004.09.002

Nerger, L., Hiller, W., 2013. Software for ensemble-based data assimilation systems-Implementation strategies and scalability. Comput. Geosci. 55, 110–118. doi:10.1016/j.cageo.2012.03.026

Nicolai-Shaw, N., Gudmundsson, L., Hirschi, M., Seneviratne, S.I., 2016. Long-term predictability of soil moisture dynamics at the global scale: Persistence versus large-scale drivers. Geophys. Res. Lett. 43, 8554–8562. doi:10.1002/2016GL069847

Njoku, E.G., Jackson, T.J., Lakshmi, V., Chan, T.K., Nghiem, S. V., 2003. Soil moisture retrieval from AMSR-E. IEEE Trans. Geosci. Remote Sens. 41, 215–228. doi:10.1109/TGRS.2002.808243

Omernik, J.M., Bailey, R.G., 1997. Distinguishing between watersheds and ecoregions. J. Am. Water Resour. Assoc. 33, 935–949. doi:10.1111/j.1752-1688.1997.tb04115.x

Owe, M., de Jeu, R., Holmes, T., 2008. Multisensor historical climatology of satellite-derived global land surface moisture. J. Geophys. Res. Earth Surf. 113. doi:10.1029/2007JF000769

PaiMazumder, D., Done, J.M., 2016. Potential predictability sources of the 2012 US drought in observations and a regional model ensemble. J. Geophys. Res. Atmos. doi:10.1002/2016JD025322

Pan, M., Wood, E.F., 2010. Impact of accuracy, spatial availability, and revisit time of satellite-derived surface soil moisture in a multiscale ensemble data assimilation system. IEEE J. Sel. Top. Appl. Earth Obs. Remote Sens. 3, 49–56. doi:10.1109/JSTARS.2010.2040585

Pan, M., Yuan, X., Wood, E.F., 2013. A probabilistic framework for assessing drought recovery. Geophys. Res. Lett. 40, 3637–3642. doi:10.1002/grl.50728

Pathiraja, S., Marshall, L., Sharma, A., Moradkhani, H., 2016a. Hydrologic modeling in dynamic catchments: A data assimilation approach. Water Resour. Res. 52, 3350–

3372. doi:10.1002/2015WR017192

Pathiraja, S., Marshall, L., Sharma, A., Moradkhani, H., 2016b. Detecting non-stationary hydrologic model parameters in a paired catchment system using data assimilation. Adv. Water Resour. 94, 103–119. doi:10.1016/j.advwatres.2016.04.021

Pickering, K.T., Owen, L.A., 1997. An introduction to global environmental issues, 2nd ed. Routledge.

Piles, M., Camps, A., Vall-llossera, M., Corbella, I., Panciera, R., Rudiger, C., Kerr, Y.H., Walker, J., 2011. Downscaling SMOS-derived soil moisture using MODIS visible/infrared data. IEEE Trans. Geosci. Remote Sens. 49, 3156–3166. doi:10.1109/TGRS.2011.2120615

Plaza, D.A., De Keyser, R., De Lannoy, G.J.M., Giustarini, L., Matgen, P., Pauwels, V.R.N., 2012. The importance of parameter resampling for soil moisture data assimilation into hydrologic models using the particle filter. Hydrol. Earth Syst. Sci. 16, 375–390. doi:10.5194/hess-16-375-2012s

Rana, A., Moradkhani, H., Qin, Y., 2016. Understanding the joint behavior of temperature and precipitation for climate change impact studies. Theor. Appl. Climatol. doi:10.1007/s00704-016-1774-1.

Rana, A., and H. Moradkhani (2016), Spatial, temporal and frequency based climate change assessment in Columbia River Basin using multi downscaled-Scenarios, *Climate Dynamics*, 47:579–600, DOI: 10.1007/s00382-015-2857-x.

Reichle, R.H., Crow, W.T., Keppenne, C.L., 2008. An adaptive ensemble Kalman filter for soil moisture data assimilation. Water Resour. Res. 44, W03423.

doi:10.1029/2007WR006357

Reichle, R.H., Kumar, S. V., Mahanama, S.P.P., Koster, R.D., Liu, Q., 2010. Assimilation of satellite-derived skin temperature observations into land surface models. J. Hydrometeorol. 11, 1103–1122. doi:10.1175/2010JHM1262.1

Risley, J., H. Moradkhani, L. Hay, and S. Markstrom 2011. Statistical Trends in Watershed Scale Response to Climate Change in Selected Basins Across the United States, AMS Earth Interaction, 15 (14) 1-26, doi: 10.1175/2010EI364.1.

Rodriguez-Fernandez, N.J., Aires, F., Richaume, P., Kerr, Y.H., Prigent, C., Kolassa, J., Cabot, F., Jimenez, C., Mahmoodi, A., Drusch, M., 2015. Soil moisture retrieval using neural networks: application to SMOS. IEEE Trans. Geosci. Remote Sens. 53, 5991–6007. doi:10.1109/TGRS.2015.2430845

Rosero, E., Yang, Z.-L., Wagener, T., Gulden, L.E., Yatheendradas, S., Niu, G.-Y., 2010. Quantifying parameter sensitivity, interaction, and transferability in hydrologically enhanced versions of the Noah land surface model over transition zones during the warm season. J. Geophys. Res. 115, D03106. doi:10.1029/2009JD012035

Ross, T., Lott, N., 2003. A climatology of 1980-2003 extreme weather and climate events. National Ocanic and Atmospheric Administration.

Samaniego, L., Kumar, R., Zink, M., 2013. Implications of parameter uncertainty on soil moisture drought analysis in Germany. J. Hydrometeorol. 14, 47–68. doi:10.1175/JHM-D-12-075.1

Seneviratne, S.I., Corti, T., Davin, E.L., Hirschi, M., Jaeger, E.B., Lehner, I., Orlowsky, B., Teuling, A.J., 2010. Investigating soil moisture-climate interactions in a

changing climate: A review. Earth-Science Rev. 99, 125–161. doi:10.1016/j.earscirev.2010.02.004

Sheffield, J., Wood, E.F., 2011. Drought: past problems and future scenarios. Routledge.

Sheffield, J., Wood, E.F., 2008. Global trends and variability in soil moisture and drought characteristics, 1950–2000, from observation-driven simulations of the terrestrial hydrologic cycle. J. Clim. 21, 432–458. doi:10.1175/2007JCLI1822.1

Sheffield, J., Wood, E.F., Chaney, N., Guan, K., Sadri, S., Yuan, X., Olang, L., Amani, A., Ali, A., Demuth, S., Ogallo, L., 2014. A drought monitoring and forecasting system for sub-sahara african water resources and food security. Bull. Am. Meteorol. Soc. 95, 861–882. doi:10.1175/BAMS-D-12-00124.1

Shukla, S., Lettenmaier, D.P., 2011. Seasonal hydrologic prediction in the United States: Understanding the role of initial hydrologic conditions and seasonal climate forecast skill. Hydrol. Earth Syst. Sci. 15, 3529–3538. doi:10.5194/hess-15-3529-2011

Shukla, S., Sheffield, J., Wood, E.F., Lettenmaier, D.P., 2013. On the sources of global land surface hydrologic predictability. Hydrol. Earth Syst. Sci. 17, 2781–2796. doi:10.5194/hess-17-2781-2013

Shukla, S., Steinemann, A.C., Lettenmaier, D.P., 2011. Drought monitoring for Washington State: indicators and applications. J. Hydrometeorol. 12, 66–83. doi:10.1175/2010JHM1307.1

Sklar, A., 1959. Fonctions de répartition à n dimensions et leurs marges. Publ. l'Institut Stat. l'Université Paris 8, 229–231.

Stainforth, D.A., Aina, T., Christensen, C., Collins, M., Faull, N., Frame, D.J.,

Kettleborough, J. a, Knight, S., Martin, A., Murphy, J.M., Piani, C., Sexton, D., Smith, L. a, Spicer, R. a, Thorpe, a J., Allen, M.R., 2005. Uncertainty in predictions of the climate response to rising levels of greenhouse gases. Nature 433, 403–406. doi:10.1038/nature03301

Steinemann, A.C., 2006. Using climate forecasts for drought management. J. Appl. Meteorol. Climatol. 45, 1353–1361. doi:10.1175/JAM2401.1

Svoboda, M., LeComte, D., Hayes, M., Heim, R., Gleason, K., Angel, J., Rippey, B., Tinker, R., Palecki, M., Stooksbury, D., Miskus, D., Stephens, S., 2002. The drought monitor. Bull. Am. Meteorol. Soc. 83, 1181–1190. doi:10.1175/1520-0477(2002)083<1181:TDM>2.3.CO;2

Thiboult, A., Anctil, F., 2015. On the difficulty to optimally implement the ensemble Kalman filter: An experiment based on many hydrological models and catchments. J. Hydrol. 529, 1147–1160. doi:10.1016/j.jhydrol.2015.09.036

Van Loon, A.F., 2015. Hydrological drought explained. Wiley Interdiscip. Rev. Water 2, 359–392. doi:10.1002/wat2.1085

Viger, R.J., 2014. Preliminary spatial parameters for PRMS based on the Geospatial Fabric, NLCD2001 and SSURGO. US Geol. Surv. doi:10.5066/F7WM1BF7

Wagner, W., Hahn, S., Kidd, R., Melzer, T., Bartalis, Z., Hasenauer, S., Figa-Saldaña, J., De Rosnay, P., Jann, A., Schneider, S., Komma, J., Kubu, G., Brugger, K., Aubrecht, C., Züger, J., Gangkofner, U., Kienberger, S., Brocca, L., Wang, Y., Blöschl, G., Eitzinger, J., Steinnocher, K., Zeil, P., Rubel, F., 2013. The ASCAT soil moisture product: A review of its specifications, validation results, and emerging

applications. Meteorol. Zeitschrift 22, 5–33. doi:10.1127/0941-2948/2013/0399

Wagner, W., Naeimi, V., Scipal, K., Jeu, R., Martínez-Fernández, J., 2007. Soil moisture from operational meteorological satellites. Hydrogeol. J. 15, 121–131. doi:10.1007/s10040-006-0104-6

Wang, A., Bohn, T.J., Mahanama, S.P., Koster, R.D., Lettenmaier, D.P., 2009. Multimodel ensemble reconstruction of drought over the continental United States. J. Clim. 22, 2694–2712. doi:10.1175/2008JCLI2586.1

Washington Department of Agriculture, 2015. Interim report: 2015 drought and agriculture.

WCRP, 2010. Drought predictability and prediction in a changing climate: assessing current capabilities, World Climate Research Programme. Barcelona, Spain.

Wilhite, D.A., 2000. Drought as a natural hazard: concepts and definitions, in: Wilhite, D.A. (Ed.), Drought: A Global Assessment. Routledge, London, pp. 3–18.

Wood, A.W., Lettenmaier, D.P., 2008. An ensemble approach for attribution of hydrologic prediction uncertainty. Geophys. Res. Lett. 35, L14401. doi:10.1029/2008GL034648

Wood, A.W., Lettenmaier, D.P., 2006. A test bed for new seasonal hydrologic forecasting approaches in the Western United States. Bull. Am. Meteorol. Soc. 87, 1699–1712. doi:10.1175/BAMS-87-12-1699

Wood, A.W., Schaake, J.C., 2008. Correcting errors in streamflow forecast ensemble mean and spread. J. Hydrometeorol. 9, 132–148. doi:10.1175/2007JHM862.1

Wood, E.F., Roundy, J.K., Troy, T.J., van Beek, L.P.H., Bierkens, M.F.P., Blyth, E., de

Roo, A., Döll, P., Ek, M., Famiglietti, J., Gochis, D., van de Giesen, N., Houser, P., Jaffé, P.R., Kollet, S., Lehner, B., Lettenmaier, D.P., Peters-Lidard, C., Sivapalan, M., Sheffield, J., Wade, A., Whitehead, P., 2011. Hyperresolution global land surface modeling: Meeting a grand challenge for monitoring Earth's terrestrial water. Water Resour. Res. 47, W05301. doi:10.1029/2010WR010090

Wood, E.F., Schubert, S.D., Wood, A.W., Peters-Lidard, C.D., Mo, K.C., Mariotti, A., Pulwarty, R.S., 2015. Prospects for advancing drought understanding, monitoring, and prediction. J. Hydrometeorol. 16, 1636–1657. doi:10.1175/JHM-D-14-0164.1

Xia, Y., Mitchell, K., Ek, M., Sheffield, J., Cosgrove, B., Wood, E., Luo, L., Alonge, C., Wei, H., Meng, J., Livneh, B., Lettenmaier, D., Koren, V., Duan, Q., Mo, K., Fan, Y., Mocko, D., 2012. Continental-scale water and energy flux analysis and validation for the North American Land Data Assimilation System project phase 2 (NLDAS-2): 1. Intercomparison and application of model products. J. Geophys. Res. Atmos. 117, D03109. doi:10.1029/2011JD016048

Xia, Y., Sheffield, J., Ek, M.B., Dong, J., Chaney, N., Wei, H., Meng, J., Wood, E.F., 2014. Evaluation of multi-model simulated soil moisture in NLDAS-2. J. Hydrol. 512, 107–125. doi:10.1016/j.jhydrol.2014.02.027

Xiao, M., Nijssen, B., Lettenmaier, D.P., 2016. Drought in the Pacific Northwest, 1920–2013. J. Hydrometeorol. 17, 2391–2404. doi:10.1175/JHM-D-15-0142.1

Yan, H., 2012. Magnitude and frequency of floods for rural, unregulated streams of Tennessee by L-Moments method. University of Arkansas.

Yan, H., DeChant, C.M., Moradkhani, H., 2015. Improving soil moisture profile

prediction with the particle filter-Markov chain Monte Carlo method. IEEE Trans. Geosci. Remote Sens. 53, 6134–6147. doi:10.1109/TGRS.2015.2432067

Yan, H., Edwards, F.G., 2013. Effects of land use change on hydrologic response at a watershed scale, Arkansas. J. Hydrol. Eng. 18, 1779–1785. doi:10.1061/(ASCE)HE.1943-5584.0000743

Yan, H., Moradkhani, H., 2016a. Combined assimilation of streamflow and satellite soil moisture with the particle filter and geostatistical modeling. Adv. Water Resour. 94, 364–378. doi:10.1016/j.advwatres.2016.06.002

Yan, H., Moradkhani, H., 2016b. Toward more robust extreme flood prediction by Bayesian hierarchical and multimodeling. Nat. Hazards 81, 203–225. doi:10.1007/s11069-015-2070-6

Yan, H., Moradkhani, H., 2015. A regional Bayesian hierarchical model for flood frequency analysis. Stoch. Environ. Res. Risk Assess. 29, 1019–1036. doi:10.1007/s00477-014-0975-3

Yan, H., Moradkhani, H., 2014. Bayesian model averaging for flood frequency analysis, in: World Environmental and Water Resources Congress 2014. American Society of Civil Engineers, pp. 1886–1895. doi:10.1061/9780784413548.189

Yossef, N.C., Winsemius, H., Weerts, A., Van Beek, R., Bierkens, M.F.P., 2013. Skill of a global seasonal streamflow forecasting system, relative roles of initial conditions and meteorological forcing. Water Resour. Res. 49, 4687–4699. doi:10.1002/wrcr.20350

Yuan, X., Ma, F., Wang, L., Zheng, Z., Ma, Z., Ye, A., Peng, S., 2016. An experimental

seasonal hydrological forecasting system over the Yellow River basin - Part 1: Understanding the role of initial hydrological conditions. Hydrol. Earth Syst. Sci. 20, 2437–2451. doi:10.5194/hess-20-2437-2016

Yuan, X., Wood, E.F., Luo, L., Pan, M., 2011. A first look at Climate Forecast System version 2 (CFSv2) for hydrological seasonal prediction. Geophys. Res. Lett. 38, L13402. doi:10.1029/2011GL047792